SIGNAL TRANSDUCTION MECHANISMS OF PAS AND HAMP DOMAINS

A Dissertation

Presented to the Faculty of the Graduate School

of Cornell University

In Partial Fulfillment of the Requirements for the Degree of

Doctor of Philosophy

by

Michael V. Airola

May 2010

SIGNAL TRANSDUCTION MECHANISMS OF PAS AND HAMP DOMAINS

Michael V. Airola, Ph. D.

Cornell University 2010

The focus of my dissertation is on the signaling mechanisms employed by PAS and HAMP domains, which are widespread signaling modules that coordinate cellular metabolism with external stimuli. A subset of PAS domains directly sense external stimuli, through an associated cofactor or ligand, and regulate the activity of an attached effector domain. In contrast, HAMP domains do not sense external stimuli and serve as signal relay modules. They are typically associated with the membrane and relay extracellular signals into intracellular responses. A subset of HAMP domains, which occur in poly-HAMP chains, are not associated with the membrane and differ from canonical HAMP domains in the region responsible for signal input.

To investigate HAMP domain signal transduction I have used the soluble receptor Aer2 as a model system. A unifying mechanism for HAMP domain signal transduction has yet to emerge, mainly due to lack of structural information. In chapter 1, I present the crystal structure of a 3-unit poly-HAMP chain from Aer2. Two distinct HAMP conformations were identified and a new model for signal transduction is presented. In Appendix 1, I present data that defines essential features of membrane associated HAMP domains. The results indicate that a signature motif: DExG, is required for HAMP domains to receive signal input across the membrane.

PAS and HAMP domains can occur within the same protein. The best-studied example is the E. coli aerotaxis receptor Aer, where direct side-on PAS and HAMP domain interactions propagate signals downstream. In Chapter 3, I present a model for

PAS and HAMP domain signal transduction in Aer2 that does not involve direct side-on interactions. This represents a new paradigm for applicable to successive PAS and HAMP domains and other similar signaling systems.

One recent controversy, in the mammalian circadian clock, is the identification of two core clock genes, PER2 and nPAS2, as heme-binding PAS proteins. A complicated feedback mechanism has been suggested where cycles in heme availability feedback to regulate the activity of PER2 and nPAS2. In chapter 2, I present data that PER2-heme interactions are non-specific and not biologically relevant to the mammalian circadian clock.

BIOGRAPHICAL SKETCH

Michael Virgil Airola was born and raised in Fresno, California. He attended Occidental College in Los Angeles, CA obtaining a Bachelor of Arts in Chemistry and conducted research on "Crack-free mesoporous transparent silica monoliths" under the direction of Prof. Ralph Amey. During his junior year, he had the pleasure of studying abroad at the University of Limerick, Ireland. In 2004, he joined the Chemistry and Chemical Biology Department of Cornell University to pursue a doctoral degree and conducted research on the "Signaling mechanisms of PAS and HAMP domains" under the supervision of Prof. Brian R. Crane. While at Cornell he met the love of his life: his fiancé, Krystal Etter. In his free time, he enjoys watching or playing soccer, grilling and hanging out with friends, eating delicious food, and exploring nature.

To my parents and Krystal for all their love and inspiration

ACKNOWLEDGMENTS

I was told graduate school would be one of the best times of my life. Some days I didn't always feel that way but as I look back it has been a wonderful journey and I have many people to thank for that.

First and foremost I want to thank my fiancé, Krystal Etter, for being there every step of the way. Her love, support and advice during tough times kept me moving and I am so thankful to have such a wonderful person in my life. From my parents, I could not ask for anything else. They have provided me with all the love a son could ask for and helped guide me through life's decisions. For this I am extremely grateful. To my brothers, Dave and John, and their significant others, Melanie and Brooke, I thank you for your constant love and friendship. To Richard and Renee Etter, thank you for treating me as your own son and always believing in me. I wish you could both be here to see this and I hope to make "The Professor" nickname come true.

Sometimes things work out better than you could ever imagine. Having an advisor like Brian Crane definitely falls into this category. He has inspired me in many ways and I thank him for all his patience, guidance, and motivation during both the good and bad years. Having a second "Crane" to talk to has been one of the most scientifically enlightening experiences. Talking to Alex almost always gave a different direction to approach my problems, minus the "Did you try adding some BOG? ... that could help." suggestion, and really helped me develop as an independent thinker.

Additionally, I consider myself very lucky to have had Holger Sondermann on my committee. He always treated me as a scientific equal, even when I was just starting out, and I have valued all his scientific and personal advice. Thanks to my other committee member Rick Cerione for his support and guidance. I will always remember his "You're doing fine. Why did you want to talk to me?" line, which

perhaps unknowingly gave me a little boost of confidence.

The Crane lab atmosphere has made such an amazing place to work over the past six years. For some reason, every member Brian and Alex attract is a wonderful and kind person. Thanks to Joanne and Abiola, for introducing me to Gimmee coffee which has greatly fed my coffee addiction. I had a lot of fun on our morning walks to Mann and back. To Bhumit, I thoroughly enjoyed sharing my and hearing about your research. This really helped to foster my interest in *in vivo* studies. Personally, you have been a great friend. To Ken and Brian Z, I enjoyed all the "smack talk" and taking your guys money in poker. Thanks for the golfing, babbling conservations on the same topic for way too long, and overall good times. Jaya's smile and charm was always on show and she was a great friend when I needed it. To Doowon, thank you for all the fun and soccer talk, as well as all your hard work in lab and your significant contributions to the following work. To Sudhamsu, for really "feeling it" and acting goofy with me. Thanks to Gaby for her laughter and for teaching me how to do a little salsa dancing before my first time out with Krystal. To Kevin Hoke, for teaching me electrochemistry and help interpreting data. It has been great working with everyone else and I've enjoyed learning about cricket from Anand, hearing hilarious jokes from Xiaoxiao, fun discussions with Tom, and hearing the Ria giggle in the office. I've also been lucky to work with some talented rotation students and very nice people: Anupam Chakravarty, Ushati Das, and Nattakan "Bee" Sukomon.

The majority of my dissertation work didn't start until fairly recently. I remember Brian asking me if I wanted to work on a "real heme-binding PAS domain", i.e. Aer2. For this I have our collaborator Kylie Watts to thank, who started our collaboration. It has been a fun couple of years and has turned out better than I imagined. In addition, much thanks to our collaborators Jing Du and John Dawson, at the University of South Carolina, for their nice MCD work on PER2.

To my friends at Cornell for all the good times we spent bowling, grilling, hiking, playing sports, poker, and even studying. Ryan and Chris for their up for anything attitude and intense spade games long into the night. Sungsoo for being such an insightful and fun conservationalist and philosopher. Andy for being Andy. Joe version 1.0 for the poker and golfing and Joe version 2.0 for the golfing and wine parties. Katie for being a good friend and colleague. Sarah and Drew for all the good times. Finally, to all my friends in Cali and other parts of the country for keeping me updated on things outside of Ithaca in “reality”.

TABLE OF CONTENTS

Biographical sketch (iii)
Dedication (iv)
Acknowledgements (v)
Table of Contents (vii)
List of Figures (ix)
List of Tables (xi)

Chapter 1: Structure of Concatenated HAMP Domains Provides a Mechanism for Signal Transduction
1.1 Abstract 1
1.2 Introduction 2
1.3 Results 5
1.4 Discussion 24
1.5 Summary 31
1.6 Materials and Methods 32
References 35

Chapter 2: Heme-Binding to the Mammalian Circadian Clock Protein Period 2 is Non-Specific
2.1 Abstract 39
2.2 Introduction 40
2.3 Materials and Methods 43
2.4 Results 46
2.5 Discussion 62
References 71

Chapter 3: Reconstruction of the Soluble Receptor Aer2 Establishes a New Paradigm for PAS and HAMP Domain Signal Transduction
3.1 Abstract 76
3.2 Introduction 77
3.3 Results and Discussion 79
3.4 Summary 97
3.5 Materials and Methods 97
References 102

Chapter 4: Defining Features of Membrane Associated HAMP Domains
4.1 Abstract 105
4.2 Result and Discussion 106
4.3 Materials and Methods 112
4.4 Contributions 114
References 115

LIST OF FIGURES

Figure	Description	Page
1.1	Domain Architectures of Representative HAMP Containing Proteins	3
1.2	Crystal Structure of the Aer2 N-Terminal Domain Contains Three Successive and Interwoven HAMP Domains	8
1.3	Structures of the Aer2 HAMP Domains	9
1.4	Superposition of HAMP Structures Reveals Two Distinct Conformations for Providing Different Signals to Downstream Domains	10
1.5	Residue Conservation and Packing Modes of HAMP Domains	12
1.6	Sidechain Interactions of Aer2 HAMP domains	13
1.7	Solvent Exposure of HAMP Residues	14
1.8	Hydrogen Bonding Interactions Between the Connector and Helices Stabilize the Aer2 HAMP Domains	18
1.9	Network of Interacting Residues at the HAMP2 and HAMP3 Interface	21
1.10	Sequence Identity and Degree of Conservation in Concatenated HAMP2 and HAMP3 Units	22
1.11	Output Mechanism Involving “Stutter Compensation”	23
1.12	Model for HAMP Domain Signal Transduction	27
2.1	PER2 binds heme in a manner dependent on redox state	48
2.2	Heme Binding Does Not Effect the Oligomeric State of PER2	49
2.3	Magnetic circular dichroism spectra of ferric PAS A, ferrous PAS A and ferrous-CO PAS A reveal ferric and ferrous hemes are bound through His-Cys and bis-His ligation respectively	51
2.4	Secondary Structure Alignment of mPER2 with other PAS domains	52

2.5	Cysteine Modification Alters the Ferric But Not the Ferrous-Heme PER2 Spectra	55
2.6	Heme binds to the chemotaxis kinase CheA	57
2.7	Addition of YtvA induces spectral changes to ferric and ferrous heme	58
2.8	Heme Dissociation from PER2 Occurs From Multiple Sites	60
2.9	Electrochemistry of PER2-Heme Complex	63
2.10	mPER2 structure with location of possible heme binding residues	68
3.1	Secondary Structure Alignment of Heme-Binding PAS Domains	79
3.2	The N- and C-terminal HAMP domains of Aer2 do not effect the UV-Visible absorption spectra of Aer2 PAS domain	82
3.3	Aer2 PAS Domain Directly Senses Oxygen	83
3.4	Pull-Down Assays of Aer2 PAS and HAMP Domain Protein Fragments	84
3.5	SAXS Parameters for Data Validation and Interpretation	86
3.6	*Ab initio* SAXS Reconstructions of Aer2 Protein Fragments	90
3.7	Reconstructed Model of Aer2 1-402 with a Linear Domain Arrangement	92
3.8	Aer2 PAS domain dimerization affinity is dependent on the heme redox/ligation state.	95
4.1	Swarm Assays of Aer2-Tar Chimeras	107
4.2	Glutamine Residue of the DExG Motif Links AS2 to AS1	111

LIST OF TABLES

Table	Description	Page
1.1	Data collection, MAD structure solution, and refinement statistics	7
1.2	Relative Threading Scores for HAMP Sequences onto Known Conformations	19
2.1	UV-Visible Absorption and HA50 Values Obtained From Heme Titrations	54
2.2	Heme Dissociation Rate Constants for mPER2 and Other Heme-Binding Proteins	61
3.1	Summary of Aer2 173-307 Protein Expression and Crystallization	80
3.2	UV-Visible Absorption Maxima for Aer2 173-289 and 1-402	82
3.3	Aer2 1-172 SAXS Parameters for Data Validation and Interpretation	87
3.4	Aer2 1-317 SAXS Parameters for Data Validation and Interpretation	88
3.5	Aer2 1-402 SAXS Parameters for Data Validation and Interpretation	89
3.6	Dependence of Aer2 173-289 Apparent MW (MW_{app}) on Protein Concentration and Redox/Ligation State	96
4.1	Summary of Soft-Agar Assays in CheRB+ and CheRB- Strains	107
4.2	Visualization of Attractant and Repellant Induced Responses	108

CHAPTER 1

Structure of Concatenated HAMP Domains Provides a Mechanism for Signal Transduction[1]

1.1 Abstract

HAMP domains are widespread prokaryotic signaling modules found as single domains or poly-HAMP chains in both transmembrane and soluble proteins. The crystal structure of a 3 unit poly-HAMP chain from the *P. aeruginosa* soluble receptor Aer2 defines a universal parallel four-helix bundle architecture for diverse HAMP domains. Two contiguous domains integrate to form a concatenated di-HAMP structure. The three HAMP domains display two distinct conformations that differ by changes in helical register, crossing angles, and rotation. These conformations are stabilized by different subsets of conserved residues. Known signals delivered to HAMP would be expected to switch the relative stability of the two conformations and the position of a coiled-coil phase stutter at the junction with downstream helices. We propose that the two conformations represent opposing HAMP signaling states and suggest a signaling mechanism whereby HAMP domains interconvert between the two states, which alternate down a poly-HAMP chain.

[1] Reprinted from *Structure*, 18(4), Airola, M.V., Watts, K.J, Bilwes, A.M., and Crane, B.R., "Structure of Concatanated HAMP Domains Provides a Mechanism for Signal Transduction", 436-448, Copyright (2010), with permission from Elsevier

1.2 Introduction

For their survival, prokaryotes depend on two-component signaling pathways to respond to changing environmental conditions (Szurmant et al., 2007). Many of the proteins that underlie these pathways contain HAMP domains, which function as signal relay modules that couple motions of transmembrane helices to the activity of a downstream cytoplasmic output domain (Hazelbauer et al., 2008). HAMP domains were named for the type of proteins in which they were originally identified: **H**istidine kinases, **A**denylyl cyclases, **M**ethyl-accepting chemotaxis proteins (MCPs), and **P**hosphatases (Aravind and Ponting, 1999). However, they also occur with other types of output modules: for example, diguanylate cyclases (GGDEF) and phosphodiesterases (EAL). The number and variety of signaling proteins in which they are featured highlight the importance and versatility of HAMP domains to prokaryotic signal transduction. The mechanism by which HAMP domains propagate conformational changes is of great interest for understanding how signals traverse membranes. In one of the best-studied examples, HAMP domains are an essential component of transmembrane chemoreceptors (MCPs), in which they connect the last transmembrane helix (TM2) to the cytoplasmic kinase interacting domain (Hazelbauer et al., 2008). Typically, transmembrane receptors, like MCPs, contain a canonical HAMP domain as a single unit (Figure 1.1). HAMP domains can be swapped interchangeably between different proteins without loss of function, which suggests a conserved mechanism for propagating signals (Appleman et al., 2003; Hulko et al., 2006; Zhu and Inouye, 2003).

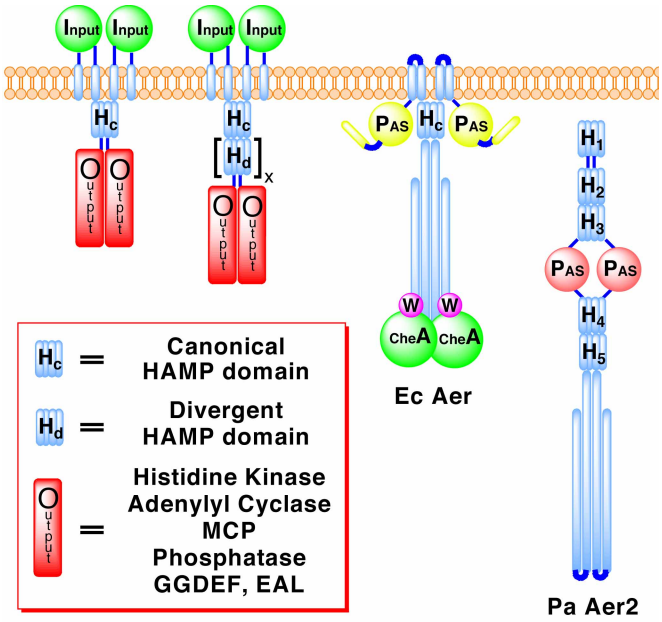

Figure 1.1. Domain Architectures of Representative HAMP Containing Proteins. Schematic depicting the location of canonical HAMP domains and poly-HAMP chains in transmembrane and soluble signaling proteins. Poly-HAMP chains, $[H_d]_x$, can extend from 2 to 31 consecutive HAMP domains. EcAer is shown binding to the histidine kinase CheA and coupling protein CheW, proteins PaAer2 also likely interacts with.

HAMP subunits (~50 residues) contain two a-helices, AS1 and AS2, bridged by a flexible connector of approximately 14 residues (Butler and Falke, 1998). NMR studies of an archeal HAMP domain of unknown function (Af1503) demonstrated that the HAMP domain folds into a parallel four-helix bundle (Hulko et al., 2006). Each of the two helices are composed of a typical heptad repeat (a-g), with hydrophobic residues in positions a and d forming a buried hydrophobic core. The flexible connector spans the length of the four-helix bundle and contains a motif of three critical residues that is found in most HAMP domains (Ames et al., 2008; Hulko et al., 2006). Cross-linking studies of the aerotaxis receptor Aer (Watts et al., 2008) and the chemoreceptor Tar (Swain and Falke, 2007) confirmed the parallel four-helix bundle architecture for the HAMP domains of these well-studied proteins.

The mechanism of signal transduction by HAMP domains has been extensively studied in the bacterial chemotaxis system and with sensor histidine kinases. In the canonical HAMP systems of MCPs and the histidine kinase NarX, signal input is received from a transmembrane helix (TM2), attached to AS1, that undergoes a "piston-like" motion induced by ligand binding to a periplasmic sensing domain (Cheung and Hendrickson, 2009; Falke and Hazelbauer, 2001). Alternatively, the TM2's of the phototransducing element NpHtrII have been shown to undergo both a horizontal displacement and a 15° clockwise rotation after light excitation (Moukhametzianov et al., 2006).

A number of mechanisms have been proposed to describe the molecular motions of HAMP domains during signal transduction. These models, which are not necessarily mutually exclusive, encompass (i) a gearbox model involving a concerted rotation of helices (Hulko et al., 2006), (ii) a dynamic model of four-helix bundle stability (Zhou et al., 2009), and (iii) a scissor-like motion with a change in helix-helix crossing angles (Swain and Falke, 2007). Additionally, a model based on cryo-electron microscopy studies of chemoreceptor assemblies suggests HAMP domains interconvert between a compact trimer of HAMP dimers and an expanded form (Khursigara et al., 2008). In each case, HAMP signaling can be described by a two-state model in which modest structural changes separate states whose conformational stabilities are closely balanced in free energy.

Pseudomonas aeruginosa contains two transducers of aerotaxis: PaAer is homologous to the membrane bound *E. coli* aerotaxis receptor Aer, whereas the second, PaAer2, lacks transmembrane helices and is a soluble receptor (Figure 1.1) (Hong et al., 2004). Aer2 contains a heme-binding PAS domain, which can signal in response to diatomic gases (K. Watts, unpublished data). A total of five HAMP domains are predicted in the full-length protein, with three N-terminal and two C-

terminal to the PAS domain. The Aer2 HAMPs belong to a group of divergent HAMPs recently identified in the gene sequences of a large number of diverse bacteria (Dunin-Horkawicz, submitted). Poly-HAMP chains (composed of repeating HAMP units) and soluble receptors, such as Aer2, are typically composed of divergent HAMP domains (Figure 1.1). The C-terminus of Aer2 contains a cytoplasmic signaling region, with a high degree of similarity to *E. coli* chemoreceptors, which likely couples the protein to the histidine kinase CheA and other components of the chemotaxis pathway (Hong et al., 2004).

Here, we present the crystal structure of the N-terminus of the soluble aerotaxis receptor Aer2 from *P. aeruginosa*, which contains three HAMP domains and represents the first structure of a di-HAMP unit. These three structures confirm the universality of the parallel four-helix bundle structure and provide a view of the diverse, low-energy conformational states available to HAMP domains. The two HAMP domains composing the di-HAMP share an extensive and interwoven interface to produce a concatenated signaling unit. The structure reveals the presence of two distinct conformations of HAMP domains, which are differentiated by changes in helical register, rotation, and crossing angle.

1.3 Results

Structure Determination and Overall Description

Sequence analysis of the N-terminal region of Aer2 (1-172) predicts that this region contains three successive HAMP domains. We overexpressed this fragment of Aer2 in *E. coli* and obtained a soluble dimer that was amenable for crystallization. Crystals of Aer2 1-172 (space group $P4_32_12$, a = b = 114.0 Å, c = 64.3 Å) grew in 1.1 M Li_2SO_4, 15-18% glycerol, 0.1 M Tris, pH 8.5, and diffracted to 2.64 Å. The structure was determined by multi-wavelength anomalous diffraction (MAD) using

selenomethionine protein crystals and refined to an R factor of 0.237 and an R_{free} of 0.270 (Table 1.1).

The structure of Aer2 1-172 is a symmetric dimer containing three HAMP domains (Figure 1.2), each similar to the NMR structure of Af1503. The basic construction of each HAMP domain consists of a monomeric unit of two parallel a-helices (AS1 and AS2) joined by an elongated connector of 12-14 residues (Figure 1.3). This unit dimerizes and coils around a central supercoil axis to form a parallel four-helix bundle. The residues of the heptad repeat point inward, forming a buried core, with the remaining residues exposed to the solvent to varying degrees. A helical insert separates HAMP1 and HAMP2, whereas HAMP2 and HAMP3 share a continuous helix, creating an interwoven, concatenated di-HAMP structure (Figure 1.2).

Two Distinct HAMP Conformations

The Aer2 HAMP domains each adopt a unique four-helix bundle. However, the three structures fall into two distinct structural conformations. Superposition shows that HAMP1 and HAMP3 adopt a conformation resembling Af1503, with only minor differences in helical tilt and orientation (Figure 1.4). In this conformation, the AS1 and AS2 helices are in-register, and the sidechains that form the hydrophobic core are positioned in the same plane to produce four layers of interacting residues (Figure 1.3).

Table 1.1 Data collection, MAD structure solution, and refinement statistics

Data Collection

	Native	Se-Met Peak	Se-Met Inflection	Se-Met Remote
Wavelength (Å)	0.97918	0.97857	0.97914	0.95682
Space group	$P4_32_12$			
Cell parameters (Å)	a = b = 114.0, c = 64.3			
Resolution (Å)	50-2.64 (2.69-2.64)	50-3.15 (3.20-3.15)	50-3.42 (3.48-3.42)	50-3.25 (3.31-3.25)
Reflections	90969	54421	43482	50373
Unique reflections	12812	13826	10963	12741
Completeness (%)	97.7 (99.2)	97.2 (99.2)	97.7 (100.0)	97.8 (99.8)
R_{sym} [a]	0.049 (0.411)	0.099 (0.433)	0.108 (0.433)	0.084 (0.464)
I/σ(I)	38.4 (4.5)	12.1 (3.2)	13.2 (3.1)	16.3 (2.9)

MAD Structure Solution Statistics

Resolution cutoff (Å)	3.42
No. of anomalous sites found	4 (of 4)
Mean figure of merit (FOM)	0.73
Overall Z-score	40.8

Refinement statistics

Resolution range	40 - 2.64 Å
R factor, %	23.7 (43.9)
R_{free}, %	27.0 (46.2)
Atoms (protein/solvent)	1231, 44
Mean B-values (Å^2)	
Overall	75.0
Main chain	63.2
Side chain	61.0
Rmsd from ideal	
Bonds mainchain	0.032 Å
Bonds sidechain	0.281 Å
Angles mainchain	0.6 deg
Angles sidechain	1.2 deg
Ramachandran plot, %	
Most favored	93.6
Additionally allowed	6.4
Generously allowed	0.0
Disallowed	0.0
Missing residues	158-172

Data for outermost resolution shell are given in parenthesis

[a] $R_{sym} = \Sigma\Sigma_j |I_j - \langle I \rangle| / \Sigma\Sigma_j I_j$

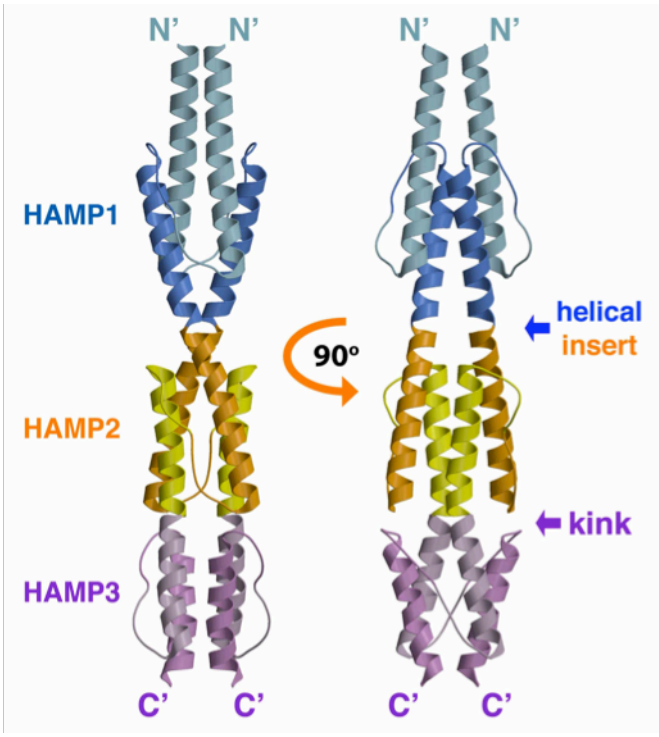

Figure 1.2. Crystal Structure of the Aer2 N-Terminal Domain Contains Three Successive and Interwoven HAMP Domains. Ribbon presentation of the Aer2 (1-172) dimer with HAMP1 (AS1: light blue, AS2: blue), HAMP2 (AS1: orange, AS2: yellow), and HAMP3 (AS1: light purple, AS2: purple). HAMP2/3 forms a concatenated structure. AS2 of HAMP1 is contiguous with AS1 of HAMP2 and AS2 of HAMP2 is contiguous with AS1 of HAMP3. HAMP3 is rotated roughly 90° relative to HAMP1 and HAMP2.

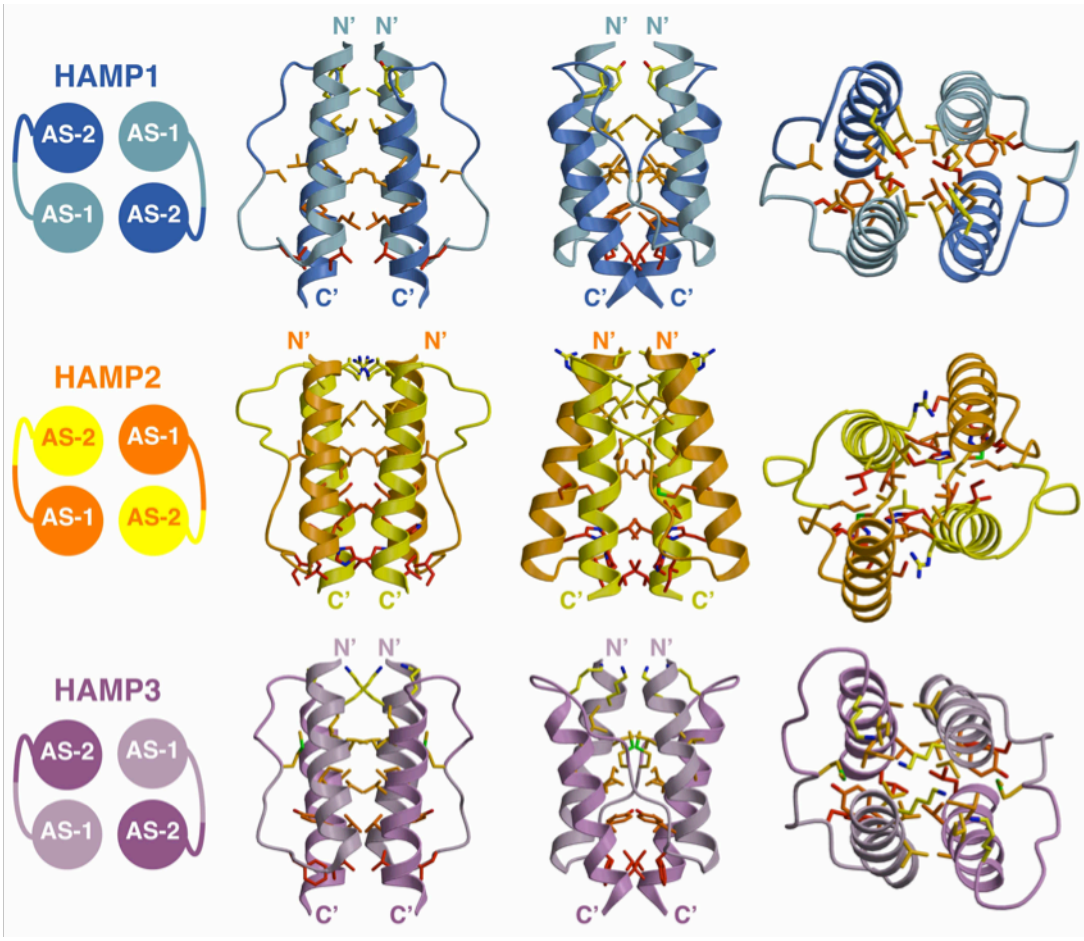

Figure 1.3. Structures of the Aer2 HAMP Domains. Side and top views (90° rotation) of individual Aer2 HAMP domains with buried side chains (Carbon: yellow to red, Nitrogen: blue, Sulfur: green). HAMP1 and HAMP3 sidechains are in-register and HAMP2 sidechains are offset. HAMP2 has an unusual trapezoidal shape (as viewed from the side) and rhombic arrangement of helices in cross section. The position of the connector and hydrophobic residue 2 (HR2) correlates with changes in helical register, helix crossing angles, and helical rotation. I88 (HR2, HAMP2) inserts between AS1 and AS2, and V33 (HR2, HAMP1) and M134 (HR2, HAMP3) pack against the periphery of AS1 and AS2.

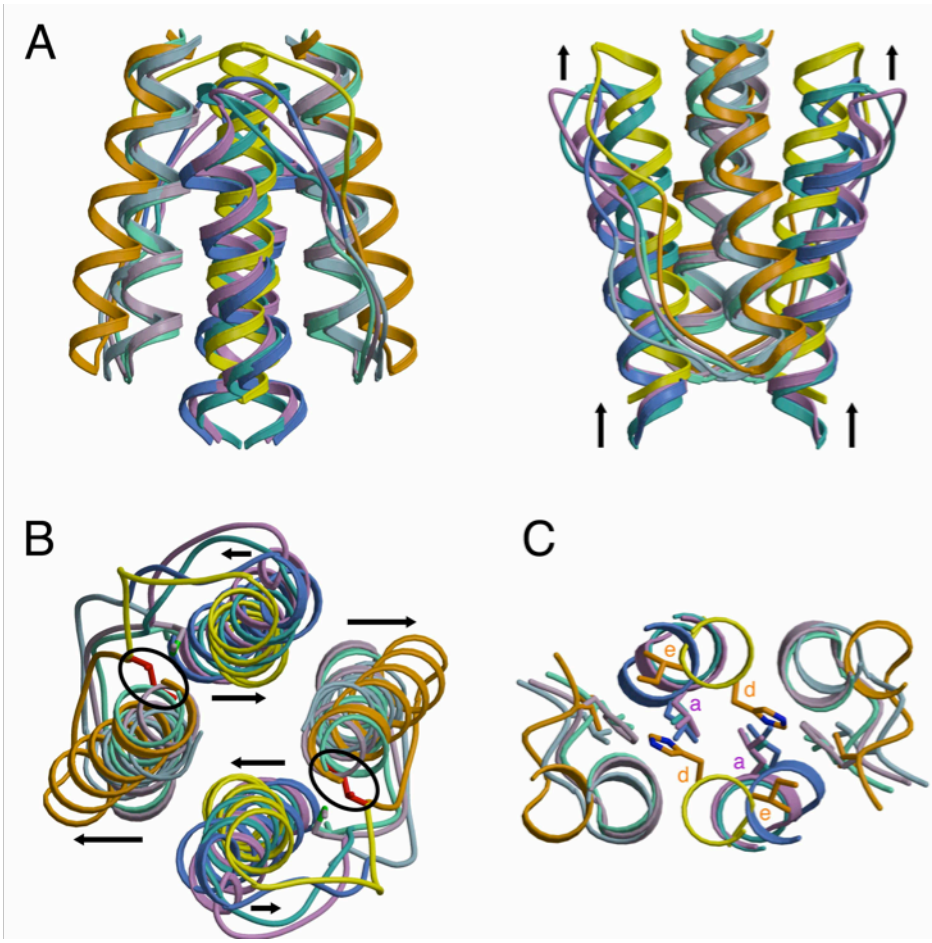

Figure 1.4. Superposition of HAMP Structures Reveals Two Distinct Conformations for Providing Different Signals to Downstream Domains. Ribbon presentation of HAMP superpositions in (A) side and (B) top views displaying differences in helix orientation between overlapping HAMP1, HAMP3, and Af1503 (AS1: light green, AS2: turquoise) helices and distinct conformation of HAMP2 (AS1: orange, AS2: yellow) with offset helices, change in helix crossing angles (black arrows), and the inserted HR2 (I88: red) residue (black circle). Note the vertical displacement of AS2 relative to AS1. (C) Distal region of HAMP domains where signal output is directly linked to the conformation of AS2. His111 (HAMP2) occupies a typical "d" position, with the analogous residue in other HAMPs (L55: HAMP1, L155: HAMP3, L326: Af1503) holding an "a" position, in which they interact with hydrophobic residue 1 (HR1) of the connector.

A defining feature of coiled-coils is the position and direction of sidechain packing. Typically, coiled-coils make knobs-into-holes interactions in which the sidechains of one helix occupy a hole formed by a set of interacting residues on an adjacent helix. Af1503 contains unusual x-da packing, with one set of sidechains directed toward the supercoil axis, in an "x" position, and a second set forming a ring of interacting residues, in "da" positions. The HAMP1 and HAMP3 sidechains do not conserve the x-da packing mode and adopt a variety of packing arrangements, including knobs into holes (a-d), x-da, and x-x layers (Figure 1.5 and Figure 1.6). HAMP1, HAMP3, and Af1503 belong to different HAMP groups, based on sequence analysis (Dunin-Horkawicz, submitted), and each group may adopt a different packing mode to stabilize a similar four-helix bundle conformation. Overall, the variety of packing modes observed demonstrates that exclusive x-da packing is not a necessary structural feature of all HAMP domains.

The conformation of HAMP2 is distinct and represents a possible alternative signaling state of HAMP domains. The unique conformation of HAMP2 arises from a combination of structural differences that affect the intra and inter subunit sidechain interactions, helix-connector interactions, and the intra and inter helix-helix crossing angles. The most notable change is an offset of the helical register between the AS1 and AS2 helices by half a helical turn (~2-3 Å), which staggers the sidechains that form the buried core (Figure 1.3). The loss of interacting residue layers essentially leads to the formation of a two-stranded coiled-coil of the AS2 helices. The AS1 helices also supercoil around the same axis but they have limited interactions with each other.

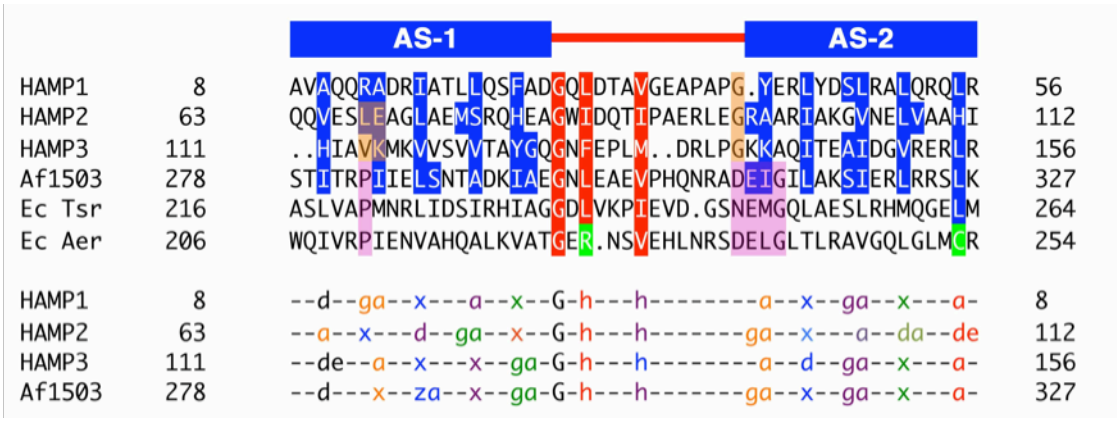

Figure 1.5. Residue Conservation and Packing Modes of HAMP Domains. Sequence alignment of representative HAMP domains: Aer2, Af1503, EcTsr, and EcAer, showing conservation of the buried core (blue) and connector motif (red) residues (top panel). The bottom panel denotes the heptad position of core residues (a, d, e, g, z = undefined, x = directed at supercoil axis), as defined by TWISTER, in a variety of packing modes: a-d, x-da (x-ga or x-de), and x-x. Sets of interacting residues are color-coded to highlight the sidechains of HAMP1, HAMP3, and Af1503 (in-register) and HAMP2 (offset) (bottom panel). “G” and “h” correspond to conserved residues of the connector motif and are also color coded with the layer of interacting residues. Position of the conserved proline residue (purple) in canonical HAMP domains corresponds to residues that occupy different heptad positions (peach) in alternative HAMP conformations. Aer2 HAMPs conserve Gly residues (peach) at the beginning of AS2, which allows close association of domains in a poly-HAMP chain, compared to the DExG motif of canonical HAMPs (purple).

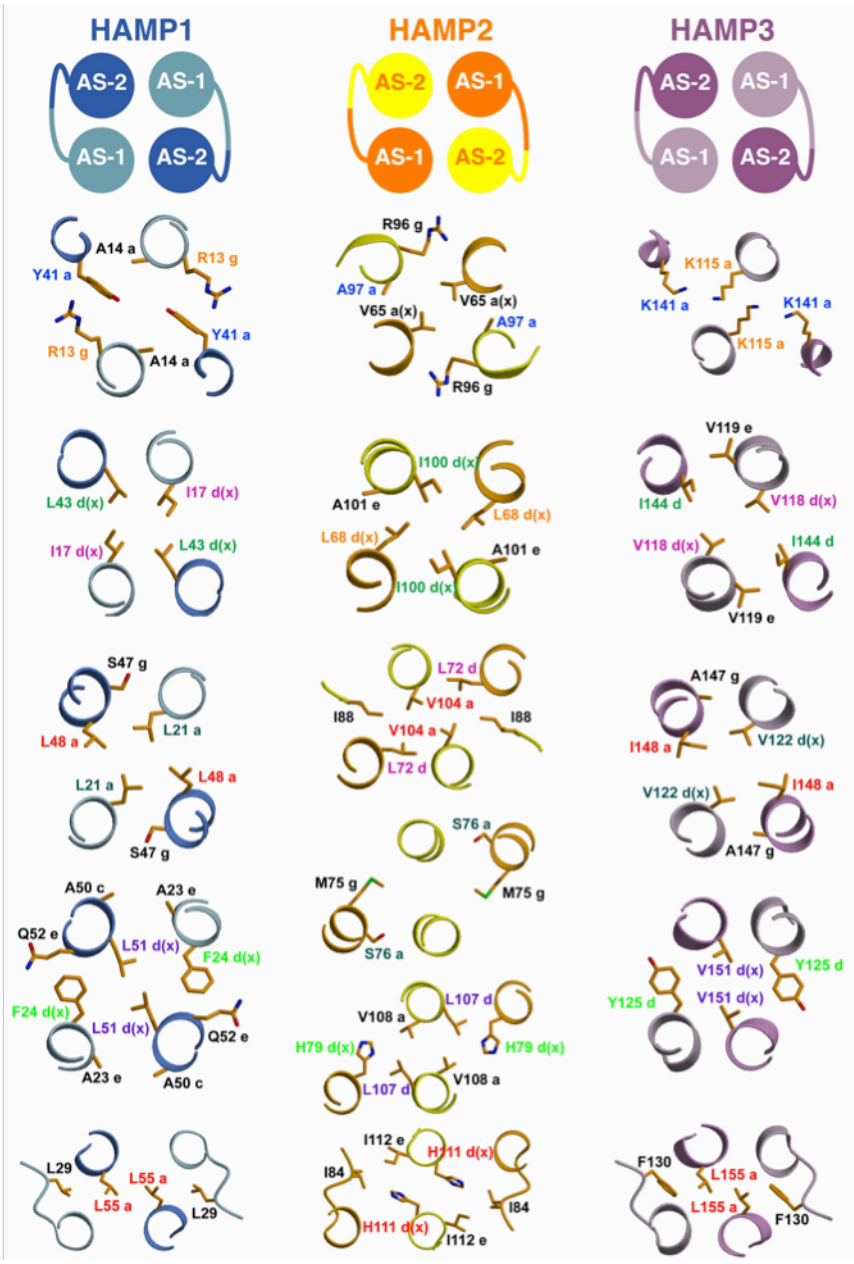

Figure 1.6. Sidechain Interactions of Aer2 HAMP domains. Cross-sections of the Aer2 HAMP domains displaying a variety of sidechain packing modes: a-d, x-da (x-ga or x-de), and x-x. Clockwise and counterclockwise rotation of AS1 and AS2 alters the corresponding sidechain positions (color-coded) in HAMP2 compared to HAMP1 and HAMP3. These changes generate a greater helix-helix separation that increases the overall solvent accessibility of HAMP2 residues at the inter-helix interface (Figure 1.7). Sidechains of HAMP2 do not occupy the same plane due to a change in helical register; they are shown with the nearest layer. Helices are viewed with the N-terminus pointing toward the viewer.

The crossing angles of the HAMP2 helices change drastically compared to the other HAMP domains, with the AS1 helices flaring out away from the supercoil axis and packing against the AS2 helices in a ridges-into-grooves manner (Figure 1.3). In turn, the AS2 helices rotate into a parallel position. Although the different packing modes of the Aer2 HAMP domains preclude an exact quantification, a general clockwise rotation of AS1 and counterclockwise rotation of AS2 relates HAMP2 to HAMP1/3. The rotation of AS1 and AS2 in opposite directions turns the sidechains forming dimer contacts outward. This increases the solvent exposure of residues at the dimer interface in AS1, which flares out, but not those of AS2, which move inward toward the supercoil axis (Figure 1.6 and Figure 1.7).

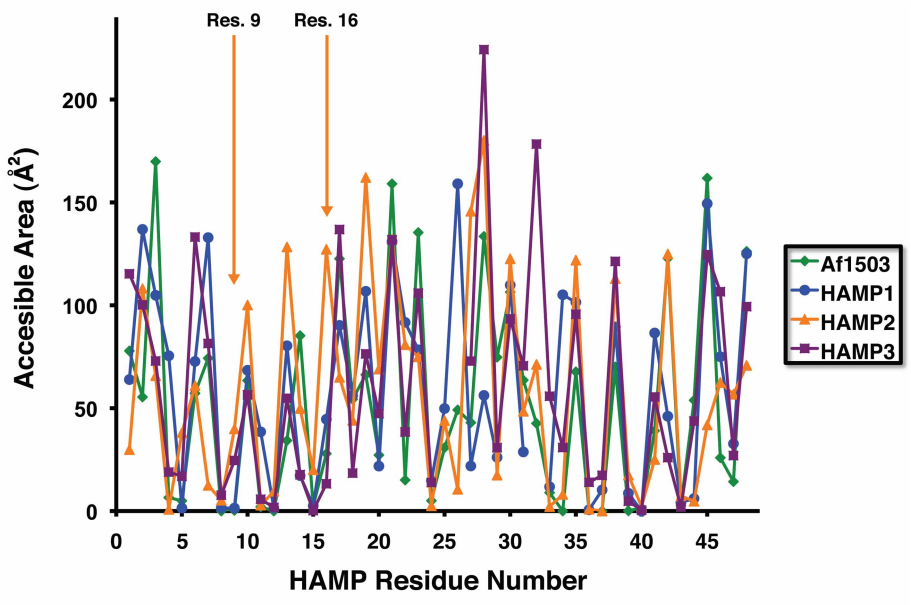

Figure 1.7. Solvent Exposure of HAMP Residues. Accessible area ($Å^2$) per residue of HAMP domain motif displaying an increased degree of solvent exposure for AS-1 residues at the dimer interface (positions 9 and 16) in HAMP2 compared to HAMP1, HAMP3, and Af1503. The increased exposure is due to helical rotation and flaring out of AS-1. Residue numbering system corresponds to the alignment in Figure 5, with residue number 1 equal to residues aligned with A10: HAMP1, V65: HAMP2, and H111: HAMP3. Solvent exposure was calculated using the CCP4 program AREAIMOL.

These changes in HAMP2 combine to form a trapezoidal four-helix bundle (Figure 1.4A). This helical rearrangement is directly coupled to an increased integration of a connector residue, I88, into the hydrophobic core of HAMP2. To our knowledge, HAMP2 is a unique parallel four-helix bundle that displays an offset ridges-into-grooves interaction; however, the structure of HAMP2 bears some resemblance to the three stranded coiled-coil of spectrin (Yan et al., 1993).

Role of the Connector in Stabilizing Alternative Conformations

Additional structural variations are found in the position and interactions of the conserved HAMP connector motif. This motif, Gly-x-HR1-x-x-x-HR2, contains two hydrophobic residues (HR1 and HR2) and begins immediately after AS1 (Figure 1.5). An extensive mutagenesis analysis of the connector region of the *E. coli* serine chemoreceptor (Tsr) found that these residues (Gly, HR1, and HR2) were the only critical residues for function (Ames et al., 2008). Mutation of G235 in Tsr to nearly any other residue led to an altered or complete loss of chemotaxis in *E. coli* cells that contained Tsr as the only chemoreceptor. Similarly, mutation of L237 (HR1) and I241 (HR2) to hydrophilic or small hydrophobic residues also led to complete loss of function. These residues each perform a significant role in stabilizing the Aer2 HAMP structures but different subsets of these conserved HAMP residues play more prominent roles in stabilizing the two distinct conformational states.

In both conformations, the Gly residue located at the C-terminus of AS1 provides the flexibility to accomplish a sharp turn, with each Gly adopting ϕ/ψ conformations disallowed by other amino acids. In the similar conformations of HAMP1 and HAMP3, the first hydrophobic residue of the motif, HR1 (L29: HAMP1, F140: HAMP3), stabilizes each structure by packing against a conserved residue of the heptad repeat in an “a” position at the end of AS2 (L55: HAMP1, L155: HAMP3) (Figure 1.4C). In contrast, the HAMP2 AS2 helices rotate counterclockwise to place

His111 (which occupies the conserved heptad position) in a “d” position where it cannot interact with I84 (HR1) of the same subunit. The counterclockwise rotation of AS2 instead brings I112 in close proximity to I84 (HR1). These structural changes are located at the C-terminal end of the HAMP domain, where the conformation of AS2 must relay signal output to a C-terminal domain.

Drastic conformational differences are observed in the position and interactions of HR2 among the three HAMPs (V33: HAMP1, I88: HAMP2, M134: HAMP3). These changes reflect the wide conformational variability and flexibility of the connector. Each interaction serves to stabilize the particular HAMP structure in a different way, which points to a concerted rearrangement of helical structure and connector interactions during conversion between HAMP signaling states. Variable extensions of the connector, combined with different helical tilts in the three conformations, allow HR2 to interact with different layers of the HAMP structure. In HAMP1, V33 (HR2) packs against the protein backbone and hydrophobic residues of layer 3: L21 and L48 (Figure 1.3). In HAMP3, a more extended conformation positions M134 (HR2) above layer 3, and the sidechain of Met134 points upward to make contact with V122 and I148 in layer2 (Figure 1.3). Again, HAMP2 adopts a more divergent conformation, fully inserting I88 (HR2) between AS1 and AS2, where it makes hydrophobic contacts with residues above and below (L68, A101, L72, V104, M75, and V108) (Figure 1.3). The position of I88 in HAMP2 reveals why HR2 has such a critical role for HAMP function and suggests that other HAMP domains may utilize a similar interaction.

Complementary to the roles of HR1 and HR2, the connector stabilizes each HAMP domain through hydrogen bond interactions. These interactions do not involve the non-critical sidechains of the connector but rather occur primarily between the sidechains of AS2 and the connector peptide backbone. For HAMP1 and HAMP3, the resulting structural outcome is a close association of the connector with the AS2 helix

(Figure 1.8). In contrast, the HAMP2 connector resides between AS1 and AS2 (N-terminal to HR2) and is closely associated with AS2 (C-terminal of HR2). At the center of this junction is N105 in AS2, which hydrogen bonds to the carbonyl oxygen and the amide nitrogen of the I88 (HR2) peptide backbone. The Asn sidechain is highly conserved in homologous Aer2 HAMP2-3 units (Figure 1.7) and is ideal to link conformational changes of AS2 with a rearrangement of the connector. This may explain why Asn is prevalently found in this position for many HAMP domains (Dunin-Horkawicz, submitted). The HAMP domains of MCPs are an exception, and other residues capable of hydrogen bonding (e.g. Arg or Ser) could perform a similar function.

Threaded HAMP Sequences

The differences in helix orientation and sidechain packing between the Aer2 and Af1503 HAMP domains prompted us to test if each HAMP sequence was specific for only one HAMP conformation. The Rosetta program is a powerful tool that has been used to evaluate the compatibility of protein sequences with different 3-dimensional structures (Ambroggio and Kuhlman, 2006; Das and Baker, 2008). Using Rosetta Design, which applies a potential function incorporating terms for stereochemistry, sterics, solvation, and electrostatics (see Methods for a more detailed description), each sequence was threaded onto all four known HAMP conformations to generate one native and three altered conformations. The threaded structure was given a score, in Rosetta energy units (REUs), that represents the compatibility of each sequence and associated sidechain conformations with the experimentally determined fixed backbone structure.

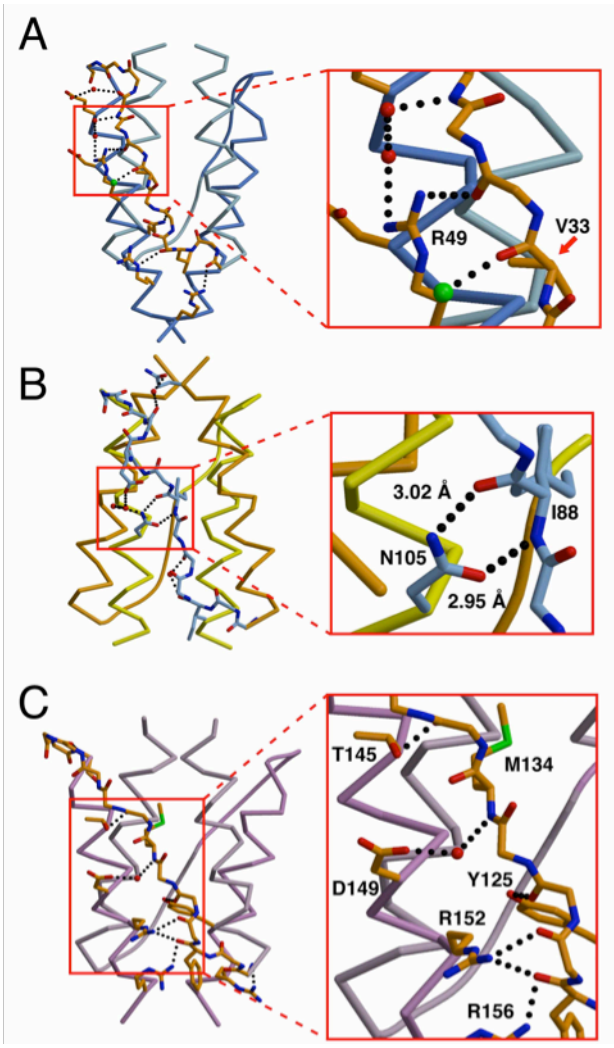

Figure 1.8. Hydrogen Bonding Interactions Between the Connector and Helices Stabilize the Aer2 HAMP Domains. Variable hydrogen bonding interactions and associations between the connector (peptide backbone) and helices (Ca trace) stabilize the different conformations of (A) HAMP1, (B) HAMP2, and (C) HAMP3. N105 hydrogen bonds (dotted line) with the peptide backbone to stabilize the position of the inserted I88 residue (hydrophobic residue 2: HR2) in HAMP2 (inset B). R49 forms a hydrogen bonding network with the connector peptide backbone and two water molecules (red). Peptide backbone of V33 (HR2) in HAMP1 forms a salt bridge with a chlorine atom (green) (inset A). D149 of HAMP3 forms a salt bridge with a water molecule (red) to the amide nitrogen of M134 (HR2) (inset C).

The HAMP1, HAMP3, and Af1503 structures, which all share the in-register conformation but contain different packing modes (e.g. x-da, x-x), had comparable REUs for their native sequence but had much higher scores when threaded with the other sequences (Table 1.2). This indicates that each HAMP sequence favors a specific packing mode to stabilize a common conformational state. In contrast, the HAMP2 sequence was compatible with the out-of-register structure of HAMP2 and the in-register structure of HAMP1. This suggests that HAMP2 could adopt a conformation similar to HAMP1 during signal transduction. When the HAMP3 and Af1503 sequences were threaded onto the HAMP2 structure, the resulting REUs were only slightly higher than with their native structures. This suggests that a HAMP2 conformation would be accessible for the HAMP3 and Af1503 sequences. In contrast, HAMP1 did not thread well onto the distorted four-helix bundle of HAMP2, which may indicate that HAMP1 could adopt a HAMP2-like structure, but only with an altered backbone conformation and packing mode.

Table 1.2. Relative Threading Scores for HAMP Sequences onto Known Conformations. Numbers refer to the Rosetta Design Score, given in Rosetta Energy Units (REUs), with lower scores being more stable. The lowest stable score is highlighted in grey for each conformation in our two-state model.

Protein Sequences	**Conformations**			
	HAMP1	**HAMP2**	**HAMP3**	**Af1503**
Hamp1	38	2047	1347	5510
Hamp2	358	-74	2792	1001
Hamp3	1555	564	145	2599
Af1503	1085	304	1667	148
Aer	2016	613	1615	6773
Mt Rv3645	212	506	937	4616
NarX	1757	416	490	1298
Tar	1985	486	431	3000
Tsr	1606	459	255	885

We then threaded the sequences of other canonical HAMP domains of unknown structure onto each known structure. Again, each sequence was most compatible with only one of either the HAMP1, HAMP3, or Af1503 structures, supporting the hypothesis that each HAMP domain sequence favors a distinct packing mode (Table 1.2). Interestingly, all the sequences threaded well onto the HAMP2 structure, with REUs close in value to the lowest score obtained from HAMP1, HAMP3, or Af1503. This may be a reflection of the more expanded conformation of HAMP2, which allows for a greater degree of freedom in sidechain size. For these reasons, one could expect a HAMP2-like structure to be more dynamic than a HAMP1, HAMP3, or Af1503 conformation. Overall, the threading analysis suggests that both canonical and divergent HAMP sequences are compatible with both an in-register conformation and a more dynamic, out-of-register, HAMP2-like conformation.

The Concatenated Di-HAMP 2-3 Unit

Concatenated HAMP2-3 gives the first view of a di-HAMP structure and provides insight into signal transduction by poly-HAMP systems. HAMP2 and HAMP3 not only share a contiguous helix, but their interface is also highly interwoven. The sidechains of K115 and K141 in HAMP3 are directed upward and insert into the HAMP2 structure to form a polar pocket with H79 and H111 (Figure 1.9). Sequence analysis of homologous Aer2 HAMP2-3 units reveals a high degree of residue conservation at this interface (Figure 1.10). Two conserved Gly residues at both the beginning and end of the connector are necessary to achieve the close proximity between HAMP2 and HAMP3. A number of hydrogen bonds are formed between HAMP2 and HAMP3, including one between the connector peptide backbones of G82 and K140, and others between various sidechains (Figure 1.9). Structurally, these two HAMP domains are highly integrated and may function as a single unit containing two opposing conformations.

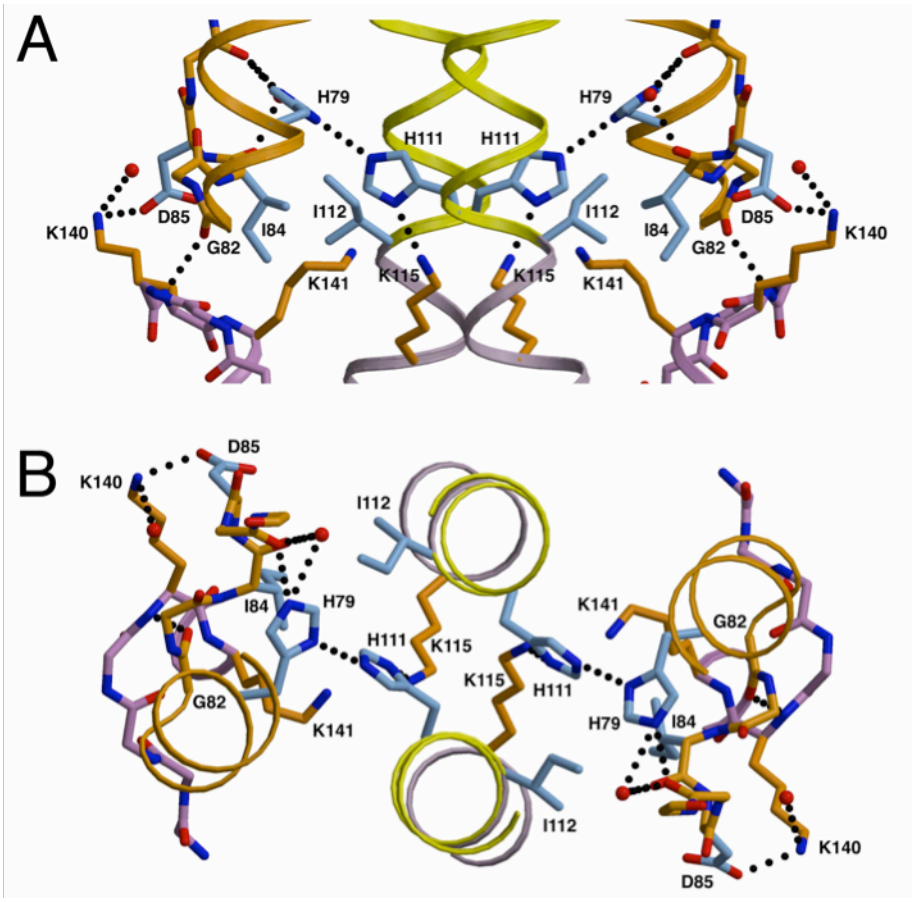

Figure 1.9. Network of Interacting Residues at the HAMP2 and HAMP3 Interface. Side (A) and top (B) views of the concatenated HAMP2 and HAMP3 interface reveal an extensive network of interactions that stabilize the observed structure and suggest that a concerted conformational rearrangement occurs during signal transduction. Salt bridges between neighboring sidechains (H79, H111, and K115) form a polar pocket that stabilizes the burial of hydrophilic groups. Direct hydrogen bonds formed between sidechains (D85 and K140) and the peptide backbone of conserved glycines (G86 and G139) of the connector display the interwoven nature of the di-HAMP structure. Red balls represent water molecules, and hydrogen bonds are denoted by dotted lines.

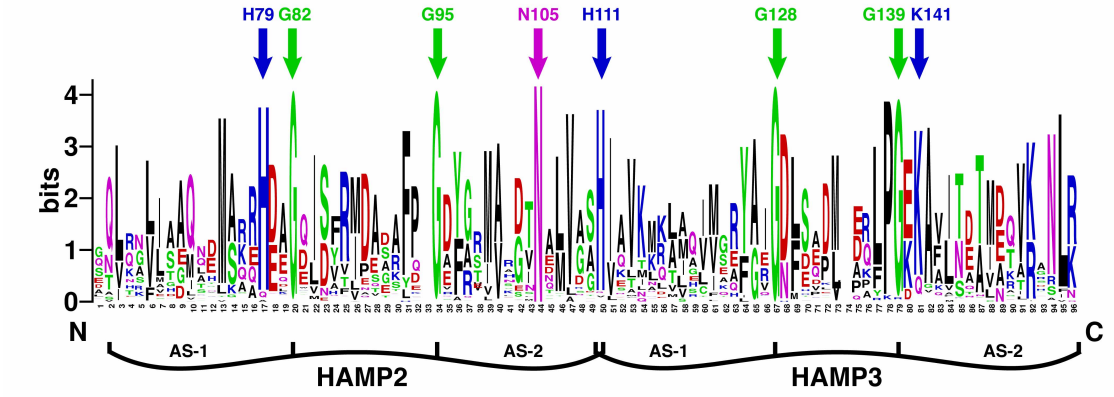

Figure 1.10. Sequence Identity and Degree of Conservation in Concatenated HAMP2 and HAMP3 Units. Weblogo of proteins homologous to Aer2 HAMP2-3 (residues 63-156), with the sequence identity and conservation indicated by letter height. The Gly residues at the beginning and end of the connector in both HAMP domains, as well as N105 in AS-2 of HAMP2, which are crucial for stability, are absolutely conserved. Residues at the interface of HAMP2 and HAMP3 also display a high degree of conservation, with both His79, His111, and K141 being almost completely conserved.

Unlike the interwoven HAMP2-3 unit, a helical insert separates HAMP1 and HAMP2 of Aer2. However, analysis of 132 sequences homologous to Aer2 1-156 (identified using pBLAST) found that Aer2 was the only protein containing this helical linker. Thus, this element is unlikely to be functionally important. Altogether, signal transduction through poly-HAMP systems is most likely to involve concerted structural changes that propagate through concatenated, repeating units.

Output Mechanism Involving "Stutter Compensation"

Insight into how HAMP domains may propagate signals downstream is gained by examining the similar heptad discontinuities between continuous AS2 and AS1 helices of the concatenated HAMP2/3 unit and between canonical AS2 helices and downstream output helices (OHs) (Figure 1.11). As discussed in other HAMP sequences (Stewart and Chen, 2009; Zhou et al., 2009), at both of these junctions the heptad repeat of continuous helices contains a "stutter" (Lupas and Gruber, 2005), differing by the insertion of four (or deletion of 3) residues. In Aer2 HAMP2, this

stutter occurs at the end of AS2. It alters the heptad position of H111 to a "d" position (Figure 1.4) and aligns the heptad repeat to match that of AS1 of HAMP3 (Figure 1.11). However in HAMP1/3, the same residue (L55/L155) is in an "a" position and will thus offset the heptad repeat of a continuous coiled-coil from ideal packing. To compensate for the offset, the stutter could move to AS1 of a downstream HAMP, as observed in HAMP2 (Figure 1.11), or output helix (OH). Critical residues at these junctions may alternately occupy a core heptad position (a or d) to an e or g position.

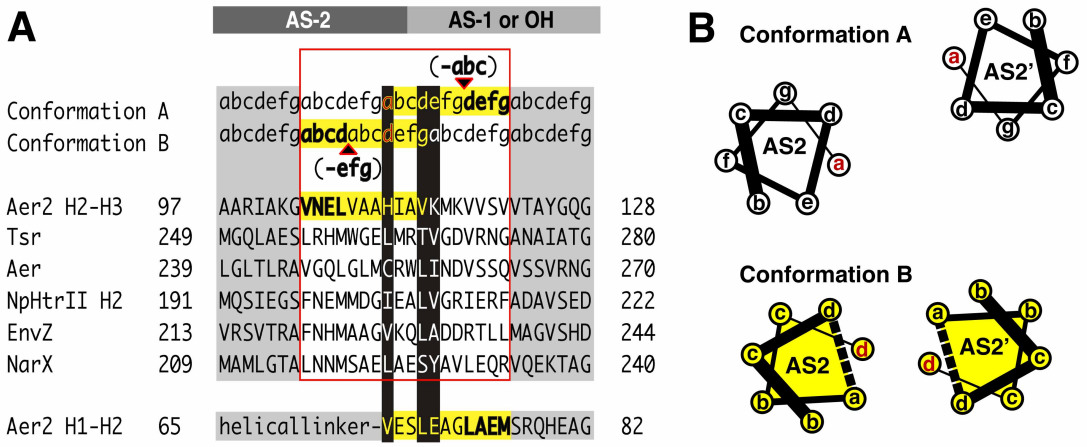

Figure 1.11. Output Mechanism Involving "Stutter Compensation." (A) Model for signal transfer that shifts the position of a stutter on either side of the AS2 junction with AS1 (poly-HAMPs) or output helices (OH) (canonical HAMPs). Helical junctions are shown for representative HAMP domains and Aer2 HAMP 2-3. Stutters (bold) are defined as either an insertion of four residues or a deletion of three residues in the heptad repeat (a-g) and effect adjacent residues (yellow highlight). Residues at the junction switch heptad positions (black highlight) and are compatible with different heptad positions. This model predicts that Aer2 HAMP2 contains a stutter (shown in bold) in AS1 (bottom sequence). Whereas the heptad assignments in HAMP2 AS-1 are as shown, the splayed helices of AS-1 do not generate a true hendecad repeat but do contain an elongated i to i+4 (E66-A70) hydrogen bond distance (3.5 Å) typical of stutters. (B) Helical wheel diagrams of AS2 helices in conformation A (HAMP1/3) and B (HAMP2) highlighting the helical rotation and translation associated with a stutter (dotted line) in AS2.

Despite the AS2 stutter realigning the heptad repeat, it may not stabilize packing of downstream helices because accommodation of the stutter couples both helix rotation and translation to the formation of a kink at the junction of HAMP2/3 (Figure 1.2). Such a kink could alter OH packing and is consistent with the recently proposed "Yin-Yang" mechanism for MCP signaling, where adjacent coiled-coil domains reciprocally influence their helix-helix packing stability (Swain et al., 2009). Notably, in MCPs, a functionally critical Pro residue at the input junction may facilitate a similar helix bending through loss of a mainchain hydrogen bond (Figure 1.5).

1.4 Discussion

A Common Signaling Mechanism

Support for a common signaling mechanism among HAMP domains comes from the fact that HAMP domains from various proteins can be swapped interchangeably to produce functional chimeras (Appleman et al., 2003; Hulko et al., 2006; Zhu and Inouye, 2003). However, signal input into HAMP domains seems to involve several alternative modes of input. In MCPs, which contain a single canonical HAMP domain, ligand binding to a perisplasmic sensing domain generates a piston-like motion in the C-terminal helix that continues through the connecting transmembrane helix (TM2) to the HAMP domain (Falke and Hazelbauer, 2001). For native Tar, ligand binding is negatively cooperative and produces an asymmetric, downward motion of TM2 from one subunit. Nevertheless, Tar does not require an asymmetric signal and functions when the input signal is contrived to be symmetric (Draheim et al., 2005; Miller and Falke, 2004). For the histidine kinase NarX, nitrate binding occurs between the two perisplasmic sensing domains resulting in a symmetric 1 Å, upward shift of the periplasmic C-terminal helices, presumably pulling TM2 upwards (Cheung and Hendrickson, 2009). Domain swapping of the periplasmic domains of Tar and NarX

results in a reverse output, consistent with the opposite displacement of TM2 (Ward et al., 2002).

Signal input to HAMP can also occur in other ways. The TM2 helices of NpHtrII, a phototransducing module from *Natronomonas pharaonis*, undergo a horizontal displacement and rotation upon light excitation (Moukhametzianov et al., 2006; Wegener et al., 2001), and the HAMP domain of Aer receives signal input from side-on interactions with an adjacent PAS domain (Taylor, 2007). In poly-HAMPs, signal input has not been biochemically characterized but most likely occurs through connecting HAMP subunits due to the highly interwoven nature of concatenated HAMPs. In our view, proposed HAMP signaling mechanisms should be consistent with the variable modes of input received by HAMPs.

A Model for HAMP Signal Transduction

The alternate structure of HAMP2 suggests a mode of signal transduction involving a change from an in-register four-helix bundle to a distorted, HAMP2-like structure. Helical displacement and rotation are two known signal inputs into HAMP that could readily shift the equilibrium between states. Both inputs merge into a screw-like motion required to interconvert HAMP conformations. The compatibility of HAMP domains with different signal inputs could be derived from a combination of structural rearrangements between opposing signaling states. The altered heptad pattern at the distal end of AS2 indicates that a HAMP2-like state would deliver a different conformational signal to a C-terminal output domain compared to HAMP1 or HAMP3. The identical heptad discontinuity at the C-terminus of canonical and poly-HAMP domains suggests a shared output mechanism and mode of signal transduction. We propose that canonical and poly-HAMP systems utilize a similar signaling mechanism and convert between the similar conformations of HAMP1, HAMP3, and Af1503 to a conformation resembling HAMP2.

Poly-HAMP Chains

The structure of concatenated HAMPs, as revealed here, raises the interesting mechanistic question of how a signal is propagated through a poly-HAMP chain. Concatenation creates a heptad discontinuity at the junction of HAMP2/3 and forms the basis for a proposed "stutter compensation" mechanism. This model is consistent with the stutters that cause a heptad shift in both AS1 and AS2 of HAMP2. Assuming that, under physiological conditions, HAMPs exhibit a two-state switching mechanism, each HAMP domain would be capable of visiting one of two states: A or B. This model predicts that in poly-HAMP chains, repeating HAMP domains would assume alternating conformations (A-B-A-...) and interconvert in a binary fashion (B-A-B-…) (Figure 1.12). Two additional points support this mechanism. First, the HAMP domains of Aer2 abide by this pattern with HAMP2 and HAMP3 assuming distinct conformations. Second, amplification of poly-HAMPs typically occurs in sets of two (Dunin-Horkawicz, submitted). An alternating mechanism would require the addition of an even number of units to maintain the sign of the signal output. If this is true, any two concatenated HAMP domains would occupy opposing signaling states at a given moment. Consequently, the di-HAMP structure of HAMP2/HAMP3 may provide a snapshot of two HAMP signaling states with reversed signal output.

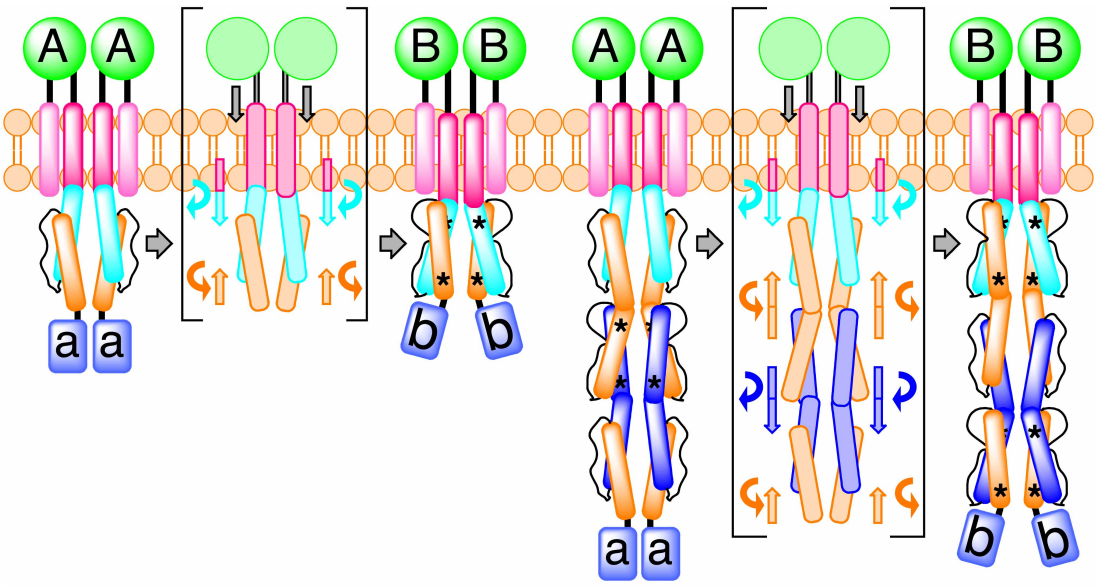

Figure 1.12. Model for HAMP Domain Signal Transduction. Schematic of a ligand dependent, two-state (A and B) HAMP domain signal transduction model highlighting the movement and rotation of helices in a canonical HAMP system and a poly-HAMP system. In the poly-HAMP system successive AS1 helices are contiguous with the preceding AS2 helices. HAMP domain structural rearrangements correspond to a change in helical register, helix-helix crossing angle, and helix rotation. Asterisks denote stutters within HAMP domains. Signal input is shown as a symmetric and downward piston-like displacement of transmembrane helix 2 (TM2), but both an asymmetric displacement or a helical rotation of TM2 would likely lead to the same conformational changes within HAMP domains.

The shared helix and extensive contacts between HAMP2/3 suggest poly-HAMP chains propagate signals through concerted rearrangements. Interconversion between the alternative conformations in our structure results in a displacement and rotation of AS1 and AS2 in opposite directions, consistent with a concerted motion in poly-HAMPs (Figure 1.12) and not unlike the proposed “gearbox” model (Hulko et al., 2006). For homologous Aer2 HAMP2-3 units, the most conserved residues were those involved in interdomain contacts. The presence of Gly residues at the beginning and end of the connector allows for the HAMP2-3 subunits to come close enough together to hydrogen bond. Structurally, these Gly residues differentiate the Aer2 HAMPs from

canonical HAMPs (which contain a DExG motif at the beginning of AS2) (Figure 1.5) and have been identified as common feature of most divergent HAMPs (Dunin-Horkawicz, submitted).

The Gearbox Model

The "gearbox" model is based on the observed x-da packing of Af1503, which has been proposed to convert into knobs into holes packing by a concerted 26° rotation of the helices (Hulko et al., 2006). However, the structures of HAMP1 and HAMP3 do not adhere to the uniform x-da packing modes upon which this model is based, although HAMP1 and HAMP3 produce the same position of the AS2 helices as seen in Af1503. In addition, sequence threading of other HAMP domains indicates that each HAMP sequence would favor a different packing mode to stabilize the same general conformation. Rotation of AS1 and AS2 in HAMP2 compared to HAMP1/3 does reflect an important feature of the gearbox model; however, large helix translations accompany the rotations.

Evidence for a HAMP2 Conformation in Canonical HAMP Domains

Helix-connector interactions distinguish HAMP domains from other four-helix bundles and play important roles in all known HAMP structures. A recent study identified the hydrophobic residues (HR1 and HR2) of the connector motif as critical to HAMP function (Ames et al., 2008). Different sets of these critical residues have prominent roles in stabilizing the alternative structures of our two-state model. In HAMP2, the conserved connector residue HR2 (I88) is the central residue in a hydrophobic pocket formed between the off-register AS1 and AS2 helices. In comparison, the corresponding residue in HAMP1 (V33), HAMP3 (M134), and Af1503 (V303) plays a less prominent role and packs weakly against the four-helix bundle. Thus, the high conservation of HR2 is more easily understood from the role it has in HAMP2, suggesting that other HAMP domains may adopt a conformation

similar to HAMP2. In contrast, HR1 plays a more prominent role in stabilizing the in-register HAMP conformation and directly interacts with an output residue in AS2 whose heptad position may correlate with signal output.

Biochemical studies also provide evidence for a HAMP2-like conformation in canonical HAMP domains. A study aimed at obtaining secondary and tertiary structure information used a library of single cysteine residue substitutions to assay residue proximity in the HAMP domain of the aspartate chemoreceptor Tar (Butler and Falke, 1998). Symmetric disulfide bonds were formed at a significantly faster rate between residues of the AS2 heptad repeat. HAMP domains are highly dynamic (Doebber et al., 2008), and the rapid degree of cross-linking suggests that structural oscillations bring the AS2 helices, but not the AS1 helices, into close proximity, as observed in the HAMP2 conformation. EPR studies of NpHtrII found that the HAMP domain oscillates between two conformations: one resembling the compact Af1503 structure and another corresponding to a more-expanded, solvent exposed conformation (Doebber et al., 2008). The most dynamic region of NpHtrII was the C-terminal region of AS1, an observation consistent with the separation of AS1 from the bundle in the highly trapezoidal structure of HAMP2.

Sequence Divergence

Although canonical and divergent HAMP domains conserve residue types in positions important for bundle formation (hydrophobic residues of the heptad repeat) and connector interactions (G-x-HR1-x-x-x-HR2), sensitive HMM-HMM (Hidden Markov-Models) are needed to recognize many divergent HAMPs (Dunin-Horkawicz, submitted). Thus, canonical and divergent HAMPs may adopt distinct subsets of conformations, and a HAMP2 conformation may only be accessible to divergent HAMPs. Additionally, protein conformations can change due to constraints of the crystal lattices. However, the similar conformations observed between the NMR

structure of Af1503 and the crystal structures of HAMP1 and HAMP3 suggest, at a minimum, that the in-register four-helix bundle is an important signaling state accessible to all HAMP domains. Furthermore, the functional importance of HR2 is best rationalized in the context of the HAMP2 conformation. Also, similar heptad discontinuities at the output helices of canonical and poly-HAMPs suggest that these modules function similarly. It follows that the distorted HAMP2 conformation would represent the opposing low-energy signaling state. Although extrapolation of the Aer2 structure into the functional dynamics of HAMP domains is at this point conjectural, the range of structural oscillation may lie somewhere near or between the two observed conformations.

Global Restructuring

As mentioned before, not all inputs to HAMP need necessarily involve a vertical helix displacement. The rearrangements that relate HAMP2 to HAMP1/3 can best be thought of as a global restructuring of the domain in which vertical helix displacements are coupled to helix rotations, tilts, and repacking of the connector. Any perturbation or interaction that favors the helix positions in one conformation over the other could, in principle, shift the equilibrium between states. In this context, structural perturbations delivered to HAMP could be asymmetric or symmetric, provided they preferentially stabilized one of the signaling states. The extensive subunit contacts displayed by HAMP domains ensures that asymmetric signals convert to a symmetric restructuring of the dimer. These inputs could include varying degrees of helix shifts and rotations, as well as direct side-on interactions from other domains, such as PAS, which is found in Aer-type sensors.

Although not definite, we believe that the HAMP2 conformation is most consistent with the kinase off state in MCPs because: (i) vertical displacement of AS1 would couple to a piston motion of TM2; (ii) the stutter in AS2 would kink and destabilize

the helices of the adaption region, which correlates with a kinase off state (Swain et al., 2009); and (iii) replacement of I241 (HR2) in Tsr with Glycine or a charged residue (D, E, K, R), changes that would destabilize a HAMP2-like state, resulted in a CW-locked (kinase on) phenotype (Ames et al., 2008).

HAMP signaling is known to be bi-directional; compatible with adaptation responses through the methylation of chemoreceptor output bundles (Hazelbauer et al., 2008), as well as the inside-out signaling mechanism of LapD (Newell et al., 2009). The HAMP domains presented here are N-terminal to the PAS domain and not in the linear path from the PAS domain to the downstream signaling domain. However, preliminary evidence indicates that HAMP2 and HAMP3, but not HAMP1, are required for proper Aer2 function (K. Watts, unpublished data). We are actively pursuing this area of research to elucidate HAMP domain function and signaling in the context of soluble receptors.

1.5 Summary

The structure of an N-terminal fragment of the soluble receptor Aer2 has expanded the known examples of accessible HAMP conformations from one to four. HAMP2 represents a novel four-helix bundle and connector arrangement whose unique structure provides the basis for a two-state model of HAMP signaling that involves a complicated set of structural rearrangements. The two conformations we implicate in signaling are distinguished by changes in helical register, crossing angle, rotation, and likely dynamics. The conformational differences are greatest at the C-terminal output region, where the rhombic distortion of HAMP2 is most dramatic. Interconversion would shift a stutter on either side of connecting helical junctions, and could serve as an output mechanism. Moreover, a vertical displacement or rotation of AS1 caused by like movements in preceding N-terminal domains could readily induce the

conformational switch. Overall, complex remodeling of the HAMP domain could be exploited to send signals to C-terminal output domains or through concatenated poly-HAMP chains.

1.6 Materials and Methods

Protein Expression and Purification

HAMP1-3 comprising residues 1-172 of the gene encoding *Pseudomonas aeruginosa* PAO1 Aer2 was cloned into the pET28a vector between NdeI and XhoI restriction sites, which added a cleavable N-terminal His-tag. For overexpression the plasmid was transformed into BL21 (DE3) cells, grown at 37° C in Luria Broth (LB) to an OD_{600} = 0.6 and incubated with 100 mM IPTG at 23° C for 6 hrs before harvesting cells. Protein was purified using a Ni-NTA column following the manufacturers recommended protocol (Qiagen). After thrombin digestion His-tag free protein was applied to a Superdex 75 26-60 Hi-Prep Column equilibrated with 20 mM Tris, pH 7.5, 50 mM NaCl. Concentrated protein was aliquoted, flash frozen, and stored at -80° C.

To generate Se-Met protein, the Aer2 plasmid was transformed into B834 (DE3) cells, which are auxotrophic for methionine. An overnight culture in LB was spun down and washed twice with autoclaved water, then added to M9 minimal media supplemented with 19 standard amino acids and L-selenomethionine (50 mg/L). All Se-Met purification buffers contained 10 mM dithiothreitol (DTT) and Se-Met protein was purified otherwise as described for the native protein.

Crystallization and Data Collection

Crystals of native Aer2 1-172 protein (20 mg/mL) were grown by vapor diffusion against a reservoir containing 1.1 M Li_2SO_4, 15-18% glycerol, and 0.1 M Tris, pH 8.5 overnight at room temperature. Se-Met Aer2 1-172 protein (60 mg/mL) crystallized in

the same space group ($P4_32_12$) against a reservoir of 1.35 M $(NH_4)_2SO_4$, 12-15% glycerol, 0.1 M Tris, pH 8.5. Solutions containing 1.25 M Li_2SO_4 or 1.5 M $(NH_4)_2SO_4$, 18% glycerol, 0.1 M Tris, pH 8.5 were used as cryoprotectants. Native diffraction data were collected at the APS NE-CAT 24-ID-E beamline on an ADSC Quantum 315 CCD. MAD data were collected at the Cornell High Energy Synchrotron Source (CHESS) F2 beamline on an ADSC Quantum 210 CCD. Data were processed with HKL2000 (Otwinowski and Minor, 1997).

Structure Determination and Refinement

Diffraction data for Se-Met protein were processed with SOLVE (Terwilliger and Berendzen, 1999) and RESOLVE (Terwilliger, 2000) to generate initial electron density maps based on anomalous diffraction from Se-Met sites (figure of merit = 0.73, resolution cutoff = 3.42 Å). The structure was built into initial maps with XFIT (McRee, 1999) and then used for refinement against the high resolution native data set (Brunger et al., 1998). Structure refinement was carried out using CNS, amidst cycles of manual model building, minimization, B-factor refinement, and solvent molecule placement to produce the final model (R-factor = 23.7 %, R_{free} = 27.0%) (Table 1.1).

Superposition of HAMP structures

Superpositions of the Aer2 and Af1503 HAMP domains were carried out using (i) Ca atoms of AS1, AS1', AS2, and AS2' helices or (ii) Ca atoms of AS1 and AS1' with both giving similar results. For optimal clarity, all figures are shown from the superposition of AS1 and AS1' Ca atoms.

Threading, Energy Minimization, and Energy Determination

The Rosetta Design program was used to generate and calculate all threaded sequences and their corresponding energy scores. The conformation of each sidechain was determined by sampling all rotamer conformations on a fixed backbone and calculating the corresponding energies of all combinations. The rotamer combination

with the lowest score was taken as the final model and represents the final overall score reported. The Rosetta Design energy function calculates threading scores by evaluating a number of factors. These factors include attractive and repulsive Lennard-Jones potentials, solvation (Lazardis-Karplus solvation model), internal energy of side chain rotamers (from Dunbrack's statistics), intra-residue clashes, salt bridges, phi and psi angles (Ramachandran preferences), hydrogen bonding interactions and void volume of residues (tightness of packing).

Sequence Analysis

Sequence alignment of Aer2, Af1503, Tar, and Aer HAMP domains was generated using ClustalW and manually adjusted as presented. Homologs of Aer2 1-156 (HAMP1-3) and 63-156 (HAMP2-3) were identified using pBLAST against the nr database (non-redundant protein sequences) (Altschul et al., 1997) and returned 132 homologous protein sequences. An alignment of the top 100 sequences homologous to Aer2 63-156 (E-value cutoff = 4×10^{-5}) was generated using ClustalW and used to visualize HAMP2-3 sequence conservation in a WebLogo (Crooks et al., 2004).

Sequence alignment of the AS2/AS1 and AS2/OH junctions of various HAMP proteins was generated using ClustalW. Heptad positions were determined using the program TWISTER (Strelkov and Burkhard, 2002). TWISTER first assigns the heptad positions "a" and "d" based on orientation relative to the supercoil axis. Remaining positions are determined based on these initial assignments.

Solvent Exposure

Solvent exposures of each HAMP domain were calculated using the CCP4 program AREAIMOL, which determines the solvent accessibility of all atoms in a protein structure based on proximity to neighboring atoms and summarizes the data per residue.

REFERENCES

Altschul, S.F., Madden, T.L., Schaffer, A.A., Zhang, J.H., Zhang, Z., Miller, W., and Lipman, D.J. (1997). Gapped BLAST and PSI-BLAST: a new generation of protein database search programs. Nucleic Acids Research *25*, 3389-3402.

Ambroggio, X.I., and Kuhlman, B. (2006). Design of protein conformational switches. Current Opinion in Structural Biology *16*, 525-530.

Ames, P., Zhou, Q., and Parkinson, J.S. (2008). Mutational analysis of the connector segment in the HAMP domain of Tsr, the Escherichia coli serine chemoreceptor. Journal of Bacteriology *190*, 6676-6685.

Appleman, J.A., Chen, L.L., and Stewart, V. (2003). Probing conservation of HAMP linker structure and signal transduction mechanism through analysis of hybrid sensor kinases. Journal of Bacteriology *185*, 4872-4882.

Aravind, L., and Ponting, C.P. (1999). The cytoplasmic helical linker domain of receptor histidine kinase and methyl-accepting proteins is common to many prokaryotic signalling proteins. Fems Microbiology Letters *176*, 111-116.

Brunger, A.T., Adams, P.D., Clore, G.M., DeLano, W.L., Gros, P., Grosse-Kunstleve, R.W., Jiang, J.S., Kuszewski, J., Nilges, M., Pannu, N.S.*, et al.* (1998). Crystallography & NMR system: A new software suite for macromolecular structure determination. Acta Crystallographica Section D-Biological Crystallography *54*, 905-921.

Butler, S.L., and Falke, J.J. (1998). Cysteine and disulfide scanning reveals two amphiphilic helices in the linker region of the aspartate chemoreceptor. Biochemistry *37*, 10746-10756.

Cheung, J., and Hendrickson, W.A. (2009). Structural Analysis of Ligand Stimulation of the Histidine Kinase NarX. Structure *17*, 190-201.

Crooks, G.E., Hon, G., Chandonia, J.M., and Brenner, S.E. (2004). WebLogo: A sequence logo generator. Genome Research *14*, 1188-1190.

Das, R., and Baker, D. (2008). Macromolecular modeling with Rosetta. Annual Review of Biochemistry *77*, 363-382.

Doebber, M., Bordignon, E., Klare, J.P., Holterhues, J., Martell, S., Mennes, N., Li, L., Engelhard, M., and Steinhoff, H.J. (2008). Salt-driven equilibrium between two conformations in the HAMP domain from Natronomonas pharaonis - The language of signal transfer? Journal of Biological Chemistry *283*, 28691-28701.

Draheim, R.R., Bormans, A.F., Lai, R.Z., and Manson, M.D. (2005). Tryptophan residues flanking the second transmembrane helix (TM2) set the signaling state of the Tar chemoreceptor. Biochemistry *44*, 1268-1277.

Falke, J.J., and Hazelbauer, G.L. (2001). Transmembrane signaling in bacterial chemoreceptors. Trends in Biochemical Sciences *26*, 257-265.

Hazelbauer, G.L., Falke, J.J., and Parkinson, J.S. (2008). Bacterial chemoreceptors: high-performance signaling in networked arrays. Trends in Biochemical Sciences *33*, 9-19.

Hong, C.S., Shitashiro, M., Kuroda, A., Ikeda, T., Takiguchi, N., Ohtake, H., and Kato, J. (2004). Chemotaxis proteins and transducers for aerotaxis in Pseudomonas aeruginosa. Fems Microbiology Letters *231*, 247-252.

Hulko, M., Berndt, F., Gruber, M., Linder, J.U., Truffault, V., Schultz, A., Martin, J., Schultz, J.E., Lupas, A.N., and Coles, M. (2006). The HAMP domain structure implies helix rotation in transmembrane signaling. Cell *126*, 929-940.

Khursigara, C.M., Wu, X.W., Zhang, P.J., Lefman, J., and Subramaniam, S. (2008). Role of HAMP domains in chemotaxis signaling by bacterial chemoreceptors. Proceedings of the National Academy of Sciences of the United States of America *105*, 16555-16560.

Lupas, A.N., and Gruber, M. (2005). The structure of alpha-helical coiled coils. Fibrous Proteins: Coiled-Coils, Collagen and Elastomers *70*, 37-+.

McRee, D.E. (1999). XtalView Xfit - A versatile program for manipulating atomic coordinates and electron density. Journal of Structural Biology *125*, 156-165.

Miller, A.S., and Falke, J.J. (2004). Side chains at the membrane-water interface modulate the signaling state of a transmembrane receptor. Biochemistry *43*, 1763-1770.

Moukhametzianov, R., Klare, J.P., Efremov, R., Baeken, C., Goppner, A., Labahn, J., Engelhard, M., Buldt, G., and Gordeliy, V.I. (2006). Development of the signal in sensory rhodopsin and its transfer to the cognate transducer. Nature *440*, 115-119.

Newell, P.D., Monds, R.D., and O'Toole, G.A. (2009). LapD is a bis-(3 ',5 ')-cyclic dimeric GMP-binding protein that regulates surface attachment by Pseudomonas fluorescens Pf0-1. Proceedings of the National Academy of Sciences of the United States of America *106*, 3461-3466.

Otwinowski, Z., and Minor, W. (1997). Processing of X-ray diffraction data collected in oscillation mode. Macromolecular Crystallography, Pt A *276*, 307-326.

Stewart, V., and Chen, L.L. (2009). The S helix mediates signal transmission as a HAMP domain coiled-coil extension in the NarX nitrate sensor from Escherichia coil K-12. Journal of Bacteriology *Published online 4 December 2009*.

Strelkov, S.V., and Burkhard, P. (2002). Analysis of alpha-helical coiled coils with the program TWISTER reveals a structural mechanism for stutter compensation. Journal of Structural Biology *137*, 54-64.

Swain, K.E., and Falke, J.J. (2007). Structure of the conserved HAMP domain in an intact, membrane-bound chemoreceptor: A disulfide mapping study. Biochemistry *46*, 13684-13695.

Swain, K.E., Gonzalez, M.A., and Falke, J.J. (2009). Engineered Socket Study of Signaling through a Four-Helix Bundle: Evidence for a Yin-Yang Mechanism in the Kinase Control Module of the Aspartate Receptor. Biochemistry *48*, 9266-9277.

Szurmant, H., White, R.A., and Hoch, J.A. (2007). Sensor complexes regulating two-component signal transduction. Current Opinion in Structural Biology *17*, 706-715.

Taylor, B.L. (2007). Aer on the inside looking out: paradigm for a PAS-HAMP role in sensing oxygen, redox and energy. Molecular Microbiology *65*, 1415-1424.

Terwilliger, T.C. (2000). Maximum-likelihood density modification. Acta Crystallographica Section D-Biological Crystallography *56*, 965-972.

Terwilliger, T.C., and Berendzen, J. (1999). Automated MAD and MIR structure solution. Acta Crystallographica Section D-Biological Crystallography *55*, 849-861.

Ward, S.M., Delgado, A., Gunsalus, R.P., and Manson, M.D. (2002). A NarX-Tar chimera mediates repellent chemotaxis to nitrate and nitrite. Molecular Microbiology *44*, 709-719.

Watts, K.J., Johnson, M.S., and Taylor, B.L. (2008). Structure-function relationships in the HAMP and proximal signaling domains of the aerotaxis receptor Aer. Journal of Bacteriology *190*, 2118-2127.

Wegener, A.A., Klare, J.P., Engelhard, M., and Steinhoff, H.J. (2001). Structural insights into the early steps of receptor-transducer signal transfer in archaeal phototaxis. Embo Journal *20*, 5312-5319.

Yan, Y., Winograd, E., Viel, A., Cronin, T., Harrison, S.C., and Branton, D. (1993). Crystal-Structure of teh Repetitive Segments of Spectrin. Science *262*, 2027-2030.

Zhou, Q., Ames, P., and Parkinson, J.S. (2009). Mutational analyses of HAMP helices suggest a dynamic bundle model of input-output signalling in chemoreceptors. Mol Microbiol *73*, 801-814.

Zhu, Y., and Inouye, M. (2003). Analysis of the role of the EnvZ linker region in signal transduction using a chimeric Tar/EnvZ receptor protein, Tez1. Journal of Biological Chemistry *278*, 22812-22819.

CHAPTER 2

Heme Binding to the Mammalian Circadian Clock Protein Period 2 is Non-Specific[2]

2.1 Abstract

The mammalian circadian clock synchronizes physical and metabolic activity with the diurnal cycle through a transcriptional-posttranslational feedback loop. An additional feedback mechanism regulating clock timing has been proposed to involve oscillation in heme availability. Period 2 (PER2), an integral component in the negative feedback loop that establishes circadian rhythms in mammals, has been identified as a heme binding protein. However, the majority of evidence for heme binding is based upon in vitro heme binding assays. We sought to ascertain if these largely spectral assays could distinguish between specific and non-specific heme interactions. Heme binding properties by a number of other well-characterized proteins, all with no known biological role involving heme interaction, corresponded to those displayed by PER2. Site-directed mutants of putative heme-binding residues identified by MCD were unable to locate a specific heme-binding site on PER2. Protein film electrochemistry also indicates that heme binds PER2 non-specifically on the protein surface. Our results establish the inability of typical in vitro assays to easily distinguish between specific and non-specific heme binding. We conclude that heme binding to PER2 is likely to be non-specific and does not involve the hydrophobic pocket within the PER2 PAS domains that in other PAS proteins commonly recognizes cofactors. These

[2] Reproduced with permission from *Biochemistry*, Apr 22 (Epub date), *Just Accepted*, Airola, M.V., Du, J, Dawson, J.H., and Crane, B.R., "Heme Binding to the Mammalian Circadian Clock Protein Period 2 is Non-Specific", Copyright 2010 American Chemical Society

findings also question the significance of in vivo studies that implicate heme interactions with the clock proteins PER2 and nPAS2 in biological function.

2.2 Introduction

In mammals, physical and metabolic activity is synchronized with the diurnal cycle by the circadian clock (Harms et al., 2004; Lowrey and Takahashi, 2004; Reppert and Weaver, 2002; Young and Kay, 2001). The clock acts as a gestalt, where the interactions of a few core clock gene products result in a remarkably precise molecular timepiece. The basic mechanism of the clock involves two transcriptional activators, CLOCK and bMAL1, whose activity oscillates over a twenty-four hour cycle. Heterodimerization of CLOCK and bMAL1 initiates the transcription of various clock controlled genes (CCGs) as well as two sets of core clock genes: period (per1, per2, and per3) and cryptochrome (cry1 and cry2) (Harms et al., 2004; Lowrey and Takahashi, 2004; Reppert and Weaver, 2002; Young and Kay, 2001). Time is set by a delayed transcriptional and post-translational feedback loop dependent on the cellular location and levels of the Period (PER1 and PER2) and Cryptochrome (CRY1 and CRY2) proteins. After transcription of per and cry genes is initiated, their corresponding proteins begin to accumulate in the cytoplasm and eventually translocate into the nucleus where they inhibit transcriptional activity of the CLOCK/bMAL1 complex. Consequently, transcription of the per and cry genes halts, ultimately decreasing the levels of PER and CRY low enough to restore activity to the CLOCK/bMAL1 complex, thereby starting the cycle anew.

A large number of clock genes contain PAS domains that sustain the clock through protein-protein interactions (Hennig et al., 2009; Reppert and Weaver, 2002; Young and Kay, 2001). The PAS domain is a common protein fold present in almost every division of life. They often function as sensory domains regulating the activity of an

attached catalytic domain or an intermolecular partner. A variety of cofactors have been identified to bind inside the hydrophobic pocket of different PAS domains enabling a diverse set of signals to be sensed and relayed. For example, the bacterial protein FixL exploits a heme functional group to respond to oxygen depletion, modulating the activity of a downstream histidine kinase domain (Gillesgonzalez and Gonzalez, 1993). Alternatively, the fungal photoreceptor Vivid (VVD) utilizes an FAD molecule to synchronize metabolic activity to changing levels in blue light (Zoltowski et al., 2007).

In addition to binding cofactors, some PAS domains participate primarily in protein-protein interactions. The PAS domains of the mammalian clock protein PER2 fall into this class with the recent crystal structure lacking any bound cofactors (Hennig et al., 2009). Another member is the Drosophila melanogaster clock protein Period (dPER) which contains two PAS domains, both devoid of a cofactor. dPER's role in signal transduction appears to involve a change in dimerization between homodimerization and heterodimerization with the Drosophila Timeless clock protein (Hennig et al., 2009; Yildiz et al., 2005). A further example is the aryl hydrocarbon receptor nuclear translocator (ARNT), a basic helix-loop-helix (bHLH)/PAS protein that forms heterodimeric transcriptional complexes with other bHLH/PAS proteins (Kewley et al., 2004). ARNT complex formation with aryl hydrocarbon receptor (AhR) is mediated by ligand binding by AhR. However, complex formation with hypoxia inducible factor alpha (HIF-a) has analogy to clock protein interactions, being dependent on protein localization and degradation (Kewley et al., 2004). It is unclear if these apo-PAS domains require cofactors for function in vivo (Erbel et al., 2003; Scheuermann et al., 2009) but their increasing representation within the PAS family suggests signaling mechanisms independent of any cofactor. In keeping with this,

many PAS domains overexpressed in E. coli do not purify with a bound cofactor (Erbel et al., 2003; Hennig et al., 2009; Morais Cabral et al., 1998; Yildiz et al., 2005).

Recent evidence has implicated that heme participates in a feedback loop that regulates the circadian clock. Heme addition is capable of synchronizing gene expression in NIH (3T3) cells (Kaasik and Lee, 2004). In turn, the clock controls transcription of d-aminolevulinate synthase 1 (ALAS1), the rate-limiting enzyme for heme biosynthesis (Panda et al., 2002; Zheng et al., 2001). Furthermore, core clock components have been identified as heme binding proteins. Neuronal PAS domain protein 2 (nPAS2), a transcription factor homologous to CLOCK, has been shown to bind heme through its PAS domains and function as a gas-based sensor (Dioum et al., 2002; Koudo et al., 2005; Mukaiyama et al., 2006). PER2 has also been shown to bind heme through its PAS domains (Kaasik and Lee, 2004; Kitanishi et al., 2008) and a downstream region of the protein that contains a putative novel heme-binding motif (Yang et al., 2008). Because of these interactions, heme has been suggested to modulate the activity of nPAS2 and the stability of PER2 (Kitanishi et al., 2008; Yang et al., 2008). In addition, heme is the ligand for the nuclear steroid receptor REV-Erba, a crucial element of the clock that regulates transcription of bMAL1 (Raghuram et al., 2007; Yin et al., 2007). Thus binding of heme to clock proteins could generate a feedback mechanism where the clock controls levels of heme through ALAS1 expression and heme reciprocally regulates clock proteins by directly affecting their activity and stability.

To address the role of heme in the regulation of the circadian clock we tested the hypothesis that the PAS domains of PER2 bind heme. In agreement with a previous study (Kitanishi et al., 2008) we found that PER2 is capable of binding heme through its PAS domains. However, site-directed mutational analysis was unable to disrupt binding of heme to PER2 in any significant way. Heme is a hydrophobic molecule that

is known to aggregate in aqueous solution and require detergents to maintain monodispersity (Brown et al., 1970; Travascio et al., 1998). This led us to test if heme was binding to PER2 in a non-specific manner due to hydrophobic and general ligand interactions. As a control, heme binding to well characterized proteins, encompassing a breadth of functionalities, was assayed. None of these proteins utilize a heme moiety in vivo but surprisingly all were found to bind heme in vitro in a manner comparative to PER2 and nPAS2. Our data suggests that the observed spectral changes reported for PER2 and nPAS2 are due to non-specific binding of heme to hydrophobic patches and exposed ligands on the surface of these proteins.

2.3 Materials and Methods

Cloning, Expression, and Purification. mPER2 DNA fragments encoding for amino acids 1-506, 1-320, 972-1257 were PCR amplified and cloned into pET28 using NdeI or NheI and XhoI restriction sites. mPER2 mutants were generated using the QuikChange Site-Directed Mutagenesis Kit (Stratagene). All clones were confirmed by complete nucleotide sequencing. For overexpression of His-tagged PER2 proteins, plasmids were transformed into BL21 (DE3) cells. An overnight culture was used to inoculate 2 L of Luria Broth (LB). Cells were grown at 37 °C to an OD600 = 0.4 and then the temperature was reduced to 18 °C. After 1 hr at 18 °C (OD600 = 0.8 -1.0) protein expression was induced with addition of 100 mM IPTG. Cells were harvested by centrifugation 20 hrs after induction and cell pellets were stored at -80 °C. All PER2 proteins were purified using standard metal affinity chromatography procedures. All protein buffers contained either 1-2 mM DTT or 0.5-1 mM TCEP to prevent disulfide formation. Overnight digestion with thrombin produced His-Tag free protein as assessed by SDS-PAGE. To remove soluble aggregates all proteins were further purified by size exclusion chromatography on a Superdex 200 26-60 Hi-Prep

Column. YqeH, CheA, and YtvA were purified as previously described (Bilwes et al., 1999; Moglich and Moffat, 2007; Sudhamsu et al., 2008). Incorporation of heme into purified protein was accomplished by incubation of a slight molar excess of hemin solution to PER2 proteins. The resulting solution was desalted on a Biorad 10-DG desalting column to remove excess heme. The heme precursor, d-levulinic acid, was also added to E. coli cells harboring the PER2 plasmid at the time of induction, but did not result in any heme incorporation into PER2.

Cysteine Modification. A protein sample of PER2 129-506 (1mM) was incubated with 3mM TCEP for 1 hour to ensure reduction of all cysteine residues. Reduced protein was incubated with 20 mM iodoacetamide for 30 min in Tris buffer, pH 8.0, 150 mM NaCl. The reaction was quenched with a 5-fold excess of DTT. Protein was desalted and further purified by gel filtration.

UV-Visible Absorption Spectroscopy. Absorption spectra for mPER2 (1-506) and PAS A were recorded at 25 °C in stoppered quartz cuvettes with an Agilent 8453 UV-Visible Absorption Spectrophotometer. Ferric samples were prepared in an anaerobic glovebox by diluting concentrated protein in previously degassed sample buffer. Subsequent treatment with dithionite produced the ferrous species.

Magnetic Circular Dichroism Spectroscopy. MCD spectra were measured with a magnetic field strength of 1.41 T by using a JASCO J815 Spectropolarimeter. This instrument was equipped with a JASCO MCD-1B electromagnet and interfaced with a Silicon Solutions PC through a JASCO IF-815-2 interface unit. All spectral measurements for PAS A were carried out with a 0.2-cm quartz cuvette at 4 °C. Ferric samples were prepared by diluting concentrated protein into previously degassed sample buffer. Complete reduction of the heme iron was accomplished by adding a few microliters of concentrated sodium dithionite solution (25 mg/ml H2O) with a microliter syringe. Ferrous-CO adducts were prepared by bubbling CO gas into the

ferrous PAS A samples. UV-Visible absorption spectra were recorded with a Cary 400 Spectrophotometer interfaced to a Dell PC before and after the MCD measurements to verify sample integrity.

Heme Titration Assay. Hemin-Cl (sigma) was resuspended in 0.01 M NaOH, filtered using a 0.1-micron filter and diluted with 100 mM Tris, pH 7.5, 100 mM NaCl to generate a dilute heme solution. Purified protein was titrated stepwise into heme solution and thoroughly mixed. Spectra were recorded after each protein addition. The heme solution was pretreated with dithionite to generate ferrous heme. Titrations with ferrous heme were carried out with degassed solutions, under anaerobic conditions, in stoppered cuvettes. Direct calculation of binding constants was complicated by the presence of multiple heme-binding sites that varied depending on the protein studied. To determine a comparable value for binding affinity we calculated heme absorption 50% (HA50) values by taking the ratio of protein concentration to heme concentration at half the maximum absorbance change. All titrations were carried out with a similar heme concentration ranging from 3.2 – 4.5 mM, except for PER2 (1-506), where the titration employed 10 mM heme.

Heme Dissociation Kinetics. Hemin loss was measured using the H64Y/V68F apomyoglobin assay described by Hargove et. al. (Hargrove et al., 1994). Purified proteins were pre-equilibrated with hemin in a 5 to 1 molar ratio. The reaction was measured as an increase in absorbance at 410 nm or 600 nm (for YtvA 600 nm was chosen because of the interfering absorption from the flavin cofactor at 410 nm) upon addition of 6 fold molar excess of apomyoglobin H64Y/V68F to the protein of interest. Measurements were carried out with an Agilent 8453 UV-Visible Absorption Spectrophotometer at 25 °C and in 0.2 M Na Phosphate, pH 7.0, 0.45 M Sucrose buffer. Rate constants were calculated by fitting the data to either single and bi-

exponential decay functions with Mathematica 7.0. The reported values are the average of three independent experiments.

Electrochemistry. Glassy carbon electrodes were polished using 0.3 mm alumina slurry and repeatedly sonicated in water to remove excess alumina. Protein or heme solutions were applied to the electrode surface and incubated for 1 min to allow for adhesion. Cyclic voltammetry was performed using a CH Instruments Model 630B potentiostat, a saturated calomel reference electrode (SCE), a platinum wire as a counter electrode, and 10 mM NaCl, as a supporting electrolyte. Buffer solutions were purged with nitrogen to remove oxygen prior to the beginning of experiments.

2.4 Results

Heme Binds to the PAS Domains of PER2. To investigate the potential role of heme interaction with PER2 in regulating the mammalian circadian clock we carried out a biochemical characterization of the PAS domains of PER2 with respect to heme binding. A truncated fragment of PER2 (1-506), containing both PAS A and B, was overexpressed in E. coli BL21 (DE3) cells in LB media. Purified protein did not contain any detectable amounts of heme or any other cofactors. To ensure the availability of heme during overexpression the heme precursor 5-aminolevulinic acid (δ-ALA) was added to the growth media, however; this also did not result in any heme incorporation into PER2.

To test whether PER2 was capable of binding heme in vitro, protein and cofactor were incubated together and run on a Superdex 200 (H26-60) size exclusion column. Heme coeluted with all PER2 fragments that contained the PAS domains thereby confirming that PER2 has the capacity to bind heme. Vitamin B12 has been reported to compete with heme in binding to the PAS domains of PER2 (Kaasik and Lee, 2004). Our size-exclusion assay indicated Vitamin B12 does not bind to PER2 (1-

506). As a control, FAD, a common cofactor found in other PAS domains, was tested and found also not to bind to PER2 (1-506).

Heme binding by PER2 was characterized using UV-Visible absorption spectroscopy. The PER2-heme complex displayed a Soret peak at 424 nm with broad a/b peaks at 572 nm and 548 nm. Reduction with dithionite shifted the Soret peak to 426 nm with a/b peaks at 560 and 530 nm (Figure 2.1A). A truncated form of PER2 (1-320) containing only the PAS A domain had a similar spectrum to PER2 (1-506) for both ferric and ferrous states (Figure 2.1B). However, PAS A had a reduced capacity for heme binding (1 to 1 molar ratio of protein to heme in Figure 2.1B) compared to PER2 (1-506) (1 to 2 molar ratio of protein to heme in Figure 2.1A)) demonstrating PAS A alone cannot account for all of the heme binding in PER2 (1-506). These results indicate that heme is low-spin hexacoordinate when bound to both PAS A (1-320) and PER2 (1-506). All spectra were identical to those previously reported for the PAS domains of PER2 and nPAS2, suggesting heme is bound in a similar fashion to that observed in those studies (Dioum et al., 2002; Kitanishi et al., 2008; Koudo et al., 2005; Mukaiyama et al., 2006; Yang et al., 2008).

Size-Exclusion Chromatography. To determine the oligomeric state of the PAS domains of PER2, both purified PER2 (1-506) and PAS A were individually applied to a Superdex 200 column. Both PER2 (1-506) and PAS A eluted at volumes consistent with the formation of a dimer, with apparent molecular weights (MWs) of 150 kDa (actual MW = 56 kDa) and 95 kDa (actual MW = 35 kDa). The elution volume of PER2 (1-506) was identical in the absence and presence of heme indicating no change in oligomeric state upon initial heme binding (Figure 2.2). Prolonged incubation of heme with PER2 formed higher order PER2 oligomers due to enhanced cysteine oxidation and formation of inter-PER2 disulfide bonds. Incubation in an

anaerobic environment in the presence of reducing agents prevented disulfide formation and did not lead to higher order oligomerization.

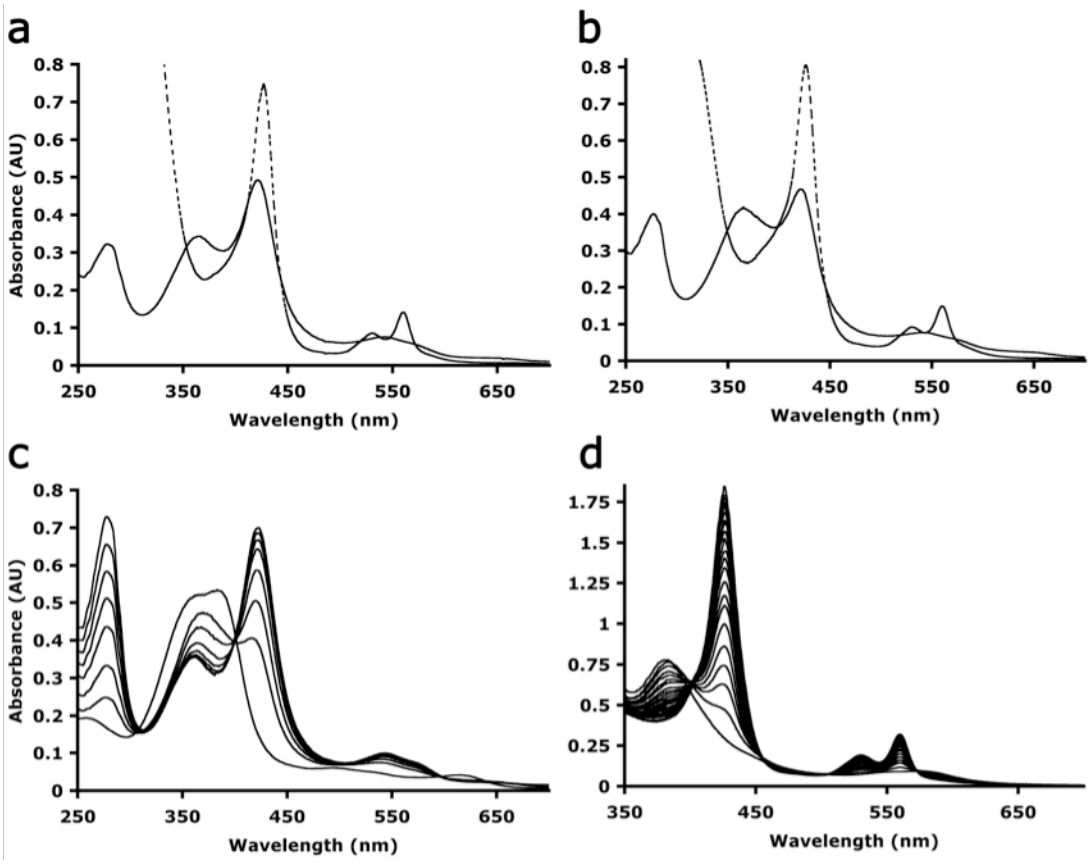

Figure 2.1. PER2 binds heme in a manner dependent on redox state. (A) UV-Visible absorption spectra of PER2 (1-506) reconstituted with heme (5 mM, pH 7.5) before (------) and after (- - -) treatment with dithionite. (B) UV-Visible absorption spectra of PAS A [PER2 (1-320)] reconstituted with heme (4 mM, pH 7.5) before and after treatment with dithionite. (C) Titration of ferric heme (10 mM) with PER2 (1-506) (1.5, 3, 5, 6.5, 8, 9.5, 11 mM). (D) Titration of ferrous heme (10 mM) with PER2 (1-506) (2.1, 4.2, 6.3, 8.4, 10.5, 12.6, 14.7, 16.8, 19.0, 21.1, 23.2, 25.3, 27.4, 29.5, 31.6, 33.7, 35.8, 37.9, 40.0, 43.9, 47.8, 59.5 mM).

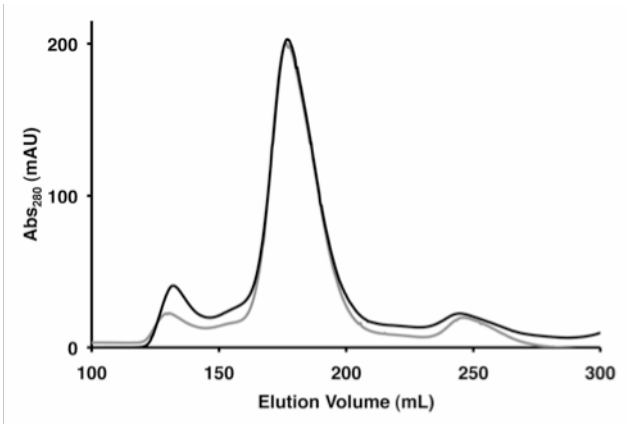

Figure 2.2. Heme Binding Does Not Effect the Oligomeric State of PER2. The elution profiles of PER2 (1-506) with heme bound (black) and without heme bound (grey) are identical and indicate PER2 (1-506) forms a dimer with an apparent MW = 150 kDa (actual MW = 56 kDa).

MCD Identification of Axial Ligands for PAS A in Ferric and Ferrous Forms.

Magnetic circular dichroism (MCD) spectroscopy is a useful method for determining heme coordination modes as it can identify the ligands (number and type), spin state, and oxidation state of the heme center (Cheek, 2000). MCD spectra can be either positive or negative, providing greater fingerprinting capability in comparison to traditional absorption spectra, which only have positive sign features. We sought to characterize the ligand set for the isolated PAS A domain of PER2 using MCD spectroscopy. The overall shape and peak position of ferric PAS A was very similar to that of imidazole-bound ferric cytochrome P450cam, which is well known to represent hexacoordinate Cys/imidazole ligation (Dawson et al., 1982), as well as the recently reported MCD spectral results on butyl-imidazole bound His60Cys nitrophorin 1 (H60C_NP1) (Vetter, 2009). (Figure 2.3A). This indicates that the ligation state of the ferric heme in PAS A also features His/Cys coordination. Reduction of PAS A with sodium dithionite to ferrous PAS A results in formation of a six coordinate low-spin

complex with MCD spectral characteristics very similar to those of the deoxyferrous H93G myoglobin bis-imidazole adduct (Figure 2.3B), which has nitrogenous ligation in both the proximal and distal sites (Du et al., 2008). Thus, unlike ferric coordination, the ferrous ligation state of PAS A is most likely bis-His. In addition, both ferrous PAS A and PER2 (1-506) are capable of binding carbon monoxide. The MCD spectra of ferrous-CO PAS A were identical to that of myoglobin with CO bound, which indicates that His and not Cys serves as the trans ligand to carbon monoxide in ferrous PAS A (Collman et al., 1976) (Figure 2.3C). We note that MCD in the wavelength range tested does not differentiate bis-His from bis-Met coordination , however; analysis of the mPER2 crystal structure (Hennig et al., 2009) did not indicate the positioning of any two Met residues capable of bis-Met coordination in PAS A or PAS B alone. Furthermore, the identification of His as the trans ligand for the ferrous-CO complex also suggests Met residues are not involved in heme coordination.

Heme Binding by PAS A and Site Directed Mutants. Having established the PAS A ferric and ferrous heme complexes as His-Cys and bis-His coordinated we sought to identify the specific residues acting as axial ligands. PAS A contains six histidine residues and six cysteine residues that could serve as the axial ligands for bound heme. Alignment with FixL, a heme binding PAS domain of known structure, revealed H232 and H238 to most likely serve as the axial ligand for heme given that they hold analogous positions in the alpha C helix of the PAS fold compared to the heme-ligating histidine residue in FixL and ecDOS (Figure 2.4) (Key and Moffat, 2005; Miyatake et al., 2000; Suquet et al., 2005). Each histidine residue in PAS A was individually mutated to an alanine in an effort to disrupt or alter heme binding.

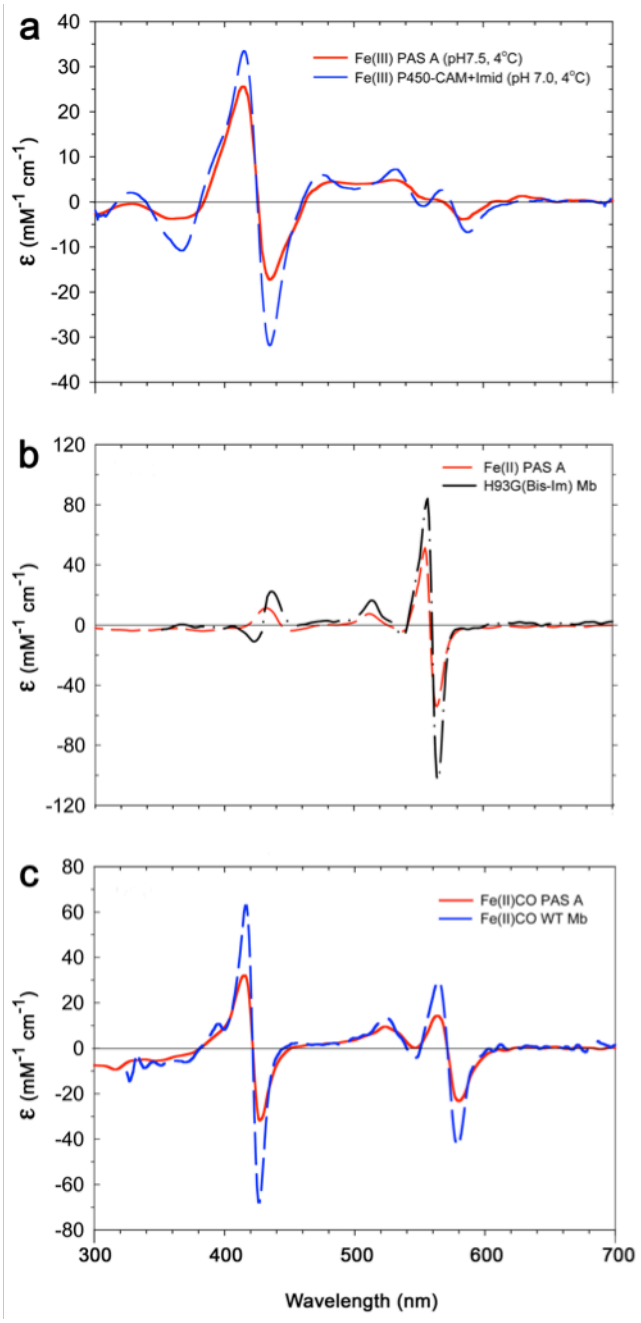

Figure 2.3. Magnetic circular dichroism spectra of ferric PAS A, ferrous PAS A and ferrous-CO PAS A reveal ferric and ferrous hemes are bound through His-Cys and bis-His ligation respectively. A) MCD spectra of ferric PAS A (red) and ferric cytochrome P450-Camphor with imidazole bound (blue). B) MCD spectra of ferrous PAS A (red) and ferrous H93G horse heart myoglobin with bis-imidazole ligation (black). C) MCD spectra of ferrous-CO PAS A (red) and ferrous-CO wild type horse heart myoglobin (blue). All spectra are reported in e(mM-1cm-1) units.

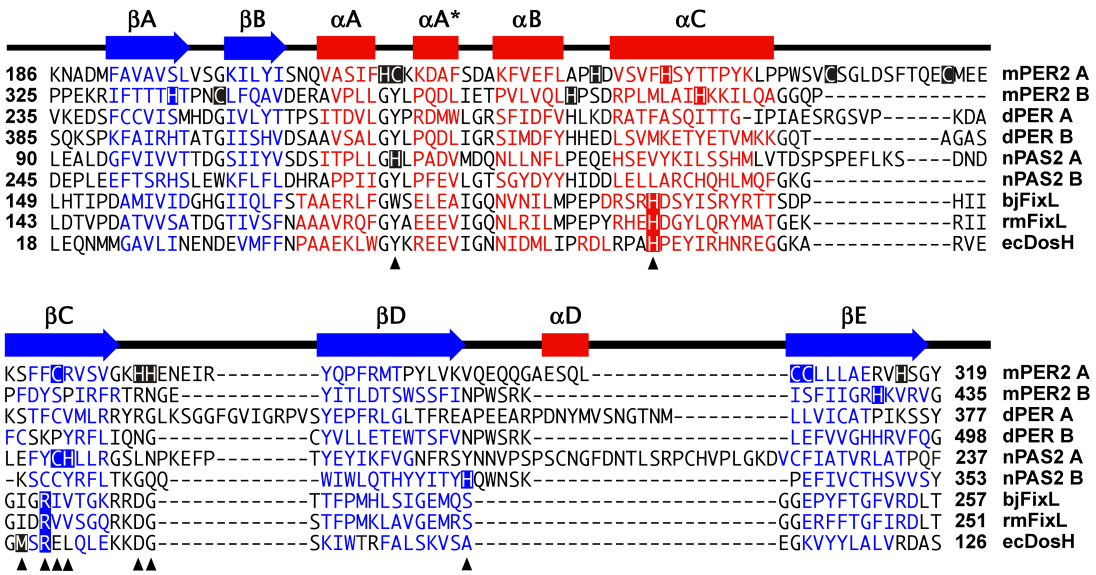

Figure 2.4. Secondary Structure Alignment of mPER2 with other PAS domains. mPER2 (PAS A: 186-319; PAS B: 325-435), dPER (PAS A: 235-377; PAS B: 385-498), nPAS2 (PAS A: 90-237; PAS B: 245-353), bjFixL (149-257), rmFixL (143-251), and ecDOS (18-126). Secondary structure information is derived from mPER2 (3GDI), dPER (1WA9), bjFixL (1DP9), rmFixL (1EW0), ecDOS (1VB6). Jpred3 (Cole et al., 2008) was used to predict the secondary structure of nPAS2. Alpha helices (red) and beta strands (blue) are colored accordingly. All cysteine and histidine residues in mPER2 are highlighted. All residues implicated in heme binding are highlighted and denoted with black triangles below. Alignments were generated with ClustalW and manually adjusted as presented.

Titration experiments were carried out with WT and mutant proteins by addition of purified protein to either free ferric or ferrous heme (Figure 2.1C and 1D). Spectral changes were monitored for a shift in Soret, a/b peaks, as well as for changes in relative binding potency (Table 2.1). We developed a method to measure the relative potency of heme binding that could account for multiple non-specific sites. So called HA50 values were calculated by taking the molar ratio of protein to heme concentration at half the maximum absorbance change in the Soret peak. This allows free heme to be the limiting factor and avoids the open-ended participation of weaker and weaker binding sites at high heme concentrations. Thus HA50 values report on the

average potency of heme binding of a specific protein and are most useful to compare closely related proteins. Changes in HA50 can reflect either changes in stoichiometry, binding affinity, or both. If 2x HA50 < 1, there are multiple sites present with dissociation constants (KD) lower than that of the free heme concentration. With 2xHA50 = 1; one strong binding site is most likely present. With 2xHA50 > 1, one or more sites with KD greater than the free initial heme concentration is present. Binding affinity was found to be redox state dependent for PAS A and PER2 (1-506), with ferric heme having a higher affinity for both proteins in comparison to ferrous heme (Kitanishi et al., 2008). Although H277/278A double mutant displayed a ten-fold reduction in HA50 values for ferrous heme, spectral shapes were identical to that seen in WT. This indicated there must be an alternative binding site involving a nearby histidine residue capable of substituting for H277/278. In addition, the H277/278A mutant showed no change in affinity for ferric heme. Thus, ferric and ferrous hemes preferentially bind to different sites on PAS A. Furthermore, our analysis failed to identify a specific residue responsible for heme binding.

Cysteine Modification Alters Ferric, But Not Ferrous PER2 Spectra. To validate the identity of the ligand set for the ferric and ferrous PER2-heme complexes we conducted heme titrations with PER2 protein modified with Iodoacetimide. Treatment with Iodoacetimide irreversibly modifies solvent exposed cysteine residues to form a thioester (-CH2-S-C(=O)-) but does not modify histidine residues. As expected titration of heme with modified PER2 resulted in altered spectral properties for the ferric (Table 2.1) but not the ferrous heme-PER2 complex (Figure 2.5) confirming Cys as a ligand for ferric heme. In addition, this results indicates that the cysteine residues responsible for heme binding in PER2 are solvent accessible, either located on the surface of PER2 or in buried pocket accessible through solvent channels.

Table 2.1: UV-Visible Absorption and HA50 Values Obtained From Heme Titrations

Protein	Ferric Soret (nm)	Ferric β, α (nm)	Ferrous Soret (nm)	Ferrous β, α (nm)	Ferric HA50	Ferrous HA50
mPER2 1-506 (PAS A/B)	424	548, 572	426	530, 560	0.25	0.61
mPER2 1-320 (PAS A)	424	543, 570	426	530, 560	0.63	1.31
PAS A H214A	424	548, 572	426	530, 560	0.26	2.71
PAS A H232A	422	548, 573	426	531, 560	0.12	0.92
PAS A H238A	425	547, 572	426	529, 559	0.93	4.97
PAS A H277/278A	424	547, 572	426	530, 560	0.60	18.1
PAS A H316A	424	546, 570	426	528, 558	0.76	1.81
mPER2 972-1257	424	543, 573	426	531, 560	1.40	3.42
mPER2 129-506	424	543, 573	426	530, 560	ND	ND
mPER2 129-506 (Cys-MOD)	411	534, 567	426	529, 559	ND	ND
YqeH	409	542, 570	426	531, 560	2.63	4.76
CheAΔ289	NA	NA	426	530, 560	NA	2.72
Δ289 D371C	424	550,573	426	530, 560	6.84	1.80
YtvA	426	548, 572	428	532, 562	0.74	2.41

C-Terminal Domain of PER2 Also Binds Heme. As a control, a C-Terminal fragment of PER2, PER2 (972-1257), with no known functional role for heme binding was assayed with the above mentioned titration method. Surprisingly, titration of free heme with PER2 (972-1257) resulted in identical spectral shifts as seen with the PAS domains of PER2. In addition, heme binding occurred with approximately the same affinity as PER2 (1-506) and PAS A with HA50 values of 1.40 and 3.42 for ferric and ferrous heme (Table 2.1).

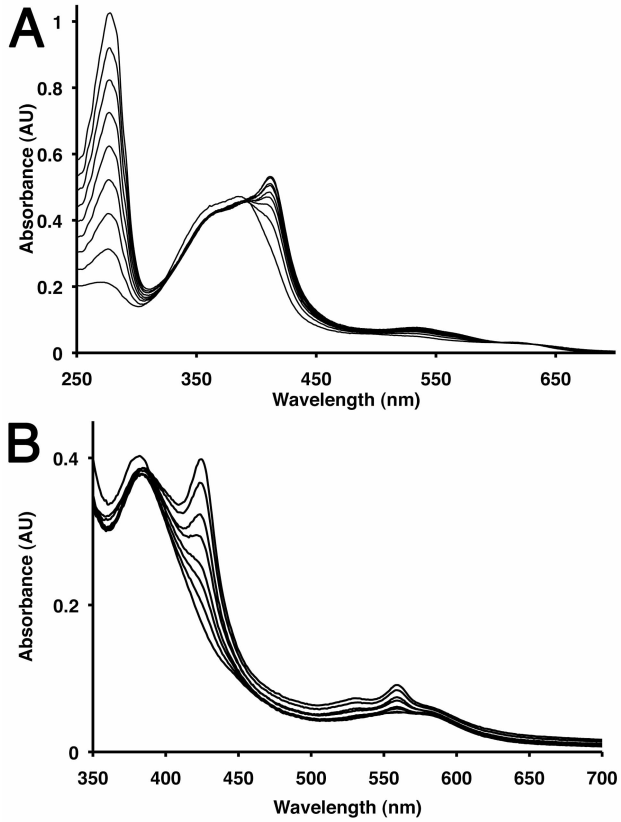

Figure 2.5. Cysteine Modification Alters the Ferric But Not the Ferrous-Heme PER2 Spectra. (A) Titration of ferric heme (8.3 mM) with PER2 (129-506) modified with iodoacetamide (0, 6, 10, 14, 18, 22, 26, 30, 34 mM). Cysteine modification alters the position of the Soret peak shifting it to 410 nm compared to unmodified PER2 with a Soret peak at 422 nm. (B) Titration of ferrous heme (8.3 mM) with PER2 (129-506) modified with iodoacetamide (0, 4.1, 8.2, 12.4, 24.7, 37, 58, 78 mM) with a Soret peak growing in at 426 nm identical to unmodified PER2.

Non-Specific Binding of Heme to Other Proteins. To test if these spectral changes were a specific property of PER2, further titration experiments were conducted with different proteins of various functions. YqeH, a GTPase from G. stearothermophilis, is involved in ribose biogenesis and has no known function related to heme (Sudhamsu et al., 2008). Addition of YqeH to ferric heme produced a Soret band at 409 nm, different from that seen with PER2, but similar to previously reported spectra of PAS A in the presence of the heavy metal mercury (Kitanishi et al., 2008). YqeH contains a

zinc-binding domain that could supply Cys ligands for heme iron coordination and account for the observed spectral differences compared to PER2. Reduction with dithionite shifted the Soret peak to 426 nm with a/b peaks at 560 and 530 nm, identical to that of PER2 and nPAS2 (Kaasik and Lee, 2004; Kitanishi et al., 2008).

Second, the well-characterized histidine kinase CheA from T. maritima was tested for heme binding (Bilwes et al., 1999). A truncated form of CheA (D289) that contains the core dimerization, kinase, and regulatory domains, but lacks cysteine residues was tested for heme binding. Interestingly, titration of ferric heme with D289 did not produce any change in peak shape but did decrease the extinction coefficient of free heme at the absorbance maximum (Figure 2.6A). However, spectral shifts identical to PER2 and YqeH were seen when D289 was added to ferrous heme (Figure 2.6B). D289 titration results demonstrate that cysteine is not required for binding ferrous heme but is required to produce the characteristic spectral changes with ferric heme.

In an attempt to induce the spectral changes in CheA observed on addition of PER2 to ferric heme, a non-native cysteine was introduced at a solvent exposed surface residue of CheA D289 (D289-D371C). The addition of D289-D371C to ferric heme produced a shoulder on the Soret peak at longer wavelength (Figure 2.6C). Difference spectra identified this shoulder as a Soret peak growing in at 424 nm, matching the heme binding signal observed for PER2 (Figure 2.6D). Thus, addition of a non-native surface cysteine residue produced spectral changes identical to PER2 but did so with a much lower binding affinity.

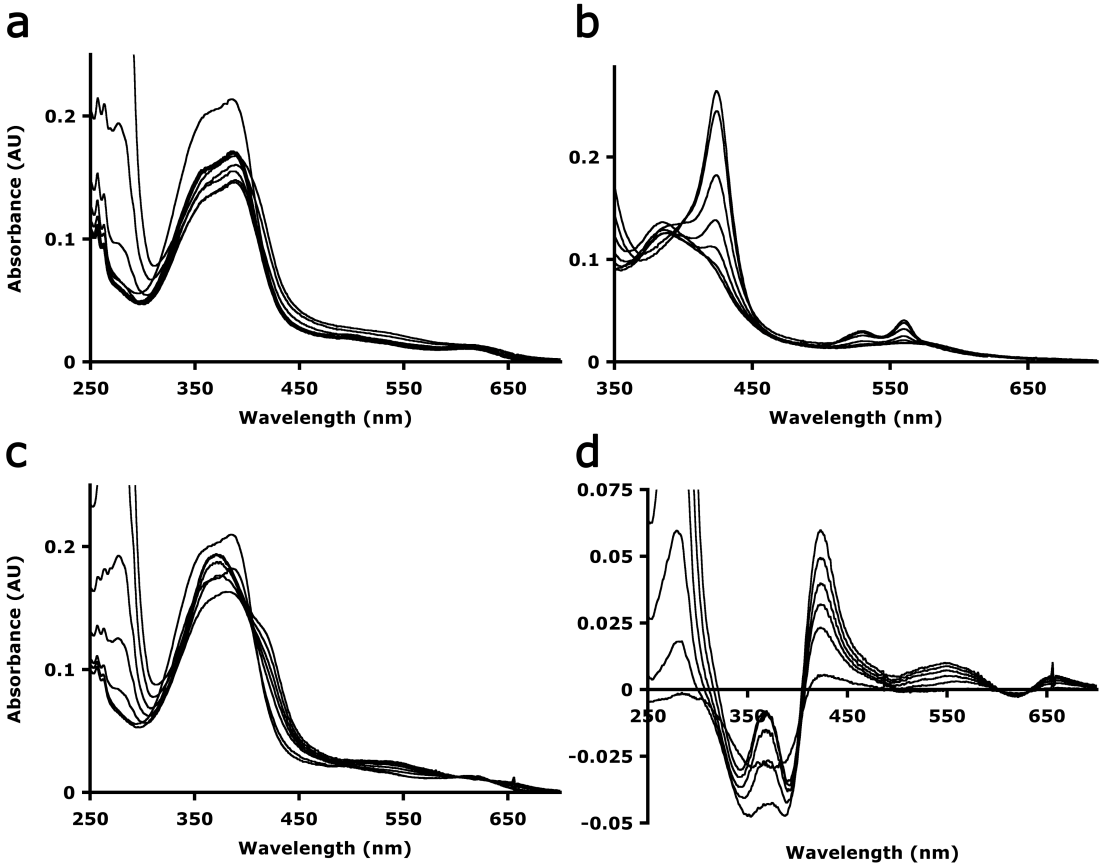

Figure 2.6. Heme binds to the chemotaxis kinase CheA. (A) Titration of ferric heme (4 mM) with CheA (0, 0.23, 0.45, 1.1, 3.5, 11.6, 35 mM). (B) Titration of ferrous heme (4 mM) with CheA (0, 0.45, 2.3, 5.8, 11.6, 23, 46.5 mM). (C) Titration of ferric heme (4 mM) with CheA D371C variant (0, 0.5, 2.5, 6.4, 12.8, 25, 45 mM). (D) Difference spectra from panel C.

PAS domains, such as PER2, typically bind cofactors in a pocket primarily formed by the central b-sheet, the aB and aC helices, and the aB-aC loop (Gilles-Gonzalez and Gonzalez, 2005). YtvA is a PAS domain protein that binds flavin mononucleotide (FMN) in this pocket (Moglich and Moffat, 2007). Since YtvA contains a native cofactor we sought to test whether YtvA could also bind heme while still maintaining FMN in its binding pocket. YtvA was first photobleached to maintain a constant FMN absorbance and induce a covalent link between the cofactor and protein (Moglich and

Moffat, 2007). Titration experiments were carried out with both ferric and ferrous heme. After subtraction of the absorbance due to FMN the resulting ferric and ferrous spectra were found to be identical to PER2 (Figure 2.7). The binding affinity of heme to YtvA was comparable to that of PER2 (1-506) and PAS A with HA50 values of 0.74 and 2.41 for ferric and ferrous heme respectively (Table 2.1). Due to the presence of covalently bound FMN, heme cannot bind in the hydrophobic pocket of the YtvA PAS domain and must therefore be interacting with residues on the surface of the protein.

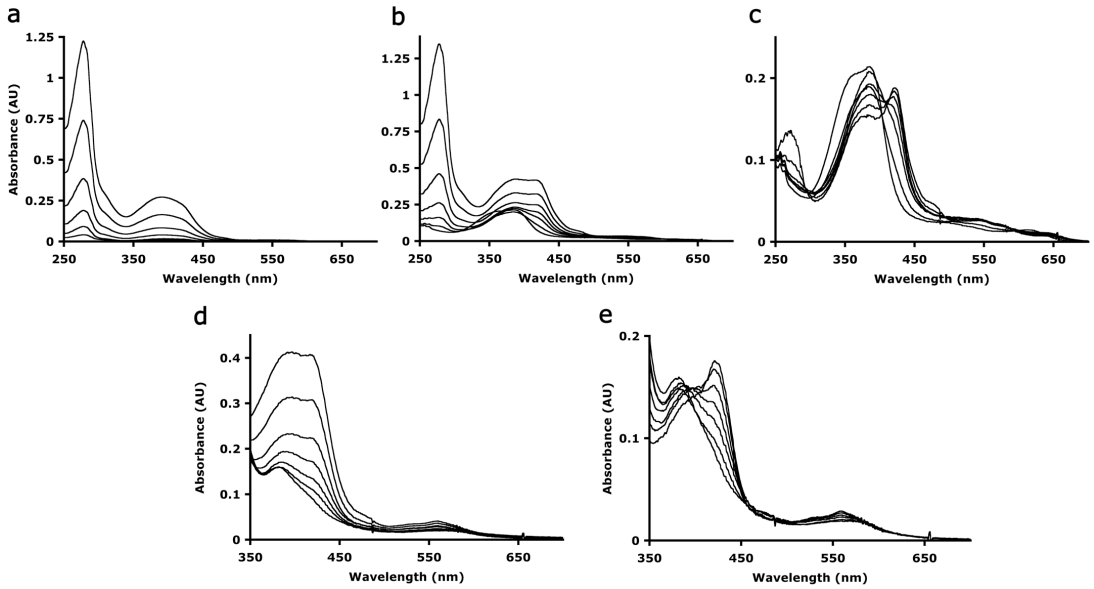

Figure 2.7. Addition of YtvA induces spectral changes to ferric and ferrous heme. (A) UV-Visible absorption spectra of YtvA (0, 1.2, 3, 6, 12, 24, & 42 mM) after photo bleaching. (B) Titration of ferric heme (4 mM) with YtvA (0, 1.2, 3, 6, 12, 24, & 42 mM). (C) Absorption spectra from titration of ferric heme with YtvA after subtraction of FMN absorbance. (D) Titration of ferrous heme (4 mM) with YtvA (0, 1.2, 3, 6, 12, 24, & 42 mM). (E) UV-Visible absorption spectra from titration of ferrous heme with YtvA after subtraction of FMN absorption.

Dissociation Rate Constant(s) of PER2 and Other Proteins Indicate Non-Specificity. HA50 values provide a qualitative means to compare relative heme-binding affinities under the same conditions but are complicated by the possibility of different heme binding stoichiometries and variable binding affinities of multiple sites. To further verify heme binding to PER2 as non-specific, we sought to evaluate binding affinities for heme. Major differences in heme-binding affinity could be due to differences in the association and/or dissociation rate constants. For association experiments, CO-heme produces a more monomeric form of free heme suitable for kinetic analysis. However, it has been shown that the heme-CO association rate constant is independent of protein structure (Hargrove et al., 1996) and overall affinity is determined by the dissociation rate constant. Previous work (Table 2.2) determined the dissociation rate constant of PER2 1-327 (PAS A) as 6.3×10^{-4} s^{-1} (Kitanishi et al., 2008), compared to the specific binding of sperm whale myoglobin, koff = 8.4×10^{-7} s^{-1} (Hargrove et al., 1996), non-specific binding of human BSA, koff = 1.1×10^{-2} s^{-1} (Hargrove et al., 1996), and bHLH-PAS A domains of the putative heme-binding CO sensor, koff =nPAS2 5.3×10^{-3} s^{-1} (Mukaiyama et al., 2006). To add to such comparisons we determined and compared the dissociation rate constants for PER2 and the other proteins that display similar heme-binding spectral properties.

We measured the dissociation rate constant of mPER2 1-320 to be 1.6×10^{-3} s^{-1} when fit as a first order process (Table 2.2, Figure 2.8), which is comparable to the previously determined value by Kitanishi et. al. (Kitanishi et al., 2008). However, both our data and that reported by Kitanishi et. al. (Kitanishi et al., 2008) was not fit well by a single exponential process. A bi-exponential process produces much better agreement with the experimental data (Table 2.2, Figure 2.8). This indicates there are at least two binding sites or two sets of binding sites for heme on PER2 with different affinities. All proteins tested had similar rate constants for heme dissociation and

occurred with at least bi-molecular processes (Table 2.2). As a control, we tested a recently identified FixL-like heme-binding PAS protein from P. aeruginosa that co-purifies with bound heme (Airola et. al., Structure, 2010, in press). In contrast, heme dissociation from the FixL-like PAS domain was a single process and the dissociation rate constant was considerably lower than PER2 at 6.9 x 10^{-5} s^{-1} (Table 2.2).

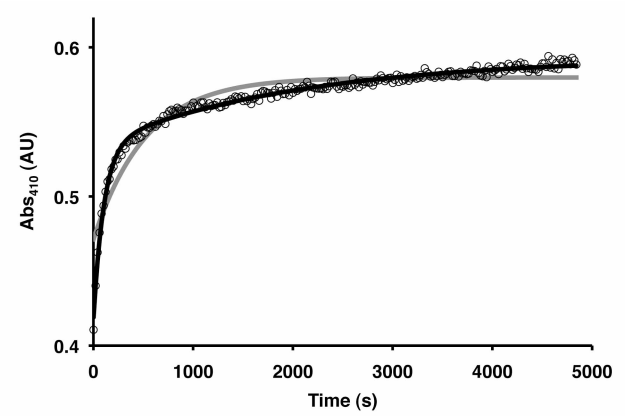

Figure 2.8. Heme Dissociation from PER2 Occurs From Multiple Sites. Heme transfer from PER2 (1-320) to H64Y/V68F apomyoglobin was measured as an increase in the Absorbance at 410 nm in 0.2 M Na phosphate, pH 7.0 and 0.45 Sucrose at 25 °C. Rate constants were calculated by analyzing the data in terms of both single (grey) and bi-exponential processes (black) (Table 2.2). The data for PER2 and other proteins was best represented by a bi-exponential process indicating multiple binding sites with different affinities.

Table 2.2: Heme Dissociation Rate Constants for mPER2 and Other Heme-Binding Proteins

Protein	koff (s^{-1})[a]	$koff_1$ (s^{-1})[b]	$koff_2$ (s^{-1})[b]	Reference
mPER2 1-320	1.6×10^{-3}	7.8×10^{-3}	4.8×10^{-4}	This work
mPER2 1-506	3.1×10^{-3}	7.6×10^{-3}	2.4×10^{-4}	This work
mPER2 972-1257	7.2×10^{-4}	1.2×10^{-3}	4.3×10^{-3}	This work
YtvA	4.8×10^{-4}	1.6×10^{-3}	1.2×10^{-4}	This work
YqeH	5.0×10^{-4}	2.2×10^{-2}	4.0×10^{-4}	This work
FixL-like PAS	6.9×10^{-5}			This work
mPER2 1-327	6.3×10^{-4}			(Kitanishi et al., 2008)
NPAS2 (bHLH-PAS A)	5.3×10^{-3}			(Mukaiyama et al., 2006)
Sw Mb[c]	8.4×10^{-7}			(Hargrove et al., 1996)
Hb α-subunit[c]	7.1×10^{-6}			(Hargrove et al., 1996)
BSA (human)[c]	1.1×10^{-2}			(Hargrove et al., 1996)

[a]rate constants were calculated assuming a single phase
[b]rate constants were calculated assuming a two step process
[c]rate constants given for 20°C
All other rate constants refer to 25°C

Electrochemistry. Protein-film voltammetry was used to evaluate the redox properties of the PER2-heme complex and thereby provide information on the local heme environment bound to PER2. A solution of concentrated PER2-heme complex was applied to a freshly polished glassy carbon electrode to generate a protein film immobilized on the electrode surface. Cyclic voltammagrams of purified PER2-heme complex displayed a reduction peak at E° = -396 mV relative to SCE, which is characteristic of solvent exposed heme bound to a protein surface (Reedy et al., 2008) (Figure 2.9). Subsequent scanning to higher potentials did not reveal a corresponding oxidation reaction, which may indicate that ferrous heme is no longer in electrochemical contact with the electrode surface. In comparison, free heme immobilized on the electrode surface displayed coupled reduction and oxidation peaks with E° = -372 mV (Figure 2.9). This confirms that the reduction peak for the PER2-heme complex is not due to free heme directly binding to the electrode surface. In the

case of the heme protein complex, reduction may cause heme to dissociate from PER2 due to PER'2 lower binding affinity for ferrous heme; thus no corresponding oxidation peak is observed. However, there is also the possibility that the initial reduction peak was due to catalytic reduction of a small amount of oxygen that could not be purged from the protein-heme complex. Such a scenario would also preclude observation of an oxidation peak. Although these two possibilities are difficult to distinguish; they both are consistent with heme being bound to a solvent exposed site on PER2.

2.5 Discussion

Potential roles for heme in the regulation of the circadian clock continue to emerge (Dioum et al., 2002; Ishida et al., 2008a, b; Kaasik and Lee, 2004; Kitanishi et al., 2008; Koudo et al., 2005; Mukaiyama et al., 2006; Raghuram et al., 2007; Rogers et al., 2008; Yang et al., 2008; Yin et al., 2007). Direct heme interactions have been suggested to regulate the stability and transcriptional activity of the clock components PER2 and nPAS2. However, much of the supporting evidence has been based upon biochemical assays of purified proteins (Dioum et al., 2002; Ishida et al., 2008a, b; Kitanishi et al., 2008; Koudo et al., 2005; Mukaiyama et al., 2006; Yang et al., 2008). To examine the biological relevance of these in vitro assays, we tested a number of well-characterized proteins with no role for heme binding. Interestingly, all of these proteins were found to bind heme in a manner comparable to PER2. This then raises the question: is heme binding to PER2 biologically relevant?

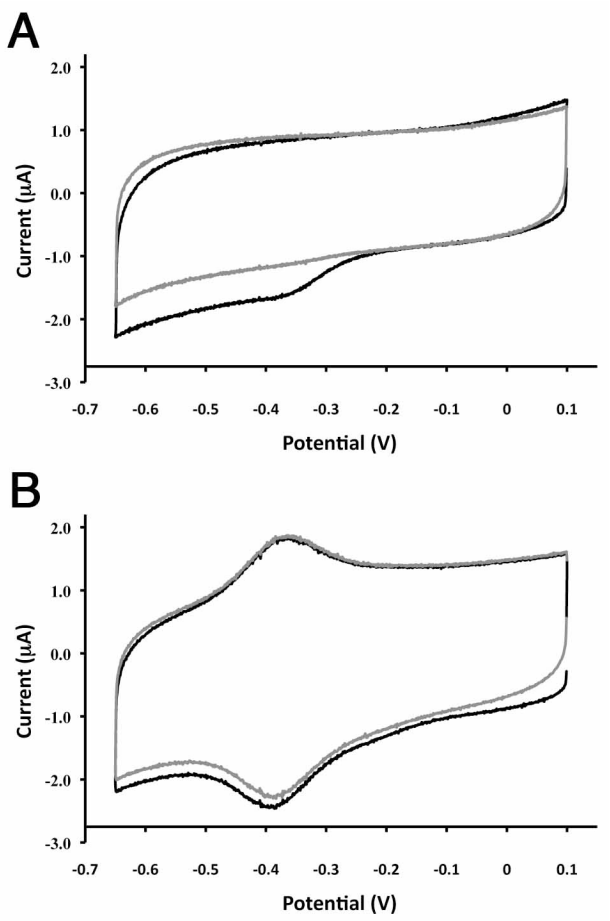

Figure 2.9. Electrochemistry of PER2-Heme Complex. A) Cyclic voltammogram of PER2-heme complex immobilized on glassy carbon electrode. B) Cyclic voltammogram of heme immobilized on glassy carbon electrode under the same conditions as (A). Black and grey traces denote the first and second potential sweeps. All scan rates were 100 mV/s.

Our initial characterization of PER2 confirmed that the PAS domains bind heme, in agreement with a previous report (Kitanishi et al., 2008). PER2 formed a stronger association with ferric heme compared to ferrous heme. Electrochemical analysis of PER2-heme complex suggests that heme may dissociate from PER2 upon reduction, consistent with redox-dependent binding location and affinity. With the methods of

UV-Visible absorption and MCD spectroscopy we identified that the PAS A domain of PER2 binds ferric heme as His-Cys coordinated and ferrous heme as bis-His coordinated. Site-directed mutagenesis identified the histidine residues 277 and 278 as the primary histidine axial ligands to ferrous heme. Replacement of these residues with alanine only affected the affinity for ferrous heme but not ferric heme. Although the affinity for ferrous heme was much less in the double mutant the same changes in spectral features were observed as with the native protein. Thus, heme binding to PER2 can occur at multiple sites.

We then examined heme binding to a number of previously characterized proteins with no known role for heme binding. As with PER2 and nPAS2, overexpression of these proteins in E. coli did not result in any heme incorporation. However, our in vitro assay determined all proteins tested were capable of binding heme. All proteins assayed displayed binding affinities for heme similar to PER2 and produced identical UV-Visible absorption spectra (Table 2.1). These results question the effectiveness of spectral assays of this type to differentiate between specific and non-specific heme binding.

Rate constants for heme dissociation were in the same range for the PER2 PAS domains and the control proteins strongly indicating that heme binding to PER2 is non-specific (Table 2.2). Furthermore, the dissociation rate constants are high compared to the specific heme-binding proteins Sw Mb, Hb a-subunit, and FixL-like PAS. Multiple non-specific sites were confirmed by fitting the experimental data using a bi-exponential decay. For the specific heme binding FixL-like PAS domain, heme dissociation was modeled well as a single first order process.

Moreover, the identify and type of axial ligand coordination in PER2 was dependent on the redox state of heme, which indicates that ferric and ferrous heme bind to different sites on the protein. The presence of a cysteine residue in the

polypeptide sequence is absolutely required to bind ferric heme as evidenced by a Soret peak at 424 nm and broad a/b peaks at 572 and 548 nm. If no surface cysteine residues are present, the addition of protein to ferric heme will not induce any spectral changes indicative of heme binding, as observed for CheA D289. However, with the introduction of a surface cysteine residue into D289 the characteristic heme binding signals were recapitulated. Thus, any solvent exposed cysteine is likely capable of binding ferric heme and generating the associated spectral response. Modification of solvent exposed cysteine residues altered the ferric spectra of PER2 indicating that ligand binding does occur on the protein surface. Alternatively, a surface cysteine residue is not required to bind ferrous heme, as native D289 and cysteine-modified PER2 displayed the usual spectral changes upon ferrous heme titration. Hence, surface histidine residues are sufficient to produce the typical ferrous spectra with Soret peak at 426 nm and sharp a/b peaks at 560 and 530 nm. Cys-His coordination for ferric heme, and bis-His coordination for ferrous heme were confirmed by MCD spectroscopy. MCD experiments also verify that a cysteine or methionine residue is not involved in binding ferrous heme with histidine serving as the trans axial ligand to bound CO in ferrous PAS A. Redox dependent binding has been reported for the putative novel-heme binding motif, Ser-Cys841-Pro-Ala, of PER2 in a region outside the PER2 PAS domains (Yang et al., 2008). UV-Vis spectral changes found that this motif bound ferric heme and gave rise to spectra identical to the PER2 PAS domains, but was unable to bind ferrous heme. This data is also consistent with ferric heme binding Cys-His coordinate and ferrous heme binding bis-His coordinate.

To analyze potential heme-binding modes for the PAS domains of PER2 and nPAS2 we examined a secondary-structure based alignment with other PAS domains of known structure and heme-binding function (Figure 2.4). FixL and ecDOS are bacterial heme binding PAS domains whose axial ligand is a highly conserved

histidine residue found in the alpha C helix of the PAS fold (Key and Moffat, 2005; Miyatake et al., 2000; Suquet et al., 2005). Although PER2 and nPAS2 do not conserve this histidine residue, it is plausible that they harbor a different histidine residue that is specific for heme. However, sequence alignments failed to identify any conserved residues that might point to a novel heme-binding motif shared between PER2 and nPAS2. Analysis of the mPER2 PAS domain structure (Hennig et al., 2009) found that all proposed heme ligation residues are positioned at a solvent exposed site, consistent with our biochemical analysis (Figure 2.10). In addition, we have shown that when the PAS domain pocket is blocked by a cofactor, such as FMN in YtvA, the PAS domains still bind heme in a manner similar to the PER2 protein.

The recent crystal structure of the mPER2 PAS domains (PDB: 3GDI) allows for a structural analysis of potential heme binding ligands (Hennig et al., 2009). A previous study identified Cys215 and Cys270 in PAS A to be important for ferric heme interactions (Kitanishi et al., 2008). A double mutant: C215A, C270A, resulted in spectral perturbations of ferric heme bound to PER2 PAS A, as analyzed by UV-Visible absorption, Electron Paramagnetic Resonance (EPR), and Resonance Raman (RR) spectroscopy. However, the double mutant displayed identical spectra for ferrous and ferrous-CO heme iron states compared to wild type. All UV-Visible absorption, EPR, and RR spectra of the single Cys mutants were identical to wild type. Nonetheless Cys215 was proposed as the primary heme interacting residue for ferric heme because the C215A mutant displayed an altered heme circular dichroism (CD) spectrum, whereas the C270A mutant did not (Kitanishi et al., 2008). Cys215 is located on a surface exposed region of PAS A that also contains His214, His277, and His278, all in close proximity and thus would be capable of both bis-His and His-Cys ligation (Figure 2.10). H277/278A and H214A PAS A mutants have lowered affinities for ferrous heme, consistent with this as the primary site for heme interaction in PAS

A. Furthermore, given the position of Cys270 on the buried face of the PAS A b-sheet, a Cys-His heme coordination mode involving Cys270 could only be possible with substantial structural distortion of the PAS A domain. Other interaction sites capable of bis-His and His-Cys ligation may be possible in a PAS A/A homodimer. In the crystal structure of the PAS domains of PER2 (Hennig et al., 2009), dimerization is mediated by the PAS B domains with no observed interaction between the PAS A domains. But, truncation of PAS B allows the PAS A domains to dimerize (Kitanishi et al., 2008), as determined by size-exclusion chromatography.

The binding of ferrous heme to PER2 also shows many characteristics similar to those of de-novo designed heme proteins. Rojas et al. (Rojas et al., 1997) reported the heme binding properties of 30 different peptides predicted to fold into four-helix bundles. This library of proteins contained on average 4.3 histidine residues and 4.9 methionine residues capable of heme ligation. None of the proteins contained cysteine residues. The authors found that 15 of 30 sequences bound heme similar to b-type cytochromes with a soret peak at 412 nm for ferric heme and a broad a/b band centered around 550 nm. Upon reduction the soret peak was shifted to 426 nm with sharp alpha and beta peaks at 560 and 530 nm respectively, identical to that observed for PER2. Another study (Rau et al., 2000) used a combinatorial synthesis approach to design and test 426 amphiphilic anti-parallel four helix bundles. Of the 426 proteins assayed, 399 were found to bind heme and give rise to a Soret band at 414 nm for the ferric state and a b-type cytochrome spectra, identical to PER2 and proteins described by Rojas et. al. (Rojas et al., 1997), for the ferrous state.

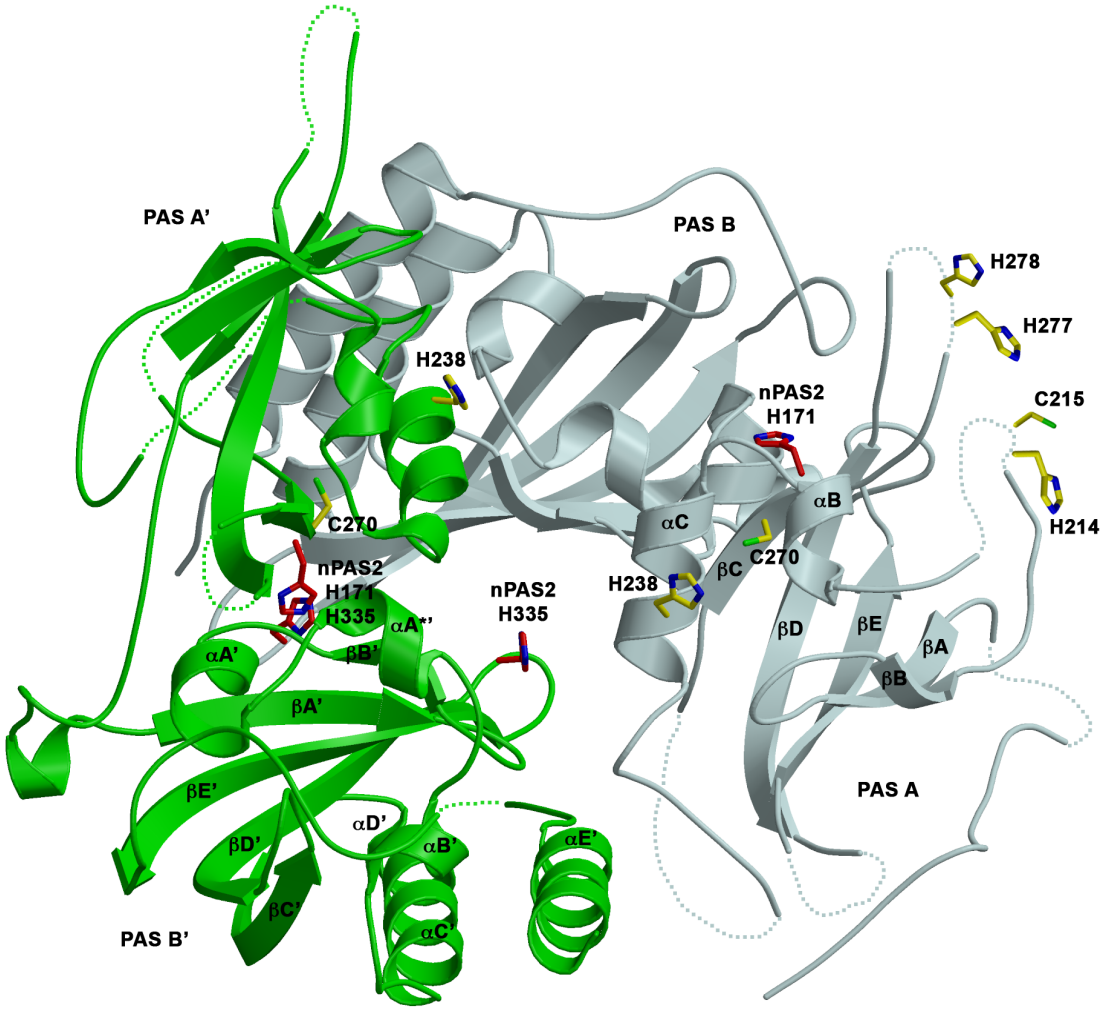

Figure 2.10. mPER2 structure with location of possible heme binding residues. Ribbon representation of mPER2 PAS A/B dimer (3GDI): molecule 1 (PAS A and PAS B), molecule 2 (PAS A' and PAS B'). Side chains are shown for residues H214, C215, H238, C270, H277, and H278 in mPER2 (yellow) and C170, H171, H335 in nPAS2 (red). H119 of nPAS2 is not shown but corresponds to C215 of PER2. Residues with missing density are depicted as a dotted line and were manually drawn. The secondary structure elements of the PAS fold are labeled for PAS A and PAS B'.

From the variety of protein folds assayed it is clear that the spectral signals indicative of heme binding do not require a specific mode of interaction between heme and a conserved protein architecture. Any polypeptide sequence containing both a cysteine and histidine residue is sufficient to induce the spectral changes observed for

PER2. Considering the low solubility of free heme, it is most likely that binding occurs at surface histidine and cysteine residues aided by hydrophobic patches on the surface of each protein. Heme has long been known to form homo-oligomers in aqueous solution (Brown et al., 1970). Additionally, heme binds non-specifically to phospholipid bilayers and associates with membrane skeletal proteins due to its high hydrophobicity (Liu et al., 1985; Tipping et al., 1979). Given the evidence against the specificity of heme binding to PER2 we urge caution in the interpretation of results from previous in vitro assays and question the biological relevance of heme binding in relation to the clock protein PER2. We note that the in vitro heme interactions observed for nPAS2 are very similar to those of PER2, and in our view, this also calls into question their biological relevance.

If heme binding to PER2 and nPAS2 is not biologically relevant the question remains how does heme feedback into the clock to coordinate circadian timing (Dioum et al., 2002; Kaasik and Lee, 2004; Kitanishi et al., 2008; Raghuram et al., 2007; Yang et al., 2008; Yin et al., 2007; Zheng et al., 2001). The identification of heme as the ligand for the nuclear receptors REV-erba and REV-erbb may provide this connection (Raghuram et al., 2007; Yin et al., 2007). Both REV-erba and REV-erbb bind heme specifically through their ligand binding domains (LBDs). Heme binding causes REV-erba to recruit the nuclear receptor corepressor – histone deacetylase 3 (NCoR-HDAC3) complex, which results in decreased transcription of bMAL1, a necessary component for active transcription of clock and clock controlled genes (Raghuram et al., 2007; Yin et al., 2007). Noteworthy is the fact that overexpression of the REV-erb LBDs in E. coli produces proteins that purify with bound heme and display UV-Visible absorption spectra different from those of PER2 and nPAS2. In contrast, there are no reports of any purified fragment of nPAS2 or PER2 protein containing heme after overexpression in E. coli. In all cases PER2 and nPAS2 must be

reconstituted in vitro with free hemin (Dioum et al., 2002; Ishida et al., 2008a, b; Kitanishi et al., 2008; Koudo et al., 2005; Mukaiyama et al., 2006; Yang et al., 2008). PER2 has been shown to bind to heme immobilized on a heme-agarose column (Kaasik and Lee, 2004; Yang et al., 2008). In light of the evidence presented here, this interaction likely represents non-specific heme binding on the surface of the PER2 protein, and does not involve the buried hydrophobic cavity of the PAS core. To date there has been no spectral or other evidence from PER2 or nPAS2 purified from mammalian cell lines that indicate PER2 or nPAS2 interact with heme. Given that in vitro heme binding to nPAS2 and PER2 is likely non-specific, heme influence over the mammalian circadian clock is most likely dominated by its interaction with the Rev-erb's, or other factors yet to be identified.

REFERENCES

Bilwes, A.M., Alex, L.A., Crane, B.R., and Simon, M.I. (1999). Structure of CheA, a signal-transducing histidine kinase. Cell *96*, 131-141.

Brown, S.B., Dean, T.C., and Jones, P. (1970). Aggregation of ferrihaems - dimerization and protolytic equilbria of protoferrihaem and deuteroferrihaem in aqueous solution. Biochemical Journal *117*, 733-&.

Cheek, J., Dawson, J.H. (2000). Handbook of porphyrins and related macrocycles, Vol 7 (New York: Academic Press).

Cole, C., Barber, J.D., and Barton, G.J. (2008). The Jpred 3 secondary structure prediction server. Nucleic Acids Res. *36*, W197-W201.

Collman, J.P., Sorrell, T.N., Dawson, J.H., Trudell, J.R., Bunnenberg, E., and Djerassi, C. (1976). Magnetic circular-dichroism of ferrous carbonyl adducts of cytochromes P-450 and P-420 and their synthetic models - further evidence for mercaptide as 5th ligand to iron. Proceedings of the National Academy of Sciences of the United States of America *73*, 6-10.

Dawson, J.H., Andersson, L.A., and Sono, M. (1982). Spectroscopic investigations of ferric cytochrome P-450-cam ligand complexes - identification of the ligand trans to cysteinate in the native enzyme. Journal of Biological Chemistry *257*, 3606-3617.

Dioum, E.M., Rutter, J., Tuckerman, J.R., Gonzalez, G., Gilles-Gonzalez, M.A., and McKnight, S.L. (2002). NPAS2: A gas-responsive transcription factor. Science *298*, 2385-2387.

Du, J., Sono, M., and Dawson, J.H. (2008). The proximal and distal pockets of the H93G myoglobin cavity mutant bind identical ligands with different affinities: Quantitative analysis of imidazole and pyridine binding. Spectroscopy-an International Journal *22*, 123-141.

Erbel, P.J.A., Card, P.B., Karakuzu, O., Bruick, R.K., and Gardner, K.H. (2003). Structural basis for PAS domain heterodimerization in the basic helix-loop-helix-PAS transcription factor hypoxia-inducible factor. Proceedings of the National Academy of Sciences of the United States of America *100*, 15504-15509.

Gilles-Gonzalez, M.A., and Gonzalez, G. (2005). Heme-based sensors: defining characteristics, recent developments, and regulatory hypotheses. Journal of Inorganic Biochemistry *99*, 1-22.

Gillesgonzalez, M.A., and Gonzalez, G. (1993). Regulation of the Kinase-Activity of Heme Protein Fixl from the 2-Component System Fixl/Fixj of Rhizobium-Meliloti. Journal of Biological Chemistry *268*, 16293-16297.

Hargrove, M.S., Barrick, D., and Olson, J.S. (1996). The association rate constant for heme binding to globin is independent of protein structure. Biochemistry *35*, 11293-11299.

Hargrove, M.S., Singleton, E.W., Quillin, M.L., Ortiz, L.A., Phillips, G.N., Olson, J.S., and Mathews, A.J. (1994). HIS(64)(E7)-]TYR APOMYOGLOBIN AS A REAGENT FOR MEASURING RATES OF HEMIN DISSOCIATION. Journal of Biological Chemistry *269*, 4207-4214.

Harms, E., Kivimae, S., Young, M.W., and Saez, L. (2004). Posttranscriptional and posttranslational regulation of clock genes. Journal of Biological Rhythms *19*, 361-373.

Hennig, S., Strauss, H.M., Vanselow, K., Yildiz, O., Schulze, S., Arens, J., Kramer, A., and Wolf, E. (2009). Structural and Functional Analyses of PAS Domain Interactions of the Clock Proteins Drosophila PERIOD and Mouse PERIOD2. Plos Biology *7*, 836-853.

Ishida, M., Ueha, T., and Sagami, I. (2008a). Effects of mutations in the heme domain on the transcriptional activity and DNA-binding activity of NPAS2. Biochemical and Biophysical Research Communications *368*, 292-297.

Ishida, M., Ueha, T., and Sagami, I. (2008b). Functional analysis of heme-PAS domain mutants of NPAS2: transcriptional activity and DNA-binding activity. Febs Journal *275*, 130-130.

Kaasik, K., and Lee, C.C. (2004). Reciprocal regulation of haem biosynthesis and the circadian clock in mammals. Nature *430*, 467-471.

Kewley, R.J., Whitelaw, M.L., and Chapman-Smith, A. (2004). The mammalian basic helix-loop-helix/PAS family of transcriptional regulators. International Journal of Biochemistry & Cell Biology *36*, 189-204.

Key, J., and Moffat, K. (2005). Crystal structures of deoxy and CO-bound bjFixLH reveal details of ligand recognition and signaling. Biochemistry *44*, 4627-4635.

Kitanishi, K., Igarashi, J., Hayasaka, K., Hikage, N., Saiful, I., Yamauchi, S., Uchida, T., Ishimori, K., and Shimizu, T. (2008). Heme-binding characteristics of the isolated PAS-A domain of mouse Per2, a transcriptional regulatory factor associated with circadian rhythms. Biochemistry *47*, 6157-6168.

Koudo, R., Kurokawa, H., Sato, E., Igarashi, J., Uchida, T., Sagami, I., Kitagawa, T., and Shimizu, T. (2005). Spectroscopic characterization of the isolated heme-bound PAS-B domain of neuronal PAS domain protein 2 associated with circadian rhythms. Febs Journal *272*, 4153-4162.

Liu, S.C., Zhai, S., Lawler, J., and Palek, J. (1985). Hemin-mediated dissocation of erythrocyte-membrane skeletal proteins. Journal of Biological Chemistry *260*, 2234-2239.

Lowrey, P.L., and Takahashi, J.S. (2004). Mammalian circadian biology: Elucidating genome-wide levels of temporal organization. Annual Review of Genomics and Human Genetics *5*, 407-441.

Miyatake, H., Mukai, M., Park, S.Y., Adachi, S., Tamura, K., Nakamura, H., Nakamura, K., Tsuchiya, T., Iizuka, T., and Shiro, Y. (2000). Sensory mechanism of oxygen sensor FixL from Rhizobium meliloti: Crystallographic, mutagenesis and resonance Raman spectroscopic studies. Journal of Molecular Biology *301*, 415-431.

Moglich, A., and Moffat, K. (2007). Structural basis for light-dependent signaling in the dimeric LOV domain of the photosensor YtvA. Journal of Molecular Biology *373*, 112-126.

Morais Cabral, J.H., Lee, A., Cohen, S.L., Chait, B.T., Li, M., and Mackinnon, R. (1998). Crystal structure and functional analysis of the HERG potassium channel N terminus: a eukaryotic PAS domain. Cell *95*, 649-655.

Mukaiyama, Y., Uchida, T., Sato, E., Sasaki, A., Sato, Y., Igarashi, J., Kurokawa, H., Sagami, I., Kitagawa, T., and Shimizu, T. (2006). Spectroscopic and DNA-binding characterization of the isolated heme-bound basic helix-loop-helix-PAS-A domain of neuronal PAS protein 2 (NPAS2), a transcription activator protein associated with circadian rhythms. Febs Journal *273*, 2528-2539.

Panda, S., Antoch, M.P., Miller, B.H., Su, A.I., Schook, A.B., Straume, M., Schultz, P.G., Kay, S.A., Takahashi, J.S., and Hogenesch, J.B. (2002). Coordinated transcription of key pathways in the mouse by the circadian clock. Cell *109*, 307-320.

Raghuram, S., Stayrook, K.R., Huang, P.X., Rogers, P.M., Nosie, A.K., McClure, D.B., Burris, L.L., Khorasanizadeh, S., Burris, T.P., and Rastinejad, F. (2007). Identification of heme as the ligand for the orphan nuclear receptors REV-ERB alpha and REV-ERB beta. Nature Structural & Molecular Biology *14*, 1207-1213.

Rau, H.K., DeJonge, N., and Haehnel, W. (2000). Combinatorial synthesis of four-helix bundle hemoproteins for tuning of cofactor properties. Angew. Chem.-Int. Edit. *39*, 250-+.

Reedy, C.J., Elvekrog, M.M., and Gibney, B.R. (2008). Development of a heme protein structureelectrochemical function database. Nucleic Acids Res. *36*, D307-D313.

Reppert, S.M., and Weaver, D.R. (2002). Coordination of circadian timing in mammals. Nature *418*, 935-941.

Rogers, P.M., Ying, L., and Burris, T.P. (2008). Relationship between circadian oscillations of Rev-erb alpha expression and intracellular levels of its ligand, heme. Biochemical and Biophysical Research Communications *368*, 955-958.

Rojas, N.R.L., Kamtekar, S., Simons, C.T., McLean, J.E., Vogel, K.M., Spiro, T.G., Farid, R.S., and Hecht, M.H. (1997). De novo heme proteins from designed combinatorial libraries. Protein Science *6*, 2512-2524.

Scheuermann, T.H., Tomchick, D.R., Machius, M., Guo, Y., Bruick, R.K., and Gardner, K.H. (2009). Artificial ligand binding within the HIF2 alpha PAS-B domain of the HIF2 transcription factor. Proceedings of the National Academy of Sciences of the United States of America *106*, 450-455.

Sudhamsu, J., Lee, G.I., Klessig, D.F., and Crane, B.R. (2008). The structure of YqeH an AtNOS1/AtNOA1 ortholog that couples GTP hydrolysis to molecular recognition. Journal of Biological Chemistry *83*, 32968-32976.

Suquet, C., Park, H.J., Kang, C.H., and Satterlee, J.D. (2005). The X-ray crystal structures of oxy- and deoxy-EcDos heme domains indicate that signal initiation-propagation is conveyed by secondary structure conformational changes. Biophysical Journal *88*, 390A-390A.

Tipping, E., Ketterer, B., and Christodoulides, L. (1979). Interactions of Small Molecules with Phospholipid-Bilayers - Binding to Egg Phoshatidylcholine of some Organic-Anions (Bromosulfophthalein, Estrone Sulfate, Heme and Bilirubin) that Bind to Ligandin and Aminoazo-Dye-Binding Protein-A. Biochemical Journal *180*, 327-337.

Travascio, P., Li, Y.F., and Sen, D. (1998). DNA-enhanced peroxidase activity of a DNA aptamer-hemin complex. Chemistry & Biology *5*, 505-517.

Vetter, S.W., Terentis, A.C., Osborne, R.L, Dawson, J.H, Goodin D.B. (2009). Journal of Biological Inorganic Chemistry *14*, 179-191.

Yang, J.H., Kim, K.D., Lucas, A., Drahos, K.E., Santos, C.S., Mury, S.P., Capelluto, D.G.S., and Finkielstein, C.V. (2008). A novel heme-regulatory motif mediates heme-dependent degradation of the circadian factor period 2. Molecular and Cellular Biology *28*, 4697-4711.

Yildiz, O., Doi, M., Yujnovsky, I., Cardone, L., Berndt, A., Hennig, S., Schulze, S., Urbanke, C., Sassone-Corsi, P., and Wolf, E. (2005). Crystal structure and interactions of the PAS repeat region of the Drosophila clock protein PERIOD. Molecular Cell *17*, 69-82.

Yin, L., Wu, N., Curtin, J.C., Qatanani, M., Szwergold, N.R., Reid, R.A., Waitt, G.M., Parks, D.J., Pearce, K.H., Wisely, G.B., and Lazar, M.A. (2007). Rev-erb alpha, a

heme sensor that coordinates metabolic and circadian pathways. Science *318*, 1786-1789.

Young, M.W., and Kay, S.A. (2001). Time zones: A comparative genetics of circadian clocks. Nature Reviews Genetics *2*, 702-715.

Zheng, B.H., Albrecht, U., Kaasik, K., Sage, M., Lu, W.Q., Vaishnav, S., Li, Q., Sun, Z.S., Eichele, G., Bradley, A., and Lee, C.C. (2001). Nonredundant roles of the mPer1 and mPer2 genes in the mammalian circadian clock. Cell *105*, 683-694.

Zoltowski, B.D., Schwerdtfeger, C., Widom, J., Loros, J.J., Bilwes, A.M., Dunlap, J.C., and Crane, B.R. (2007). Conformational switching in the fungal light sensor vivid. Science *316*, 1054-1057.

CHAPTER 3

Reconstruction of the Soluble Receptor Aer2 Establishes a New Paradigm for PAS and HAMP Domain Signal Transduction

3.1 Abstract

PAS and HAMP domains are two common signal transduction modules important for responding to environmental changes and stresses. Here we have used a combination of techniques to reconstruct the structure of the soluble receptor Aer2, which contains a heme-binding PAS domain arranged linearly between 3 N- and 2 C-Terminal HAMP domains. The preliminary PAS structure (R factor = 0.33, R_{free} = 0.39) indicates a novel PAS fold differing from other heme binding PAS domains. Crystallographic data for different heme ligation and redox states have been collected which may provide insight into associated conformational changes in PAS structure. Solution studies indicate a change in PAS dimerization affinity dependent on heme redox and ligation state. Signal transduction in Aer2 appears to involve changes in PAS domain spatial proximity that generates a global restructuring of attached C-terminal HAMP domains. Similarities with PAS domains that contain short C-terminal signaling helices suggests a general signaling mechanism involving changes in downstream helical structure widely applicable to a variety of signal transduction modules.

3.2 Introduction

PAS (Per-Arnt-Sim) and HAMP domains are two common signal transduction motifs involved in sensing and signaling in response to changes in cellular environment (Dunin-Horkawicz and Lupas, 2010; Taylor and Zhulin, 1999). They both occur in a wide variety of signaling proteins and regulate the same large class of effectors including Histidine kinases, Adenylyl cyclases, Methyl-accepting chemotaxis proteins, Phosphotases, GGDEF, and EAL domains (Aravind and Ponting, 1999). This subset of PAS domains often bind a cofactor capable of sensing light, redox, and/or oxygen to regulate the activity of downstream effector domains (Moglich et al., 2009b). Although HAMP domains do not directly sense stimuli they also control the activity of downstream domains through signal relay mechanisms (Hulko et al., 2006). HAMP domains are typically associated with the membrane and receive signals through transmembrane helices attached to periplasmic sensing domains, which are relayed to downstream effector domains (Hazelbauer et al., 2008). In addition, a newly identified subset of HAMP domains occur in sequential poly-HAMP chains and are found in both transmembrane and soluble receptors (Airola et al., 2010).

PAS and HAMP domains can also occur together in the same signaling protein. The best-studied example is the *Escherichia coli* aerotaxis receptor Aer (EcAer) (Taylor, 2007). In EcAer, the PAS and HAMP domains are separated in sequence by two transmembrane segments that anchor the protein in the membrane. The PAS domain binds a flavin adenosine nucleotide (FAD) cofactor to monitor intracellular redox conditions and direct E. coli cells to an optimal oxygen concentration for energy production (Rebbapragada et al., 1997). Signal transduction has been shown to occur through direct side-on interactions between the PAS and HAMP domains (Watts et al., 2008), and transmitted through the C-terminal MCP-like signaling to affect the activity of the histidine kinase CheA.

Pseudomonas aeruginosa contains two transducers of aerotaxis: PaAer is homologous to the membrane bound *E. coli* aerotaxis receptor Aer, whereas the second, PaAer2, lacks transmembrane helices and is a soluble receptor (Figure 1.1) (Hong et al., 2004). Aer2 contains a heme-binding PAS domain, which can signal in response to diatomic gases (K. Watts, in preparation). Five HAMP domains are found in the full-length protein, with three N- and two C-terminal to the PAS domain. The C-terminus of Aer2 contains a cytoplasmic signaling region, with a high degree of similarity to *E. coli* chemoreceptors, which likely couples the protein to the histidine kinase CheA and other components of the chemotaxis pathway (Hong et al., 2004). Although the three N-terminal HAMP domains are located upstream of the PAS domain, the HAMP2/3 unit is required for function (K. Watts, in preparation). The mechanism of signal transduction in Aer2 is not yet known and may differ from EcAer given the different domain architectures.

Secondary structure predictions, using Jpred3 (Cole et al., 2008), of the Aer2 PAS domain indicated significant differences in elements central to signal propagation in the heme-binding PAS domains of FixL and ecDOS. Both of these well-characterized proteins utilize a distal arginine residue to stabilize oxygen binding that is located at the start of the Gβ strand (Figure 3.1) (Gilles-Gonzalez and Gonzalez, 2004; Key and Moffat, 2005). Upon oxygen dissociation a nearby methionine residue forms a six-coordinate complex in EcDOS, while FixL contains an open coordination site occupied by a water molecule. These changes in ligation state are accompanied by a rearrangement of Gβ strand. In Aer2, the loop connecting the Fα helix and Gβ strand is predicted to be significantly shorter (Figure 3.1). The arginine residues located at the start of hβ are important for Aer2 function *in vivo* (K. Watts, in preparation) suggesting Aer2 may adopt an alternative PAS fold and undergo different conformational changes, compared to FixL and ecDOS, upon changes in ligation state.

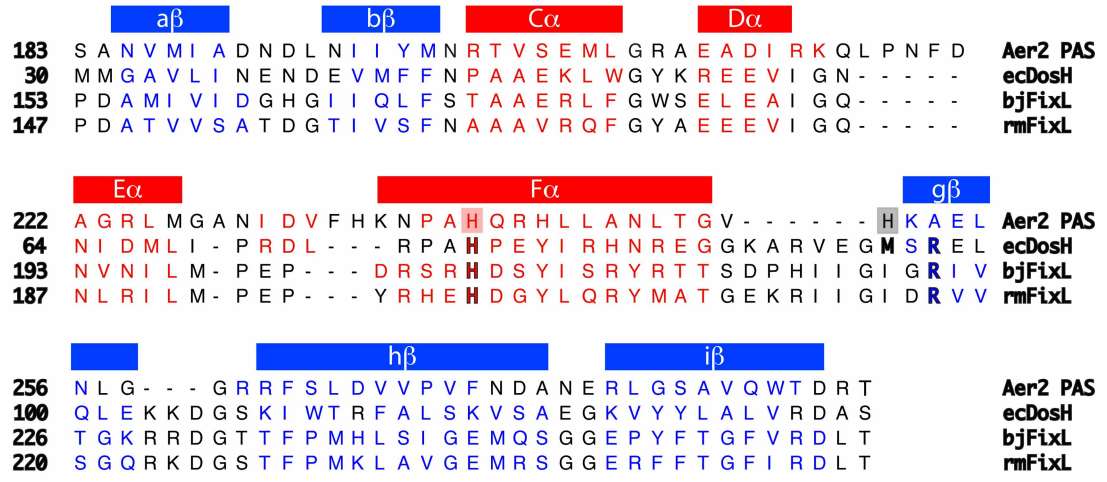

Figure 3.1. Secondary Structure Alignment of Heme-Binding PAS Domains. Alignment of heme-binding PAS domains Aer2, ecDOS, bjFixL, and rmFixL highlighting the shortened linker between the Fα helix and Gβ strand in Aer2.

Here we present a model for signal transduction in Aer2, based upon the reconstruction of Aer2 structure, which differs from EcAer and does not involve direct PAS and HAMP interactions. The crystal structure of the Aer2 PAS domain reveals a novel PAS fold and contains a C-terminal helical extension that comprises AS1 of HAMP4. Using a combination of techniques we demonstrate the Aer2 PAS domain is situated between the N- and C-terminal HAMP domains and propose a mechanism for signal transduction involving changes in PAS dimerization that is propagated by downstream helical distortions.

3.3 Results and Discussion

Crystallization of the Aer2 PAS Domain using Surface Entropy Reduction (SER)

Initial attempts at crystallizing the Aer2 PAS domain, residues 173-289, and the PAS domain containing a C-terminal extension, Aer2 173-307, identified both PAS containing fragments to crystallize under the same conditions. However, these conditions yielded only thin needle clusters unsuitable for diffraction experiments.

Successful crystallization of Aer2 173-307 was accomplished by utilizing a surface entropy reduction (SER) method, designed to reduce the entropic barrier of crystallization, by mutation of high entropy residue or residue clusters (Lys, Glu, Gln) to low entropy residues (Ala) (Cooper et al., 2007; Goldschmidt et al., 2007). Six SER mutants of Aer2 173-307 were generated (Table 3.1) with a K176A (SER A) mutation yielding single crystals diffracting to 1.9 Å after optimization (see Materials and Methods).

Table 3.1. Summary of Aer2 173-307 Protein Expression and Crystallization

Protein	Mutation	Expression	Notes
WT	-	Good; 23°C	Obtained crystal hit
SER A	K176A	Good; 23°C	Diffracted to 1.9Å
SER B	K215A, Q216A	Good; 23°C	-
SER C	K235A	Good; 23°C	-
SER D	K252A, E254A	Poor; 18°C	-
SER E	E275A	Sufficient; 18°C	Obtained crystal hit
SER F	E293A, Q294A, E295A	Good; 23°C	C-Ter degradation

Multi-wavelength anomalous dispersion (MAD) was used to determine the structure of Aer2 PAS_{Cext} (Terwilliger and Berendzen, 1999). After encountering difficulties during refinement, the crystals were identified as twinned. Identification of the correct space group (P6) and twinning operation (k, h, -l) allowed for successful statistical refinement with CNS (Brunger et al., 1998). Two protein molecules were found in the asymmetric unit with the C-terminal helix extensions packing against the accompanying PAS domain's β sheet. The interaction between the face of the PAS C-terminal helix (AS1 of HAMP4) contacting the β sheet would form part of the

hydrophobic core of HAMP4 and is not biologically relevant. However, this interaction may be similar to the PAS-HAMP interactions in EcAer. The overall PAS structure conserves some features with the other heme-binding PAS domains of known structure, FixL and ecDOS, maintaining the position of bound heme. Interestingly, the Aer2 PAS domain differs from FixL and ecDOS in the overall topology of the α helix and loop region. In Aer2, the αC is merged with αD to form an extended helix. At present the structure is not fully refined (R factor = 33, R_{free} = 39), due to twinning complications and time constraints, allowing an analysis of only general features and delaying any detailed analysis and comparison of the heme active site. All general features, including the position and residue identity of C-terminal α helical residues, discussed in the following text are clearly visible at this point in the refinement.

Redox and Ligation State Manipulation in Solution and in Crystals

The Aer2 PAS domain is capable of binding the diatomic gases O_2, nitric oxide (NO), and carbon monoxide (CO) *in vitro* (Figure 3.2 and Table 3.2) and signaling in response to diatomic gases *in vivo* (K. Watts, in preparation). Manipulation of the iron-heme redox and ligation state can be accomplished using a variety of methods. The oxy-complex is easily formed in solution by addition of 1mM ascorbate in an aerobic environment. A lack of spectral changes upon addition of CN^-, a known high affinity ligand for ferric heme, confirmed an oxygen-iron complex (Figure 3.3). Addition of the oxidizing agent $Fe(CN)_6$, to generate Fe(III) heme, followed by CN^- demonstrated that Aer2 is capable of binding CN^-. The Fe(II)-NO complex is also easily formed by addition of 1mM ascorbate supplemented with NOC-7, a NO releasing compound, and can also be carried out aerobically. This simple methodology has been applied to obtain diffraction data for the oxy complex and Fe(II)-NO iron-heme ligation states, as well as the Fe(III), Fe(III)-NO, and Fe(II) states (see Materials

and Methods). Currently, it is not known whether these experiments were successful in altering the redox and ligation state of Aer2 in crystals as the final structural model is not yet complete. Further analysis and discussion of possible redox and ligation state conformational changes in PAS structure must await completion of the final model.

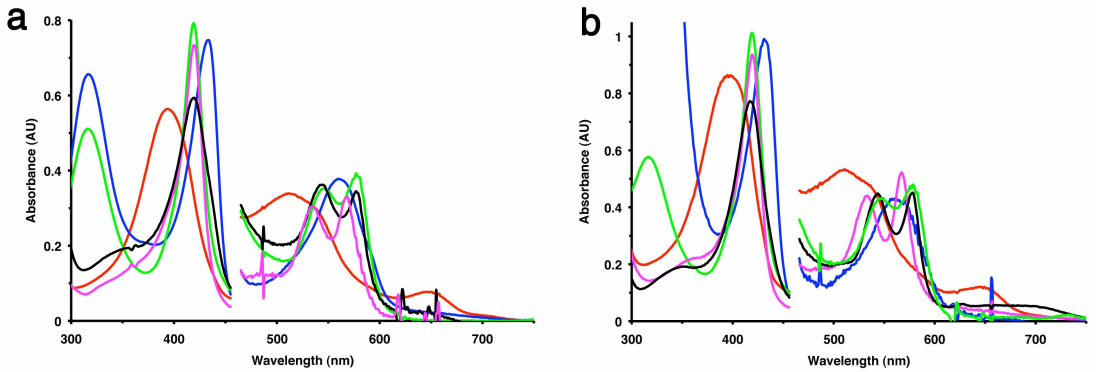

Figure 3.2. The N- and C-terminal HAMP domains of Aer2 do not effect the UV-Visible absorption spectra of Aer2 PAS domain. (A) UV-Visible absorption spectra of Aer2 PAS domain (173-289): oxy complex (black), ferrous (blue), ferric (red), ferrous-NO (green), and ferric-NO (purple). (B) Identical UV-Visible absorption spectra of Aer2 1-402 containing both the N- and C-terminal HAMP domains: oxy complex (black), ferrous (blue), ferric (red), ferrous-NO (green), and ferric-NO (purple). Region between 475-700 nm are shown five times enlarged for clarity.

Table 3.2. UV-Visible Absorption Maxima for Aer2 173-289 and 1-402.

	Absorption Maxima								
	Fe(III)			Fe(II)			Fe(II)-O2		
protein	soret	β	α	soret	β	α	soret	β	α
Aer2 173-289	393	511	646	433	560		418	543	577
Aer2 1-402	396	511	645	432	561		418	543	577

	Fe(III)-NO			Fe(II)-NO		
protein	soret	β	α	soret	β	α
Aer2 173-289	419	534	568	419	546	577
Aer2 1-402	419	533	567	420	546	578

Investigation of Direct PAS and HAMP Domain Interactions

The PAS domain of EcAer requires the associating HAMP domain to stably bind FAD (Herrmann et al., 2004). Unlike EcAer the PAS domain of Aer2 can bind heme stably in the absence of other domains. However, we sought to determine if we could detect any PAS/HAMP interactions in Aer2 by comparing the heme absorption spectra of various Aer2 proteins containing the N- and C-terminal HAMP domains. Recombinantly expressed Aer2 protein fragments containing the C-terminal HAMP domains (290-382) required a newly reported method for heme incorporation (ref Sudhamsu, 2010) involving coexpression of ferrochelatase, which catalyzes the insertion of iron into protoporphyrin IX, for full heme incorporation (see Materials and Methods). Identical spectra for all redox and ligation states were obtained for Aer2 1-402, Aer2 1-317 (data not shown), and Aer2 173-289 proteins (Figure 3.2 and Table 3.2). We conclude that the Aer2 HAMP domains are not in close proximity to, nor do they exert an influence on, the heme active site.

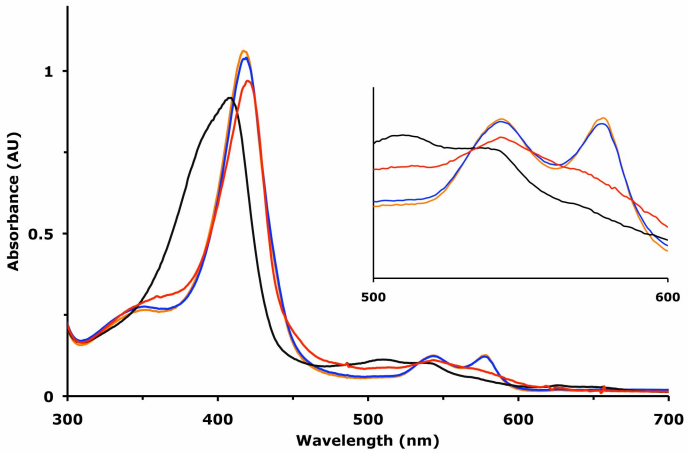

Figure 3.3. Aer2 PAS Domain Directly Senses Oxygen. UV-Visible spectrum of the Aer2 PAS domain with bound oxygen (orange), oxy-complex in the presence of CN^- (blue), Fe(III) (black), Fe(III)-CN^- complex formed upon addition of CN^- to Fe(III) state. The spectrum of the oxy-complex is unchanged upon addition of CN^- but alters its Fe(III) spectrum in the presence of CN^-.

To further investigate possible PAS/HAMP interactions we conducted pull-down assays of the individual domains (1-172, 173-289, 290-432) and domains in tandem (1-289 with 290-432) for increased sensitivity. All experiments were carried out with 40 mM Imidazole to eliminate non-specific binding of untagged proteins to Ni-NTA beads. Initial results did not detect any direct interactions (Figure 3.4). The binding affinity may be too low to detect using this method but presumably any possible interaction is not transient making this situation unlikely. The ligation state in the above mentioned results was Fe(III) with imidazole bound, which mimics oxygen binding. However, additional signaling states, including Fe(II)-O_2 and Fe(II), need to be assayed before any strong conclusions can be drawn (We note that the Fe(III) signaling state can not be assayed due to the high concentration of imidazole needed to eliminate non-specific binding but that imidazole does not effect the UV-Visible spectra of the Fe(II) state). These results do not rule out any PAS/HAMP interactions in Aer2 but do suggest that Aer2 may utilize an alternative mode of signal transduction that does not involve direct side-on interactions as represented in EcAer.

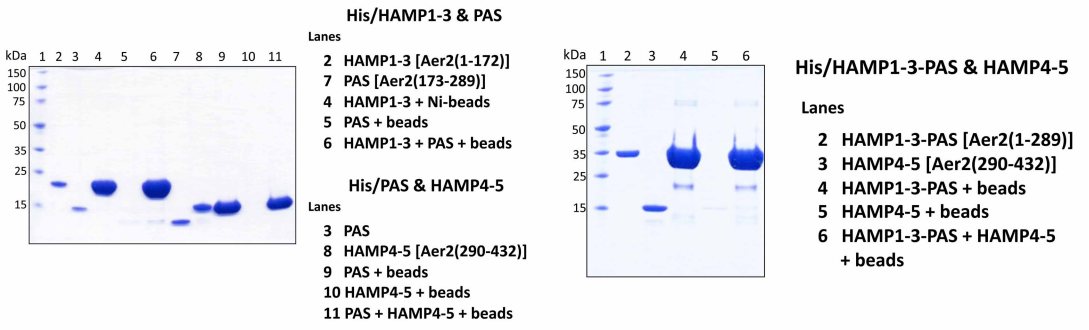

Figure 3.4. Pull-Down Assays of Aer2 PAS and HAMP Domain Protein Fragments. Pull-down assays were unable to detect binding of the PAS domain to either HAMP1-3 or HAMP4-5 fragments.

Determination of Quaternary Structure using Small Angle X-ray Scattering (SAXS)

If signal transduction in Aer2 does not involve direct PAS/HAMP interactions then it must adopt a radically different quaternary structure, as compared to EcAer, with the PAS domains not adjacent to either the N- or C-terminal HAMP domains (Figure 1.1), but rather located above or below. Small-angle X-ray scattering (SAXS) is an ideal technique for obtaining low-resolution molecular envelopes and is particularly useful to reconstruct the quaternary structure of individual domains with known atomic structures (Putnam et al., 2007). In addition, SAXS data is collected from protein samples in solution and allows comparison of different signaling states capable of detecting any large scale conformational changes (Lamb et al., 2008; Lamb et al., 2009).

SAXS data were collected for Aer2 protein fragments 1-172, 1-317, and 1-402 to allow unambiguous identification of domain arrangement through comparison. Great care was taken to ensure experimental data were suitable for SAXS analysis (see Materials and Methods). In summary, Guinier analysis and a plot of the intensity at zero scattering angle (I_0) vs. concentration (Figure 3.5) indicated all samples were monodisperse and suitable for *ab initio* reconstruction (Tables 3.3, 3.4, 3.5). Additionally, a maximum distance (D_{max}) for each receptor fragment was determined by calculating the pair-wise electron density distribution function (P(r)) (Figure 3.5 and Tables 3.3, 3.4, 3.5). Ten *ab initio* reconstructions were carried out for each protein using DAMMIN (Svergun and Koch, 2002) and the resulting models were compared and averaged using DAMAVER to generate final models (Figure 3.6). The accuracy of SAXS reconstructions can be improved by imposing symmetry constraints (Putnam et al., 2007). We imposed P2 symmetry given the inherent two-fold symmetry in HAMP structure. However, all reconstructions failed to identify the

correct two-fold axis and the presented data and reconstructions were generated without any symmetry constraints.

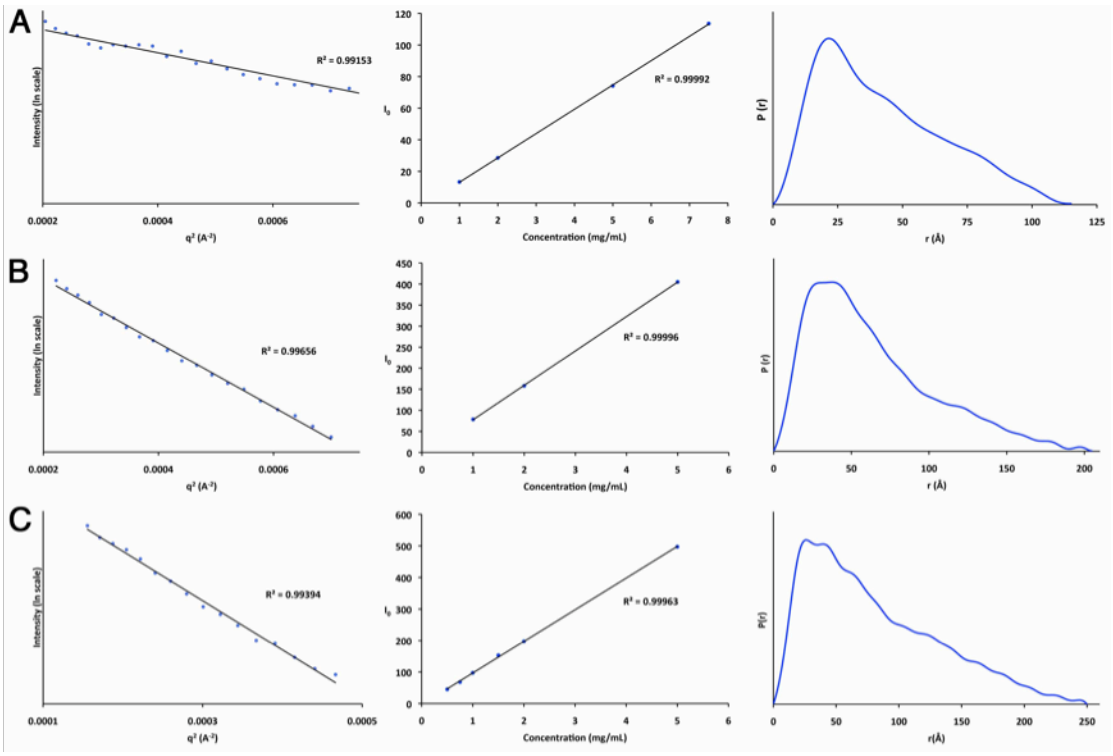

Figure 3.5. SAXS Parameters for Data Validation and Interpretation.
(A) Guinier plot, plot of intensity at zero scattering angle (I_0) vs. protein concentration (mg/mL), and plot of pair-wise electron density distribution (P(r)) vs. r (Å) for Aer2 1-172. (B) Guinier plot, plot of I_0 vs. concentration (mg/mL), and plot of P(r) vs. r (Å) for Aer2 1-317. (C) Guinier plot, plot of I_0 vs. concentration (mg/mL), and plot of P(r) vs. r (Å) for Aer2 1-402. D_{max} occurs when P(r) reaches zero. Data confirm all protein samples as monodisperse and suitable for SAXS analysis.

Table 3.3. Aer2 1-172 SAXS Parameters for Data Validation and Interpretation.

Merged Data

Experimental	
q-range	0.0125 - 0.319 $Å^{-1}$
resolution	503 - 19.7 Å
R_g (Guinier plot)	32.4 Å
R_g ((P(r))	34.1 Å
D_{max}	115 Å
Structure modeling	
Goodness of fit (χ^2)	1.02
NSD	1.00
R_g model	32.0 Å
D_{max} model	112.2 Å

Raw Data

Concentration (mg/mL)	**Rg (Guinier plot)**	**I_0 (Guinier plot)**
1	28.0 Å	13.291
2	31.0 Å	28.514
5	32.4 Å	74.1
7.5	33.4 Å	113.54

Table 3.4. Aer2 1-317 SAXS parameters for data validation and interpretation.

Merged Data

Experimental	
q-range	0.0149 - 0.319 $Å^{-1}$
resolution	422 - 19.7 Å
R_g (Guinier plot)	45.8 Å
R_g ((P(r))	52.8 Å
D_{max}	205 Å
Structure modeling	
Goodness of fit (χ^2)	1.16
NSD	0.64
R_g model	51.8 Å
D_{max} model	193 Å

Raw Data

Concentration (mg/mL)	**Rg (Guinier plot)**	**I_0 (Guinier plot)**
1	45.4 Å	78.5
2	45.4 Å	158.2
5	45.8 Å	405

Table 3.5. Aer2 1-402 SAXS parameters for data validation and interpretation.

Merged Data

Experimental	
q-range	0.01247 - 0.319 $Å^{-1}$
resolution	504 - 19.7 Å
R_g (Guinier plot)	62.7 Å
R_g ((P(r))	67.8 Å
D_{max}	250 Å
Structure modeling	
Goodness of fit (χ^2)	1.31
NSD	0.69
R_g model	66.4 Å
D_{max} model	237.8 Å

Raw Data

Concentration (mg/mL)	**Rg (Guinier plot)**	**I_0 (Guinier plot)**
0.5	57.5 Å	45.025
0.75	58.3 Å	68.05
1	59.2 Å	97.25
1.5	59.8 Å	152.8
2	61.2 Å	197.4
5	62.7 Å	497.2

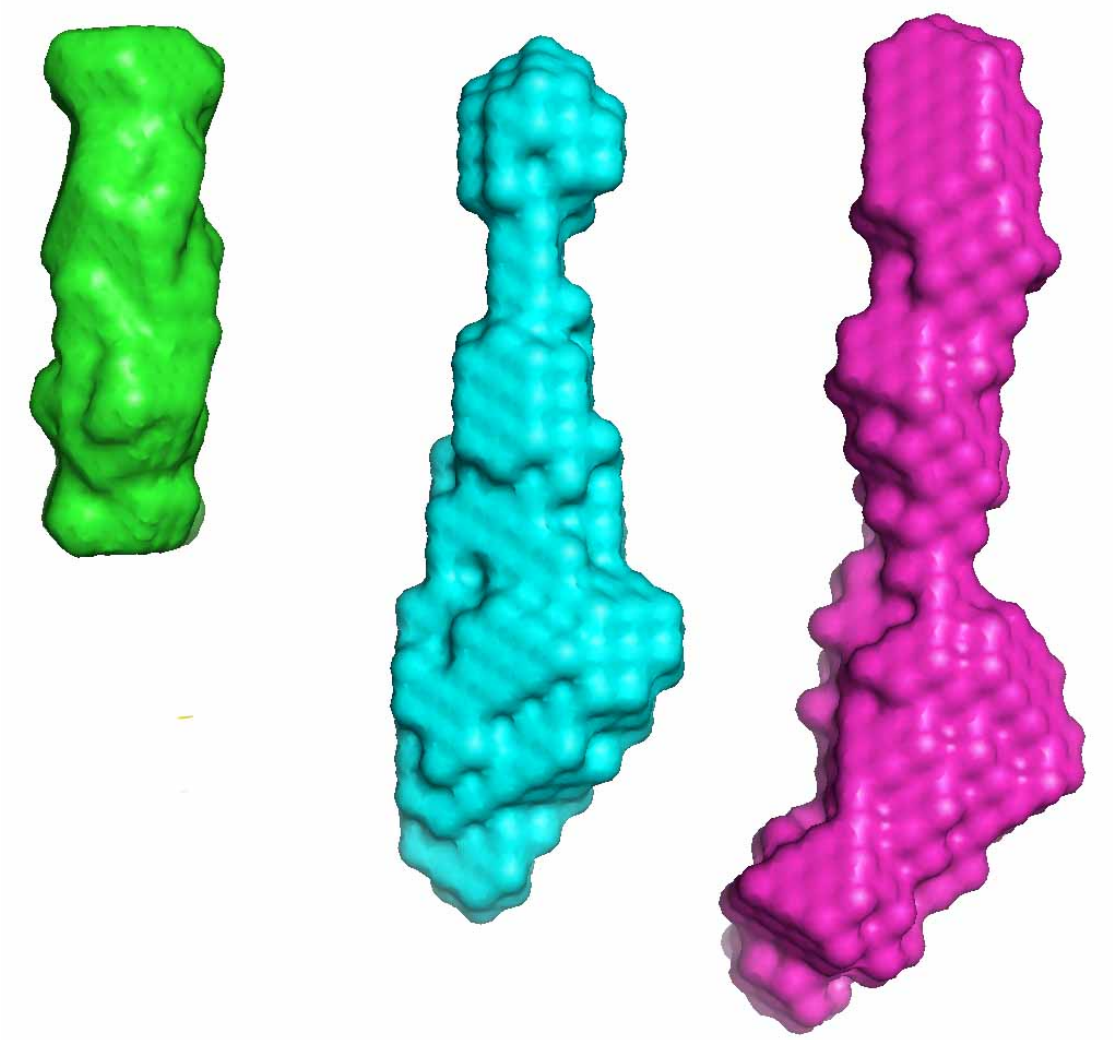

Figure 3.6. *Ab initio* SAXS Reconstructions of Aer2 Protein Fragments. Molecular envelopes of Aer2 1-172 (green) comprising only the three N-terminal HAMP domains, Aer2 1-317 (blue) containing three N-terminal HAMP domains, the PAS domain, and AS-1 and linker of HAMP4, and Aer2 1-402 (magenta) containing the three N-terminal HAMP domains, the PAS domain, and the two C-terminal HAMP domains. Molecular envelopes were generated using DAMMIN.

In agreement with previously discussed data, the D_{max} values and *ab initio* reconstructions derived from the SAXS data are consistent with a lack of direct PAS and HAMP interactions. The calculated D_{max} for each protein increased with the addition of each domain and implies a linear domain arrangement (Figure 3.6). *Ab*

initio reconstructions also clearly distinguish the three N-terminal HAMP domains, the PAS domains, and the C-terminal HAMPs (Aer2 1-402) or C-terminal PAS extension (AS1/connector of HAMP4 (290-317) in Aer2 1-317) that occur sequentially (Figure 3.6). Interestingly, the two C-terminal HAMP domains in the final averaged Aer2 1-402 model did not run parallel to the three N-terminal HAMP domains. However, this feature may be a product of an inherent flexibility between all domains or be artifactual given the highly elongated nature of the Aer2 receptor, which increases the search volume compared to globular proteins, making reconstructions less accurate.

Given the linear arrangement of domains we constructed a full-length model of Aer2 by superimposing the PAS structure C-terminal helix (AS1 of HAMP4) with the known N-terminal HAMP domain structures of Aer2. Superposition placed the β sheets of both PAS domains in close proximity, which is well characterized as the common PAS-PAS dimerization interface (Moglich et al., 2009b). Superposition with the two different HAMP conformations resulted in varying degrees of proximity and relative PAS-PAS orientations. After the final PAS structure model is complete a more thorough analysis needs to be undertaken, but superposition with Aer2 HAMP2 brought the PAS β sheets in close proximity and were slightly offset (Figure 3.7), which is similar to known PAS homodimers, while superposition with the differing conformation of Aer2 HAMP1 separated the PAS domains (data not shown). These differences may reflect a mode of signal transduction involving changes in PAS dimerization but final conclusions from this analysis must wait until the Aer2 PAS structure is fully refined. To construct the final model of Aer2 1-402 (Figure 3.7) the N-terminal HAMP domain structure (1-157) was placed slightly above the two adjacent PAS domains (173-307) and the concatenated Aer2 HAMP2-3 unit was modeled as the C-terminal HAMP domains (290-382) with a coiled-coil C-terminal extension (383-402). This final model (Figure 3.7) is fully consistent with the D_{max}

from the SAXS data and differs only slightly with the Aer2 1-402 *ab initio* reconstruction, which takes into account domain flexibility in solution.

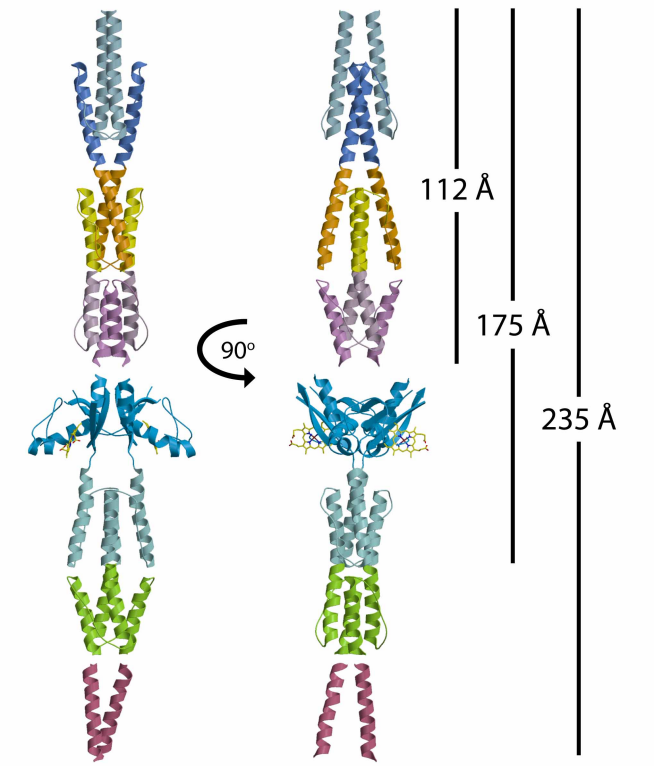

Figure 3.7. Reconstructed Model of Aer2 1-402 with a Linear Domain Arrangement. Model for Aer2 1-402 domain arrangement based on known crystal structures and SAXS data. A region of unknown structure between HAMP3 and the PAS domain would connect residues 157 and 173. D_{max} values derived from the SAXS data are displayed on right and are only consistent with the linear domain arrangement as shown. Signal transduction must occur through helix translations and rotations incurred through upstream changes in PAS dimerization.

The facilities at the SIBYLS beamline allowed us to also collect SAXS data for the ferrous redox state allowing us to ask; do large scale changes in protein structure exist between Aer2 signaling states? Superposition of the scattering curves from the ferrous and oxygen bound states revealed identical scattering curves. Thus, Aer2 does not

undergo major structural rearrangements during signal transduction. Conformational changes must be limited to minor changes in domain arrangement, unresolvable at the resolution of SAXS.

PAS Domain Dimerization

PAS dimerization is known to be a common mode of signal transduction (Moglich et al., 2009b; Zoltowski and Crane, 2008; Zoltowski et al., 2007). Given the close proximity of the Aer2 PAS domains in the full length receptor, it is likely that the Aer2 PAS domains exist as either a constitutive dimer and alter their packing interface or switch between PAS monomers, in close proximity, and a PAS-PAS homodimer. Both mechanisms would require modest changes in dimerization affinity with a switching mechanism also requiring a weak overall affinity given both the N- and C-terminal HAMP domains are constitutive dimers and would constrain PAS motions to a small volume.

Preliminary analysis using size-exclusion chromatography indicates the Aer2 PAS domain has a low affinity for dimerization which changes dependent on the redox/ligation state of the iron-heme center (Figure 3.8 and Table 3.6). At a low concentration (27 μM) the oxy complex is a monomer (MW_{app} = 12.9 kDa, MW_{actual} = 13.5) but increases its radius of hydration, which may indicate dimerization, at higher concentration. Upon oxidation to the ferric state dimerization affinity may increase with larger MW_{app}'s of 13.6 (27 μM) and 19.0 kDa (335 μM). Changes in elution volume do not necessarily involve changes in oligomeric state and may also reflect conformational changes in protein structure, i.e. unfolding of a helix (Harper et al., 2004). However, the concentration dependence of the elution volume suggests the Aer2 PAS domains do dimerize. A more thorough analysis using static light scattering will need to be conducted to confirm these results. In addition, the signaling states of Aer2 are not clearly defined and the biological relevance of the ferric state is still

unknown. Future studies should include an analysis of the ferrous signaling state, as *in vivo* studies find Aer2 responds to diatomic gases and *in vivo* may only access the ferrous and oxy complex, as well as Fe(II) complexes with both NO and CO diatomic gases, signaling states. It is of note that the similar oxygen sensing heme-binding PAS domain FixL, which cycles between Fe(II) and Fe(II)-O_2 *in vivo*, displays similar activity for both ferric and ferrous states (Moglich et al., 2009a). However, it is not known if Aer2 shares the same signaling properties as FixL.

Implications for Signal Transduction

The domain arrangement of Aer2 differs drastically from EcAer and does not involve direct side-on interactions. Aer2 represents a new paradigm for signal transduction applicable to proteins containing successive PAS and HAMP domains. Preliminary analysis indicates the Aer2 PAS domains alter their affinity for dimerization in a redox/ligation state dependent manner. Spatial rearrangement of the PAS domains would alter the position and orientation of the downstream C-terminal HAMP helices. Recently, a general mechanism for HAMP domain signal transduction has emerged (Airola et al., 2010; Zhou et al., 2009) involving a change in the heptad coiled-coil packing. This "stutter compensation" mechanism involves a shift from standard coiled-coil packing, where every 7^{th} residue is in the same position (7n), to incorporate a "stutter", an addition of 4 residues (7n +4). Stutters disrupt helical packing (Lupas and Gruber, 2005) and often result in helix kinks, as found at the interface of Aer2 HAMP2/3 (Airola et al., 2010). The structure of the Aer2 PAS domain reveals, that like other PAS domains with C-terminal helices (Moglich and Moffat, 2007), an additional four residues occur prior to the heptad repeat of HAMP4 AS1 (7n +4). We suggest that changes in PAS dimerization alter the heptad periodicity of the attached C-terminal AS1 helix, either adding or removing the helical stutter,

which induces a global rearrangement of the downstream HAMP domains propagating the signal downstream.

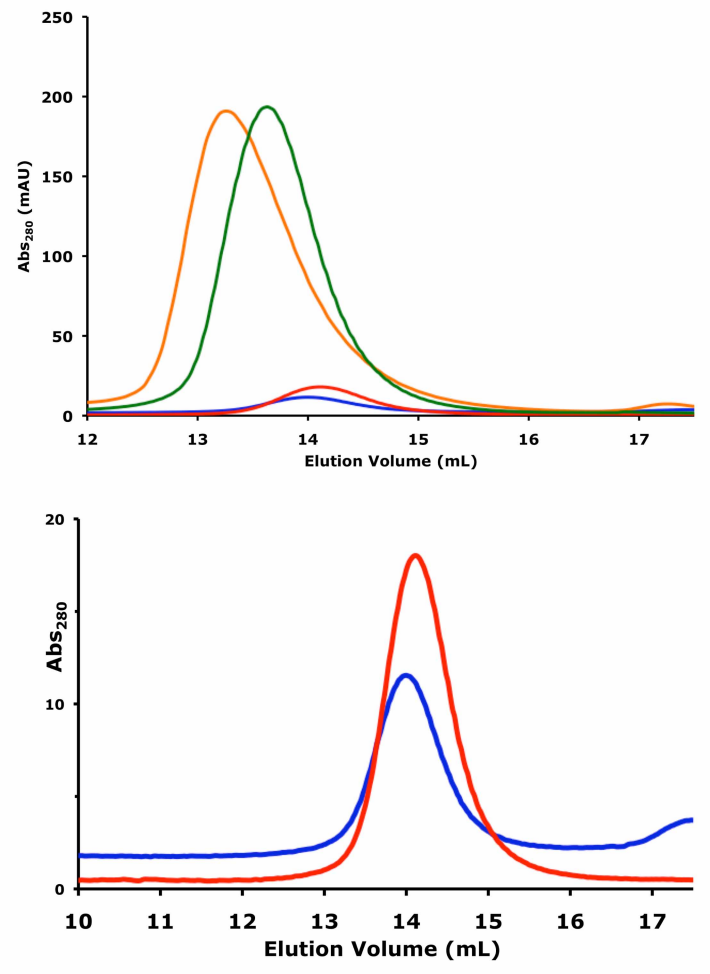

Figure 3.8. Aer2 PAS domain dimerization affinity is dependent on the heme redox/ligation state. Elution profile of Aer2 PAS domain showing an increase in apparent MW upon oxidation of heme to ferric state (27 μM, MW_{app} = 13.6 kDa, blue) (335 μM, MW_{app} = 19.0 kDa, orange) compared to oxy complex (27 μM, MW_{app} = 12.9 kDa: red) (335 μM, MW_{app} = 16.1 kDa: green). The concentration dependence of the elution volume indicates both iron-heme states support dimerization with differing affinities.

Table 3.6. Dependence of Aer2 173-289 Apparent MW (MW_{app}) on Protein Concentration and Redox/Ligation State

Concentration (μM)	Redox/Ligation State	MW_{app} (kDa)
27	Fe(II)-O_2	12.9
335	Fe(II)-O_2	16.1
27	Fe(III)	13.6
335	Fe(III)	19.0

This mechanism may have broad implications in other biological signaling systems. The junction between the Aer2 PAS domain and AS1 helix resembles a subset of PAS domains that signal to attached effector domains through short C-terminal helical segments (Moglich et al., 2009b). Sequence analysis of these short C-terminal helices suggests they form coiled-coil structures and typically occur with a 7n + 4 length. Altering the heptad periodicity of these short C-terminal helices effects downstream signaling (Moglich et al., 2009a). These signaling helices may mimic HAMP domains and an analogous mechanism involving stutter compensation may also apply in these similar signal transduction systems.

Additionally, the linear arrangement of the Aer2 PAS and HAMP domains resembles the structure of transmembrane receptors containing periplasmic PAS sensors attached to a downstream HAMP domain through a short transmembrane spanning helix. The minor conformational changes displayed by Aer2 between different signaling states are fully consistent with the constrained motions of transmembrane helices. Soluble and transmembrane receptors, such as CitA, may differ in their cellular location but utilize identical modes of signal transduction.

3.4 Summary

We have reconstructed the structure of the soluble receptor Aer2 by combining atomic resolution structures of the individual PAS and HAMP domains with solution SAXS data. The final result indicates the Aer2 PAS and HAMP domains do not directly interact and are arranged in a linear fashion, consistent with the results of both UV-Visible spectra and pull-down assays. A mechanism of signal transduction likely involves changes in PAS dimerization dependent on the signaling state of the iron-heme. Overall, the quaternary structure of Aer2 better represents the domain arrangement other successive PAS and HAMP domains and establishes a new paradigm for PAS-HAMP signaling that may be widely applicable to other signaling systems.

3.5 Materials and Methods

Protein Expression and Purification

Various fragments (1-289, 1-402, 173-289, and 173-307) of the gene encoding *Pseudomonas aeruginosa* PAO1 Aer2 were cloned into the pET28a vector between NdeI and HindIII restriction sites, which added a cleavable N-terminal His-tag. Surface entropy reduction mutants of Aer2 173-307 were generated either by PCR (SER A), overlap extension (SER B, C, D, E), or Quik-Change (SER F) using standard protocols. For overexpression, plasmids were transformed into BL21 (DE3) cells, grown at 37° C in Luria Broth (LB) to an OD_{600} = 0.6 and incubated with 100 mM IPTG at either 18°C (1-402) or 23°C (1-289, 173-289, 173-307) for 20 hrs before harvesting cells. *E. coli* ferrochelatase was coexpressed with Aer2 1-402 to promote full heme incorporation as previously described (Sudhamsu J, 2010). Proteins were purified using a Ni-NTA column following the manufacturers recommended protocol (Qiagen). After thrombin digestion His-tag free protein was applied to either a

Superdex 75 26-60 Hi-Prep Column (173-289 and 173-307) or a Superdex 200 26-60 Hi-Prep Column (1-289 and 1-402) equilibrated with either 20 mM Imidazole, pH 8.0, 50 mM NaCl (1-289, 173-289, and 173-307) or 20 mM Imidazole, pH 8.0, 100 mM NaCl, 5% glycerol (1-402). Concentrated protein was aliquoted, flash frozen, and stored at -80°C. Aer2 1-172 was purified as previously described (Airola et al., 2010).

To generate Se-Met protein, the Aer2 173-307 K176A (SER A) plasmid was transformed into B834 (DE3) cells, which are auxotrophic for methionine. An overnight culture in LB was spun down and washed twice with autoclaved water, then added to M9 minimal media supplemented with 19 standard amino acids and L-selenomethionine (50 mg/L). All Se-Met purification buffers contained 10 mM dithiothreitol (DTT) and Se-Met protein was purified otherwise as described for the native protein.

Crystallization and Data Collection

Crystals of native Aer2 173-307 K176A (SER A) protein (30-50 mg/mL) were grown by vapor diffusion against a reservoir containing 1.2-1.5 M $(NH_4)_2SO_4$, 0-15% glycerol, and 0.1 M MES pH 6.2-6.4 and appeared after 3-4 days at 17°C. The best quality crystals grew slowly over the course of 8 months to a size of 300-500 microns. Se-Met Aer2 173-307 K176A (SER A) protein (30-50 mg/mL) crystallized in the same space group (P6) under similar conditions. Solutions containing 1.65 M $(NH_4)_2SO_4$, 18% glycerol, 0.1 M MES, pH 6.2-6.4 were used as cryoprotectants. Native and MAD diffraction data were collected at the Cornell High Energy Synchrotron Source (CHESS) F2 beamline on an ADSC Quantum 210 CCD. Data were processed with HKL2000 (Otwinowski and Minor, 1997).

Structure Determination and Refinement

Diffraction data for Se-Met protein were processed with SOLVE (Terwilliger and Berendzen, 1999) and RESOLVE (Terwilliger, 2000) to generate initial electron

density maps based on anomalous diffraction from Se-Met sites (figure of merit = 0.50, resolution cutoff = 2.90 Å). A 75% complete structure was built into initial maps with XFIT (McRee, 1999) and refined against the peak data set using CNS (Brunger et al., 1998). Poor refinement statistics and poor electron density indicated possible twinning, which was confirmed by further analysis. Refinement in all hexagonal space groups with all possible twinning operations identified the correct space group as P6 with a twinning operation of k, h, -l, given the significantly lower refinement statistics (R factor = 33, R_{free} = 39) compared to other space groups/twinning operations (R factor ~ 43, R_{free} ~ 46). The current model is not yet complete but general features including helical, beta strand, and heme positions are clearly visible.

Redox and Ligation State Manipulation of Crystals

To generate different redox and ligation state species, crystals were soaked for 1-5 minutes in cryoprotectant buffer supplemented with various chemicals: oxy-complex (1 or 10 mM ascorbate), ferrous-NO (1 or 10 mM ascorbate and NOC-7), ferrous (100 mM ascorbate), ferric (1 or 10 uM $Fe(CN)_6$), and ferric-NO (10 uM $Fe(CN)_6$ and NOC-7). Addition of 100 mM ascorbate resulted in a loss of diffraction quality (2.8 Å) indicating either conformational changes associated with a change of redox state or radical damage.

UV-Visible Absorption Spectroscopy

Absorption spectra for Aer2 proteins were recorded at 25 °C in stoppered quartz cuvettes with an Agilent 8453 UV-Visible Absorption Spectrophotometer. Ferrous samples were prepared in an anaerobic glovebox by diluting concentrated protein in previously degassed sample buffer and treating with the reducing agent dithionite. Subsequent addition of the nitric oxide releasing compound NOC-7 produced the ferrous-NO complex. Ferrous-NO complexes could also be generated by addition of 1uM ascorbate and NOC-7. Oxy complexes were generated by either adding cold,

non-degassed buffer to dithionite treated ferrous Aer2 or by addition of 1 μM ascorbate to Aer2 protein in an aerobic environment. Ferric species were generated by addition of the oxidizing agent $Fe(CN)_6$. Subsequent treatment with NOC-7 produced the ferric-NO complex. Multiple rounds of buffer exchange were conducted to remove any trace of imidazole prior to spectroscopic measurements.

Size-exclusion Chromatography

The redox/ligation state of Aer2 protein was confirmed prior to and after elution for all experiments. Aer2 PAS protein samples were prepared as described and applied to an analytical Superdex 75 column. Apparent molecular weights were calculated based upon protein standards run just prior to experiments.

Small-angle X-ray Scattering Data Collection

Small-angle X-ray scattering data were collected at the SIBYLS beamline (Advanced Light Source, Lawrence Berkeley National Laboratories) using a MarCCD 165 detector capable of fast frame transfer mode. Protein samples at various concentrations and matching buffer samples were loaded into a 96 well plate and transferred to a helium purged sample chamber using a Hamilton robot. Data were collected for short (0.5 sec), long (5 sec), and short (0.5 sec) exposure times. Samples were checked for radiation damage by comparing data from both short exposure times. Guinier plots were used to evaluate potential sample aggregation and protein concentration effects. Initial data of Aer2 1-402 indicated interparticle repulsion (decreased scattering at I_o with increasing protein concentration). Buffer modification from 20mM imidazole, pH 8.0, 100 mM NaCl, 5% glycerol to 20 mM Imidazole, pH 7.0, 200 mM NaCl, 5% glycerol alleviated this effect generating monodisperse samples suitable for SAXS analysis. Ferrous samples were prepared by addition of excess dithionite in an anaerobic environment. Protein samples were loaded in a 96 well plate and sealed with an aluminum top impermeable to gas molecules. Exposure

to air was limited to a 2 sec transfer from the 96 well plate to the helium purged sample chamber in the Hamilton robot needle. Visual inspection of the samples during data collection revealed a solution color indicative of ferrous heme confirming the heme redox state as Fe^{2+}.

Small-angle X-ray Scattering Data Evaluation and Ab Initio Reconstruction

Prior to analysis the scattering from matching buffer samples was subtracted from the protein raw data to generate scattering curves due to protein alone. Guinier plots of all buffer subtracted scattering curves were analyzed using primus and used to calculate the radius of gyration (R_g) and intensity at zero scattering angle (I_o). Due to the elongated features of Aer2 proteins all values reported from the guinier plot include a range extending to R_g x 1.3. To optimize signal to noise ratios, merged data sets were created from short exposures, for small values of q, and long exposures, for large values of q. Pair-distribution functions were generated using GNOM. The resulting files were used for *ab initio* shape reconstruction using DAMMIN and did not impose symmetry constraints. Ten independent *ab initio* runs were compared and averaged using SUPCOMB and DAMAVER to generate the final molecular envelopes.

REFERENCES

Airola, M.V., Watts, K.J., Bilwes, A.M., and Crane, B.R. (2010). Structure of Concatenated HAMP Domains Provides a Mechanism for Signal Transduction. Structure *18*, 436-448.

Aravind, L., and Ponting, C.P. (1999). The cytoplasmic helical linker domain of receptor histidine kinase and methyl-accepting proteins is common to many prokaryotic signalling proteins. Fems Microbiology Letters *176*, 111-116.

Brunger, A.T., Adams, P.D., Clore, G.M., DeLano, W.L., Gros, P., Grosse-Kunstleve, R.W., Jiang, J.S., Kuszewski, J., Nilges, M., Pannu, N.S.*, et al.* (1998). Crystallography & NMR system: A new software suite for macromolecular structure determination. Acta Crystallographica Section D-Biological Crystallography *54*, 905-921.

Cole, C., Barber, J.D., and Barton, G.J. (2008). The Jpred 3 secondary structure prediction server. Nucleic Acids Research *36*, W197-W201.

Cooper, D.R., Boczek, T., Grelewska, K., Pinkowska, M., Sikorska, M., Zawadzki, M., and Derewenda, Z. (2007). Protein crystallization by surface entropy reduction: optimization of the SER strategy. Acta Crystallographica Section D-Biological Crystallography *63*, 636-645.

Dunin-Horkawicz, S., and Lupas, A.N. (2010). Comprehensive analysis of HAMP domains: implications for transmembrane signal transduction. Journal of Molecular Biology *397*, 1156-1174.

Gilles-Gonzalez, M.A., and Gonzalez, G. (2004). Signal transduction by heme-containing PAS-domain proteins. Journal of Applied Physiology *96*, 774-783.

Goldschmidt, L., Cooper, D.R., Derewenda, Z.S., and Eisenberg, D. (2007). Toward rational protein crystallization: A Web server for the design of crystallizable protein variants. Protein Science *16*, 1569-1576.

Harper, S.M., Christie, J.M., and Gardner, K.H. (2004). Disruption of the LOV-J alpha helix interaction activates phototropin kinase activity. Biochemistry *43*, 16184-16192.

Hazelbauer, G.L., Falke, J.J., and Parkinson, J.S. (2008). Bacterial chemoreceptors: high-performance signaling in networked arrays. Trends in Biochemical Sciences *33*, 9-19.

Herrmann, S., Ma, Q.H., Johnson, M.S., Repik, A.V., and Taylor, B.L. (2004). PAS domain of the Aer redox sensor requires C-terminal residues for native-fold formation and flavin adenine dinucleotide binding. Journal of Bacteriology *186*, 6782-6791.

Hong, C.S., Shitashiro, M., Kuroda, A., Ikeda, T., Takiguchi, N., Ohtake, H., and Kato, J. (2004). Chemotaxis proteins and transducers for aerotaxis in Pseudomonas aeruginosa. Fems Microbiology Letters *231*, 247-252.

Hulko, M., Berndt, F., Gruber, M., Linder, J.U., Truffault, V., Schultz, A., Martin, J., Schultz, J.E., Lupas, A.N., and Coles, M. (2006). The HAMP domain structure implies helix rotation in transmembrane signaling. Cell *126*, 929-940.

Key, J., and Moffat, K. (2005). Crystal structures of deoxy and CO-bound bjFixLH reveal details of ligand recognition and signaling. Biochemistry *44*, 4627-4635.

Lamb, J.S., Zoltowski, B.D., Pabit, S.A., Crane, B.R., and Pollack, L. (2008). Time-resolved dimerization of a PAS-LOV protein measured with photocoupled small angle X-ray scattering. Journal of the American Chemical Society *130*, 12226-+.

Lamb, J.S., Zoltowski, B.D., Pabit, S.A., Li, L., Crane, B.R., and Pollack, L. (2009). Illuminating Solution Responses of a LOV Domain Protein with Photocoupled Small-Angle X-Ray Scattering. Journal of Molecular Biology *393*, 909-919.

Lupas, A.N., and Gruber, M. (2005). The structure of alpha-helical coiled coils. Fibrous Proteins: Coiled-Coils, Collagen and Elastomers *70*, 37-+.

McRee, D.E. (1999). XtalView Xfit - A versatile program for manipulating atomic coordinates and electron density. Journal of Structural Biology *125*, 156-165.

Moglich, A., Ayers, R.A., and Moffat, K. (2009a). Design and Signaling Mechanism of Light-Regulated Histidine Kinases. Journal of Molecular Biology *385*, 1433-1444.

Moglich, A., Ayers, R.A., and Moffat, K. (2009b). Structure and Signaling Mechanism of Per-ARNT-Sim Domains. Structure *17*, 1282-1294.

Moglich, A., and Moffat, K. (2007). Structural basis for light-dependent signaling in the dimeric LOV domain of the photosensor YtvA. Journal of Molecular Biology *373*, 112-126.

Otwinowski, Z., and Minor, W. (1997). Processing of X-ray diffraction data collected in oscillation mode. Macromolecular Crystallography, Pt A *276*, 307-326.

Putnam, C.D., Hammel, M., Hura, G.L., and Tainer, J.A. (2007). X-ray solution scattering (SAXS) combined with crystallography and computation: defining accurate macromolecular structures, conformations and assemblies in solution. Quarterly Reviews of Biophysics *40*, 191-285.

Rebbapragada, A., Johnson, M.S., Harding, G.P., Zuccarelli, A.J., Fletcher, H.M., Zhulin, I.B., and Taylor, B.L. (1997). The Aer protein and the serine chemoreceptor Tsr independently sense intracellular energy levels and transduce oxygen, redox, and

energy signals for Escherichia coli behavior. Proceedings of the National Academy of Sciences of the United States of America *94*, 10541-10546.

Sudhamsu J, K.M., Airola MV, Patel BA, Yeh SR, Rousseau DL, Crane BR. (2010). Co-expression of ferrochelatase allows for complete heme incorporation into recombinant proteins produced in E. coli. Protein Expression and Purification.

Svergun, D.I., and Koch, M.H.J. (2002). Advances in structure analysis using small-angle scattering in solution. Current Opinion in Structural Biology *12*, 654-660.

Taylor, B.L. (2007). Aer on the inside looking out: paradigm for a PAS-HAMP role in sensing oxygen, redox and energy. Molecular Microbiology *65*, 1415-1424.

Taylor, B.L., and Zhulin, I.B. (1999). PAS domains: Internal sensors of oxygen, redox potential, and light. Microbiology and Molecular Biology Reviews *63*, 479-+.

Terwilliger, T.C. (2000). Maximum-likelihood density modification. Acta Crystallographica Section D-Biological Crystallography *56*, 965-972.

Terwilliger, T.C., and Berendzen, J. (1999). Automated MAD and MIR structure solution. Acta Crystallographica Section D-Biological Crystallography *55*, 849-861.

Watts, K.J., Johnson, M.S., and Taylor, B.L. (2008). Structure-function relationships in the HAMP and proximal signaling domains of the aerotaxis receptor Aer. Journal of Bacteriology *190*, 2118-2127.

Zhou, Q., Ames, P., and Parkinson, J.S. (2009). Mutational analyses of HAMP helices suggest a dynamic bundle model of input-output signalling in chemoreceptors. Mol Microbiol *73*, 801-814.

Zoltowski, B.D., and Crane, B.R. (2008). Light activation of the LOV protein Vivid generates a rapidly exchanging dimer. Biochemistry *47*, 7012-7019.

Zoltowski, B.D., Schwerdtfeger, C., Widom, J., Loros, J.J., Bilwes, A.M., Dunlap, J.C., and Crane, B.R. (2007). Conformational switching in the fungal light sensor vivid. Science *316*, 1054-1057.

CHAPTER 4

Defining Features of Membrane Associated HAMP Domains

4.1 Abstract

HAMP domains are widespread signaling modules that relay transmembrane signals into extracellular responses. Recently a subset of PAS domains, not directly associated with the membrane, were identified. The crystal structure of a 3-unit poly-HAMP chain from the soluble receptor Aer2 identified a universal architecture for all HAMP domains and determined a novel conformation. We tested whether the divergent Aer2 HAMP domains could function at the membrane. Aer2-Tar Chimera receptors (ATCs) were generated with both single and poly-HAMP domains. The results indicate a DExG motif is required to receive signal input at the membrane interface. Differing methylation responses to opposing HAMP conformations suggests HAMP domains alternate between these two states during signal transduction.

4.2 Results and Discussion

Aer2-Tar Chimeras (ATCs) were generated from the *Escherichia coli* aspartate receptor Tar by replacing the Tar HAMP domain with both single Aer2 HAMP domains and Aer2 poly-HAMP chains. The boundaries of HAMP domains are clearly defined and fusion sites were selected based on sequence alignment and known HAMP structures. Our aims were to assay essential features for HAMP domain function at the membrane, signal transduction through helical linkers, and possible signal inversion in poly-HAMP chains containing alternating conformations.

Aer2-Tar Chimeras Do Not Support Chemotaxis

ATC plasmids were transformed into *E. coli* BT3388 cells lacking all MCPs and Aer. As a control, Tar expressed from the same vector, pKG116, was also tested. All ATCs failed to support chemotaxis and lacked the defining outer ring as displayed by Tar (Figure 4.1). Receptors fell into two classes with H1 and H1-2 displaying an enlarged swarm radii indicating a CW bias (kinase on) phenotype (Table 4.1). H1-23 shared this same feature but to a lesser degree. ATCs H2, H3, and H23 displayed a CCW (kinase off) bias phenotype with a small swarm radius (Figure 4.1).

We conducted temporal assays for each receptor with increasing concentrations of aspartate. The signaling state of cells, CW (tumbling) or CCW (smooth swimming), was monitored under a microscope. Tar had random motility without aspartate and very smooth swimming immediately after addition of 1 mM aspartate. Both H1 and H1-2 had strong CW-biases, explaining their larger swarms. Neither mutant responded to changes in aspartate. All other ATC mutants had CCW bias in motility buffer and also did not respond to aspartate (Table 4.2). Western blots, using anti-Tsr antibody, confirmed all ATCs had stable expression in BT3388.

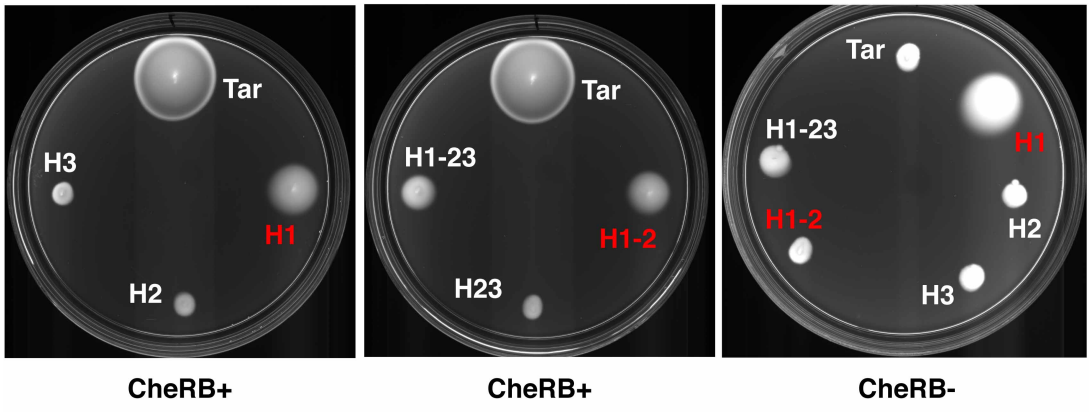

Figure 4.1. Swarm Assays of Aer2-Tar Chimeras.
Chemotactic ability of ATC mutants in *E. coli* strains BT3388 (MCP-, Aer-, CheRB+) and UU2610 (MCP-, Aer-, CheRB-). All ATC mutants lacked an outer cell ring (see Tar) diagnostic of a functioning chemotaxis system. Both ATCs containing Aer2 HAMP1 (H1) and HAMP1-2 (H1-2) had enlarged swarm diameters in CheRB+ cells indicative of a CW bias. The differential swarm diameters of H1 and H1-2 in CheRB+ and CheRB- cells suggests the methylation system responds differently to these two receptors signifying the C-terminal HAMP domains send opposing signals downstream.

Table 4.1. Summary of Soft-Agar Assays in CheRB+ and CheRB- Strains

Receptor	CheRB+	CheRB-
Tar wt	functional	CCW bias
H1	CW bias	CW bias
H2	CCW bias	CCW bias
H3	CCW bias	CCW bias
H1-2	CW bias	CCW bias
H23	CCW bias	NA
H1-23	slight CW bias	slight CW bias

The clear CW bias phenotypes of H1 and H1-2 indicated these receptors formed functional chemoreceptor arrays and activated CheA more so than wt Tar. This suggests that signal input is effectively decoupled from the kinase binding region due to non-functional HAMP domains. The second class of receptors was unable to

activate CheA, which may be due to an inability to form functional signaling clusters or an enforced CCW state.

Table 4.2. Visualization of Attractant and Repellant Induced Responses

Receptor	air	Asp+	Ni+
pKG116	CCW	NR	NR
Tar wt	CW bias	CCW	CW
H1	CW bias	NR	strong CW
H2	slight CW bias	NR	slight CW
H3	slight CW bias	NR	slight CW
H1-2	strong CW bias	NR	strong CW
H23	CCW bias	NR	slight CW
H1-23	slight CW bias	NR	slight CW
H1D	CW bias	CCW	CW
H1P	CW lock	NR	NA
H1DP	slight CW bias	NR	slight CW
H1D-2	strong CW bias	NR	strong CW
H1P-2	strong CW bias	NR	strong CW
H1DP-2	strong CW bias	NR	strong CW
H1D-23	slight CW bias	NR	slight CW
H1P-23	slight CW bias	NR	slight CW
H1DP-23	slight CW bias	NR	slight CW

Methylation and demethylation by the adaptation proteins CheR and CheB resets the zero point of MCPs to allow detection of a wide, dynamic range of chemical gradients (Hazelbauer et al., 2008). Adaptation responses can reverse HAMP domain signaling and mask underlying biases. Swarm assays were conducted in the *E. coli* CheRB- strain UU2610. The CCW class of receptors behaved identically in both CheRB- and CheRB+ cells (Table 4.1). Interestingly, removal of the adaptation system altered the phenotype of H1-2 from a CW to CCW bias (Figure 4.1), while H1

displayed a larger swarm radius. In CheRB+ cells H1 and H1-2 exhibited similar CW bias phenotypes that suggests the methylation system responds differently to these two receptors. HAMP1 and HAMP2 occupy alternate conformations in the crystal structure of Aer2 1-172 (Figure 1.2). The results suggest these different HAMP conformations send opposite signals to downstream domains.

Reconstitution of Signal Input

The Aer2 HAMP domains represent the subset of HAMP domains that are not associated with the membrane and typically concatenate to form poly-HAMP chains (Airola et al., 2010; Dunin-Horkawicz and Lupas, 2010). This subset of HAMP domains contains a conserved glycine residue at the start of AS2 to allow the close association required in a poly-HAMP chain (Airola et al., 2010). Membrane associated HAMP domains differ and contain a conserved DExG motif, thought to be important for transmembrane signal input (Dunin-Horkawicz and Lupas, 2010). In addition, the HAMP domain of Tar and other MCPs contain a highly conserved proline residue, near the beginning of AS1, which may also be important for signal input (Zhou et al., 2009).

We introduced these putative signal input motifs into ATC receptors containing HAMP1 (H1, H1-2, and H1-23) in an effort to reconstitute signal input and recouple the kinase binding region to stimuli. Both single and combined DELG and Pro mutations were introduced to determine if one, both, or either mutation could affect function. Swarm assays were conducted in BT3388 cells and all mutants again failed to support chemotaxis. We then conducted temporal assays to assess any attractant induced responses. The DELG mutant of H1 (H1D) was CW biased in air and switched to CCW a few seconds after addition of aspartate (1 μL of 10 mM) (Table 4.2). This response was slower compared to Tar, which changes to CCW instantaneously, but demonstrates that H1D is a functional receptor capable of

receiving and transmitting transmembrane signals. The Pro mutant of H1 (H1P) was CW-biased and did not respond to aspartate. The H1DP mutant, containing both DELG and Pro mutations, was CCW biased and did not respond to aspartate. The deleterious effect of the proline residue suggests, that unlike the DExG motif, it is not required for signal input in membrane associated HAMP domains.

All H1-2 DELG and Pro receptors (H1D-2, H1P-2, and H1DP-2) had CW biases and showed no response to aspartate. However, the opposite phenotype of H1-2, compared to H1, in CheRB- cells suggests this receptor would propagate an inverted response to aspartate. Actions of the adaptation system complicate our current analysis and temporal assays in a CheRB- strain may result in attractant induced responses. We hypothesize that in a CheRB- strain H1D-2 will display a CCW bias and will switch to CW after addition of aspartate. H1P-2 and H1DP-2 will most likely remain non-functional receptors.

All DELG and Pro mutations in H1-23 had a slight CW bias and did not respond to addition of aspartate. This is not unexpected as the H1-23 receptor displays only a minor CW bias in both CheRB+ and CheRB- strain. Diminished CheA activation may correlate with either a higher degree of oscillation in the C-terminal HAMP domain or a dampening effect due to the long distance of signal propagation from HAMP1 to HAMP3.

Structural Basis for the Importance of the DExG Motif

Reconstitution of H1 function by the DExG motif raises the interesting mechanistic question: Why and what role do these residues play during signal transduction? Insights are gained by analyzing the NMR structure of the Af1503 HAMP domain (Hulko et al., 2006), which adopts a similar conformation to Aer2 HAMP1 (Airola et al., 2010). The aspartate residue (D) of Af1503 hydrogen bonds with an arginine sidechain of the connector. However, this Arg is not highly conserved

and this interaction may not be significant. The glutamate residue (E) appears to play the most prominent structural role of the three residues. In Af103, the E311 sidechain hydrogen bonds with the peptide backbone of a T281 located at the start of AS1 (Figure 4.2). This interaction may couple transmembrane induced motions of AS1 to AS2 to incur a global rearrangement of HAMP domain structure. Additionally, the absence of a sidechain in G313 allows the connector to pack up against AS2 which may be facilitate proper positioning of E311.

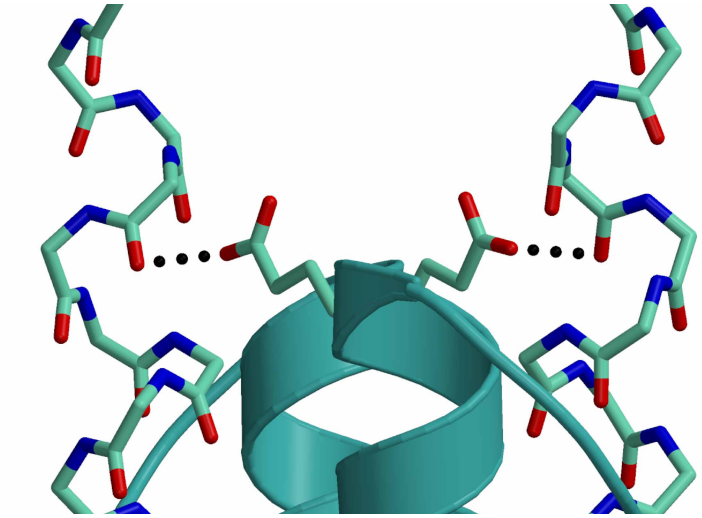

Figure 4.2. Glutamine Residue of the DExG Motif Links AS2 to AS1
A hydrogen bond between Glu311, of the DExG motif, to the peptide backbone of AS1 in Af1503 links the AS1 (peptide ball-and-stick) and AS2 (ribbon) helices. In membrane associated HAMP domains, signal input travels through transmembrane helix2 (TM2) to AS1. The glycine residue (not shown), of the DExG motif, allows the connector to pack against AS2 due to an absence of a sidechain residue.

The structure of the Af1503 HAMP domain represents only one signaling state of HAMP domains (Airola et al., 2010). Here we have demonstrated the alternative conformation of Aer2 HAMP2 does represent an opposing signaling state to the

similar conformations of HAMP1 and Af1503. In HAMP2, the AS1 and AS2 helices alter their helical register (Airola et al., 2010), and would bring T281 closer to E311 in Af1503. These conformational changes may correlate with a rearrangement of the DExG motif interactions seen in Af1503 and possibly involve D310 in a more prominent role.

Although H1D was capable of switching in response to stimuli, it failed to support chemotaxis. Unlike Tar, switching was not instantaneous and occurred 2-5 seconds after addition of aspartate. Comparatively, the adaptation response is evolutionarily tuned to Tar, and other similar MCPs, and occurs over the time course of five seconds. Thus, the lack of chemotactic function for H1D may derive simply from slow response times and require a less robust adaptation system.

Future Work

Currently, we are pursuing structural information for the DELG motif in Aer2 HAMP2. This region of HAMP2 is not involved in the crystal contacts of Aer2 1-172 and we are hopeful this mutant will crystallize under the same conditions as the wild type protein. To complete are study we are also introducing DELG and Pro mutations into ATC mutants containing HAMP2 and HAMP3 as the N-terminal HAMP domain (H2, H3, and H23) in an attempt to reconstitute signal input and verify our results for H1D. However, given the CCW phenotypes (kinase off) of these receptors it is not unlikely that after introduction of the DELG motif these receptors will remain non-functional.

4.3 Materials and Methods

Cloning and Mutation of Aer2-Tar Chimeras (ATCs)

E. coli Tar was cloned from genomic DNA into Litmus 28i with 5' XbaI-NdeI and 3' HindIII-XhoI restriction sites. An internal NdeI site in Tar was silently removed (CAT

ATC to CAC ATG). Silent mutations engineered BamHI and PmlI restriction sites at the 5' and 3' ends of the Tar HAMP domain respectively. Aer2 HAMP PCR fragments were cloned into Tar using the BamHI and PmlI sites to generate Aer2-Tar Chimeras containing different Aer2 HAMP domain fragments. Full-length ATC receptors were transferred to pKG116 containing a salicylate inducible promoter. Mutations were accomplished using either the Quik-Change strategy or overlap extension. The correct sequence for all clones was confirmed by direct nucleotide sequencing in Litmus 28i and successful transfer to pKG116 by restriction digest test.

Addition of the DELG and Pro residues into HAMP1 containing ATCs in pKG116 was accomplished by site-directed mutagenesis using the Quik-Change strategy. Mutations were confirmed by direct nucleotide sequencing of the HAMP region. Regions upstream and downstream were assumed to be correct and will be confirmed at a later date.

Soft Agar Chemotaxis Assays

Chemotactic ability of plasmid-containing E coli BT3388 lacking all native MCPs and Aer and UU2610 additionally lacking the adaptation proteins CheR and CheB was assessed at 30°C on tryptone soft agar plates containing appropriate concentrations of chloramphenicol, aspartate, and 0.5, 1, and 2 mM Na salicylate.

Visualization of Attractant and Repellant Induced Responses

Responses of plasmid-containing E. coli BT3388 and UU2610 to attractant and repellant stimuli were directly visualized under a microscope. All cells were assayed in motility buffer. Varying amounts (1, 5, or 10 μL) of stock solutions of aspartate (10 mM) and $NiCl_2$ (5 mM) were added directly to cells. Aspartate and Ni were added to the same cell drops for Tar and different cell drops for all ATC mutants and pKG116 vector control.

4.4 Contributions

M.V.A. performed all cloning and site-directed mutagenesis. Kylie J. Watts (Loma Linda University) performed all soft agar chemotaxis assays and direct visualization of responses.

REFERENCES

Airola, M.V., Watts, K.J., Bilwes, A.M., and Crane, B.R. (2010). Structure of Concatenated HAMP Domains Provides a Mechanism for Signal Transduction. Structure *18*, 436-448.

Dunin-Horkawicz, S., and Lupas, A.N. (2010). Comprehensive analysis of HAMP domains: implications for transmembrane signal transduction. Journal of Molecular Biology *397*, 1156-1174.

Hazelbauer, G.L., Falke, J.J., and Parkinson, J.S. (2008). Bacterial chemoreceptors: high-performance signaling in networked arrays. Trends in Biochemical Sciences *33*, 9-19.

Hulko, M., Berndt, F., Gruber, M., Linder, J.U., Truffault, V., Schultz, A., Martin, J., Schultz, J.E., Lupas, A.N., and Coles, M. (2006). The HAMP domain structure implies helix rotation in transmembrane signaling. Cell *126*, 929-940.

Zhou, Q., Ames, P., and Parkinson, J.S. (2009). Mutational analyses of HAMP helices suggest a dynamic bundle model of input-output signalling in chemoreceptors. Mol Microbiol *73*, 801-814.